Functionalized polythiophene thin-film transistors for low-cost gas sensor arrays

Josephine Bea Chang

Electrical Engineering and Computer Sciences
University of California at Berkeley

Technical Report No. UCB/EECS-2006-42
http://www.eecs.berkeley.edu/Pubs/TechRpts/2006/EECS-2006-42.html

April 24, 2006

FUNCTIONALIZED POLYTHIOPHENE THIN-FILM TRANSISTORS FOR LOW-COST GAS SENSOR ARRAYS

by

Josephine Bea Chang

B.S. (University of Texas, Austin) 2001
M.S. (University of California, Berkeley) 2004

A dissertation submitted in partial fulfillment of the

requirements for the degree of

Doctor of Philosophy
in

Engineering-Electrical Engineering
and Computer Sciences

in the

GRADUATE DIVISION

of the

UNIVERSITY OF CALIFORNIA, BERKELEY

Committee in charge:

Professor Vivek Subramanian, Chair
Professor Chenming Hu
Professor Don Tilley

Spring 2006

FUNCTIONALIZED POLYTHIOPHENE THIN-FILM TRANSISTORS FOR LOW-COST GAS SENSOR ARRAYS

by

Josephine Bea Chang

The dissertation of Josephine Bea Chang is approved:

Chair Date

Date

Date

University of California, Berkeley

Spring 2006

ABSTRACT

FUNCTIONALIZED POLYTHIOPHENE

THIN-FILM TRANSISTORS FOR LOW-COST

GAS SENSOR ARRAYS

by

Josephine B. Chang

Doctor of Philosophy in Electrical Engineering and Computer Sciences

University of California, Berkeley

Professor Vivek Subramanian, Chair

A low-cost electronic nose solution based on printed arrays of organic thin film transistor gas sensors is proposed. First, polythiophene organic thin film transistors are shown to be suitable for use as gas sensors. Good sensitivity to a range of gas analytes including alcohols, thiols, amines, and acids is observed down to 10 ppm. The alcohol and acid response is also reversible at low concentrations. Then, a synthetic route is demonstrated for predictably altering sensor response through the incorporation of functionalized end-capping groups. This route is used to generate an array of polythiophene sensor inks with differentiated sensor response, and effect of end-group functionality and placement are investigated. An integrated gas sensor array is fabricated using a droplet-on-demand technique as a demonstration of the possibility for low-cost manufacturing. Finally, the design of organic-based logic support circuitry for the sensor array is considered.

ACKNOWLEDGMENTS

This work has been the recipient of a generous input of time and effort from many people at Cal. Dr. Jean Fréchet's research group in the Chemistry department was an invaluable source of ideas, chemical expertise, and, most importantly, in-house synthesized materials. In particular, I would like to thank Kevin Sivula and Amanda Murphy for many useful discussions and a fruitful collaboration over the years. In my own lab group, Vincent Liu's contributions to this research are much appreciated, and Jason Lee was an invaluable resource for the device modeling and circuit simulation portion of the work. Thanks also to Steve Volkman, who was always there when I needed advice, and to Alejandro de la Fuente, for making our lab a bearable place to work. In addition, Frank Liao must be acknowledged as the true founder of this sensors project. He developed a flexible, robust experimental infrastructure that I had the good fortune to inherit. And, of course, I've been incredibly lucky to have had the privilege of working with Vivek Subramanian, my advisor, mentor, and role model over the past four years. Thanks, Vivek, for making my graduate school productive, rewarding, memorable, and fun. Thank you most of all for football and for Paul.

Dedicated to my mom and dad, who have always given me only the best,

and have hoped for this even longer and harder than I have.

TABLE OF CONTENTS

LIST OF FIGURES

Number Page

Chapter 1: **INTRODUCTION**

Electronic noses have been heralded for over a decade. The field has promised to introduce the world to sensing applications ranging from wine bottles capable of monitoring the aging of their contents to mailboxes that can sniff out bombs. However, the electronic noses commercially available today carry hefty price tags that remain well outside of the range feasible for consumer products such as smart food labels.

The introduction of electronic noses into the consumer market could enable applications ranging from medical self-diagnosis kits to indoor air-quality monitoring and smart home appliances. At the low-cost extreme, electronic noses could be used to integrate spoilage detection into pharmaceutical and food packaging and labels. All of these uses have been demonstrated using electronic nose systems [10][11]; they are unavailable today simply because of cost. Currently, commercially available electronic nose systems typically have price tags in the thousands of dollars. The sensing elements most commonly used by these systems include metal oxide and conducting polymer chemoresistors as well as quartz crystal microbalances, surface acoustic wave devices, and gas chromatography systems. The cost of sensors arrays would be significantly lowered if multiple sensing elements could be integrated onto a single substrate, allowing batch fabrication. However, with the sensing elements currently available,

integration typically requires complex processing and/or sequential subtractive steps, which are expensive.

One promising approach to lowering the cost of electronic noses is to use organic electronics for some or all of the components. This would allow leveraging of the low-cost manufacturing ideas associated with the field of organic electronics, such as printed circuits and roll-to-roll manufacturing. Transistors based on organic semiconductors are known to exhibit gas sensor responses, and may be able to provide a low-cost replacement for the gas sensor arrays currently used in electronic noses. Printing the sensor array could lower the cost of electronic noses by lowering the fabrication costs for individual sensors, by reducing the cost of integrating the array onto a single substrate, and by eliminating the sensor-to-processor attach cost, since sensors could be printed directly onto the signal processing units. Furthermore, organic electronics may also be able to provide the signal processing circuitry necessary to form a complete electronic nose system. Techniques for printing OTFTs have been under intensive development over the past decade, and many of the organic conductive materials used are similar to those used for electronic noses. So far, however, printing has not been applied for fabrication of gas sensor arrays. Many of the conducting polymers currently used for commercial electronic noses are insoluble after polymerization, and are thus typically deposited using electrochemical polymerization or plasma chemical vapor deposition.

The next two chapters contain relevant background material. Chapter 2 gives an overview of electronic nose technology, including historical development, recent research, and basic principles of operation. Chapter 3 reviews the field of organic electronics, with an emphasis on organic thin film transistors (OTFTs). The fundamental physics behind charge transport in conjugated systems and OTFT device operation is covered.

During characterization of OTFT gas sensors, signal drift due to operational and environmental instabilities is often encountered. Typically, sensor response is overlaid on top of long-term signal drift, and distinguishing the two is an important challenge. Chapter 4 addresses the stability problems associated with using organic devices, highlighting the dominant sources of signal drift and discussing strategies for avoiding or accommodating this drift.

In Chapter 5, the use of organic transistors for gas sensing is introduced in detail. Previous work on OTFT sensors and mechanism that have been proposed for the sensor response are discussed. Then, experimental results are presented describing the sensor response of polythiophene OTFT sensors to different volatile organic compounds. The sensor response of an air stable polythiophene is compared to that of a non-air stable one in order to investigate the tradeoff between sensitivity and air stability. Real-time extraction of multiple device parameters during sensing experiments is used to shed light on the mechanisms of sensor response transduction in OTFTs.

In addition to operational OTFT gas sensors, the construction of a low cost, printed gas sensor array requires a library of printable sensing materials with complementary sensitivities. A synthetic route for the generation of such an array of printable sensing materials is presented in Chapter 6. By attaching differently functionalized capping groups onto the ends of polythiophene chains, several variants of printable sensor inks were synthesized. When used in an array of OTFT gas sensors, significant sensor response differentiation was observed in these new materials. Threshold voltage response was particularly heavily influenced by the functionalized end-capping groups.

In Chapter 7, the printable materials presented in Chapter 6 are used to construct an integrated gas sensor array using fabrication methods compatible with low-cost manufacturing. The integrated sensor array shows good sensitivity to a range of organic vapors, and the differential response required for electronic noses. Integration of this sensor array with silicon-based signal processing circuitry is considered.

An all-printed process, using OTFT-based signal processing coupled with an OTFT gas sensor array, would be a potential path to ultra-low cost electronic noses. Chapter 8 examines the challenges associated with providing signal processing through OTFT-based logic. Charge transport models for organic thin films are reviewed, and based on these models, a compact SPICE device model for OTFTs is developed. This model is used to investigate circuit-design issues involved in the implementation of analog to digital conversion in OTFT-based logic, which is an important component that would need to be provided by any signal processing circuitry.

Finally, Chapter 9 summarizes the progress that has been made so far towards the realization of low-cost electronic nose systems, and discusses the work that remains in the pursuit of this goal.

Much of the technical content presented in this dissertation has been published or submitted to peer-reviewed journals or publicly presented at conferences. The relevant references are listed below:

[1] J. B. Lee, M . Heeney, S. Tierney, I. McCulloch, A. Murphy, J. Liu, J.M.J. Fréchet, and V. Subramanian, "Stability in OTFT gas sensors," Organic Thin-Film Electronics, edited by A.C. Arias, N. Tessler, L. Burgi, and J.A. Emerson (Mater. Res. Soc. Symp. Proc. 871E, Warrendale, PA), I1.5, 2005.

[2] J. B. Lee, M. Heeney, S. Tierney, I. McCulloch, A. Murphy, J. Liu, J. Fréchet, and V. Subramanian, "Polythiophene Thin-Film Transistor Array for Gas Sensing," Device Research Conference, Santa Barbara, CA, Paper IV.A-6, 2005.

[3] V. Subramanian, J. Lee and V. Liu, "Low-cost arrayed gas sensors for environmental monitoring," Materials Research Society Fall Symposium, Paper S2.1, Boston, MA, December 2005.

[4] J. B. Chang, V. Liu, V. Subramanian, K. Sivula, C. Luscombe, A. Murphy, J. Liu, and J.M.J. Fréchet, "Functionalized polythiophene thin-film transistors for low-cost gas sensor arrays," accepted for publication in Journal Appl. Phys., 2006.

[5] J. B. Chang, and V. Subramanian, "Effect of active layer thickness on bias stress effect in pentacene thin film transistors," accepted for publication in Appl. Phys. Lett., 2006.

[6] V. Subramanian, J. Lee, V. Liu, S. Molesa, "Printed Electronic Nose Vapor Sensors for Consumer Product Monitoring," IEEE International Solid State Circuits Conference, Paper 15.3, February, 2006.

Chapter 2: BACKGROUND ON ELECTRONIC NOSES

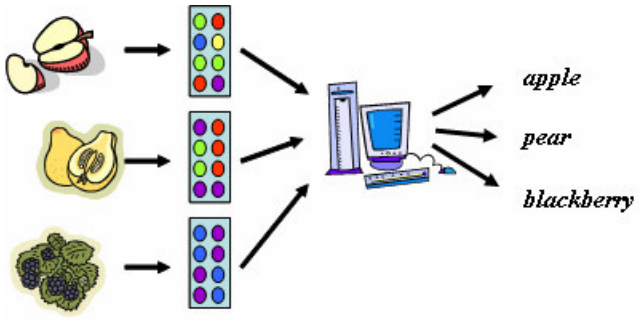

Figure 2.1: Sensing principle used by electronic noses. Odors are identified by recognizing patterns in the response of an array of sensors.

An electronic nose is a device that identifies complex odors by using pattern recognition strategies similar to those employed by the human olfactory system. Given a glass of wine, a traditional stand-alone gas sensor could be used to pin down the concentration of a single gas, like ethanol, for example. A more complex system equipped with gas chromatography/mass spectrometry may be able to break down the wine odor into various components, detecting a collage of alcohols, acids, and esters. A human nose, on the other hand, would only be able to vaguely quantify the concentration of ethanol and would be fairly inadequate at breaking down the odor into its constituent parts, but would be able to very rapidly identify the odor as wine. This is accomplished through pattern recognition; to identify the wine, the person smelling it must already know what wine generally smells like.

The human sense of smell is facilitated by approximately ten thousand odor sensors within the nose, whose response patterns are processed by the brain to search for matches to known response patterns in order to identify the odor. An electronic nose operates on similar principles, but with much fewer sensors—commercial systems use around ten to fifty sensing elements. A complete electronic nose system is generally comprised of a sampling system, a gas sensor array, and a signal processor equipped with pattern recognition capability.

Most basic gas sensors operate based on a lock-and-key strategy, in which a specific gas is picked out by a targeted sensing mechanism. Electronic noses, on the other hand, use an array of sensors with different sensitivities and selectivities. The sensors used in these applications often exhibit broad responses to a range of gases, and identification of specific odors relies on analysis of the array response with pattern-recognition algorithms. Much like that of the human nose, this type odor recognition is both more flexible and more powerful than what is possible with a single sensor. Grandma's apple pie may smell different from mom's, but they have similar odor patterns, and an electronic nose can be trained to recognize both and everything in between. Unlike a single sensor, which is typically specific, an electronic nose can operate much more generally. Rather than developing one sensor for wine monitoring, and a different one to detect bad fish, the same electronic nose template could be trained separately for different tasks.

2.1 Historical development

Electronic devices that can detect and identify gases have existed for many decades. Solid-state gas sensor devices and simple sensor arrays were first reported the 1950s. In response to increasing political awareness of environment and public health issues, basic gas sensor

research progressed rapidly over the next two decades, resulting in a wide array of different sensor transducer technologies, many of which are discussed in Section 2.4. In general, these sensors focus on the detection of specific gases using targeted transduction technologies [7]. On the other end of the spectrum, gas chromatography/mass spectrometry (GC/MS), first developed in the 1960s, allows the analysis of complex odors containing multiple components. Though it is a powerful tool that has become a mainstay of chemistry laboratories, GC/MS relies on relatively complex chemical analysis techniques. Sensor transducers, which translate chemical sensitivity into electrical, optical, or some other more manageable signal internally, are more suited for applications outside the laboratory [8].

The idea of putting an array of sensor transducers together into an intelligent, gas sensor system for odor recognition was first introduced by Persaud and Dodd in 1982 [9], and the term electronic nose was later coined in 1988 by Gardner. From the mid-1980s to the mid-1990s, an enormous amount of research activity resulted in the development of robust systems with very good sensitivity and discriminatory power [10]. Demonstrations of the abilities of electronic noses included such fine tasks as distinguish between different vintages of wine [11] and coffee beans from different countries [12].

The first instrument to hit the market, the "Sniffer" by Bacharach, Inc. in the 1960s, had only one sensing element, and so probably didn't qualify as a true electronic nose. Commercial systems equipped with sensor arrays first became available in the mid-1990s. Pioneering instruments include the MOSES, the IIT Electronic nose, and the Applied Sensor 3300. Today, bench top systems are available for laboratory use, while portable systems, some including hand held components, are available for field applications [13]. In 1998, Gardner and Bartlett predicted that "the next decade should see the cost of electron noses fall dramatically

and so they will be used not only in industry but also in every day life" [10]. So far, however, this price drop has not materialized, and commercial prices for electronic noses today remain at the same level as they were in 1998.

2.2 Biological noses

Of the five senses, the sense of smell uses the largest portion of the brain [14]. The human nose is sensitive to certain pungent odors at concentrations as low as a few parts per billion. In many ways, the artificial olfaction of electronic noses has been modeled on its biological counterpart (Figure 2.2).

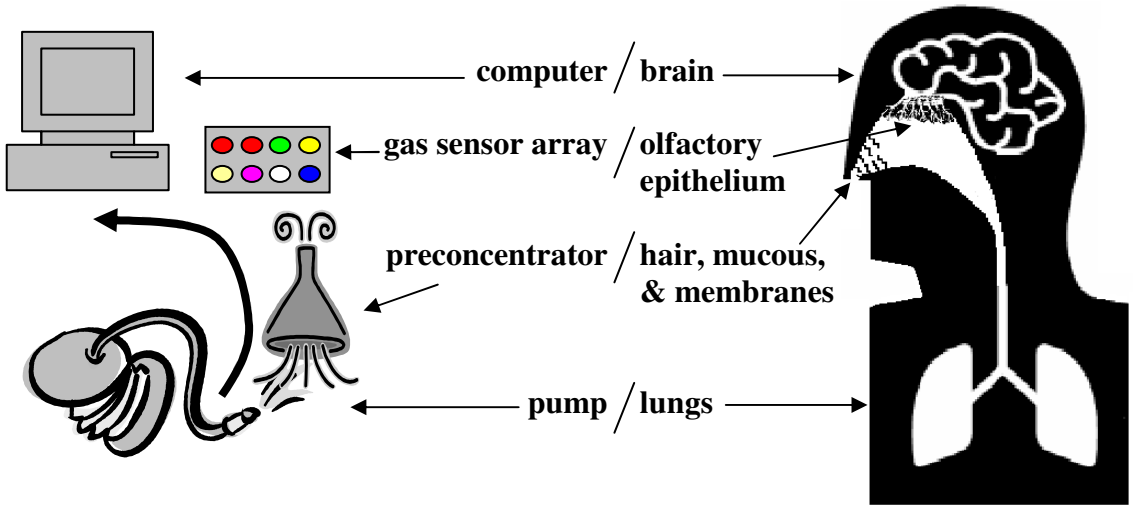

Figure 2.2: Comparison of an electronic nose with the biological olfactory system.

In humans, the lungs deliver odor-laden air the epithelium layer; the electronic nose uses a pump. The human nose is equipped with hairs, mucous, and membranes to filter and concentrate odors, while the electronic nose typically has a sampling system responsible for sample filtration as well as a conditioning system to enhance selectivity and protect the sensors.

In humans, the olfactory epithelium contains millions of receptors that interact with odorous molecules in unique ways; the electronic nose has a gas sensor array. The human sensing cells convert chemical sensor responses into a unique pattern of electronic nerve impulses, which travel through a complex network of neurons before reaching the brain for interpretation. Similarly, the chemical sensors in the electronic nose produce a pattern of electrical signals that is read and interpreted by a computer using pattern classification algorithms [14].

Despite these similarities, however, the electronic noses available today still fall far short of the capabilities of the human nose. The most obvious disparity is that electronic noses have far less sensors. The cost of designing and manufacturing an electronic nose rises quickly with the size of the gas sensor array, and it is unlikely that any man-made system will be able to approach the millions of receptors present in human noses any time in the near future. As a result, the human nose is still preferred for many demanding olfactory tasks, and sensory panels remain a mainstay in the food and perfume industries. And for tasks requiring extreme sensitivity, such as sniffing out drugs and contraband at airports, a dog's nose still easily outperforms any man-made instrument. However, with careful design of the sensor array, and in applications where the relevant range of odors is limited, an electronic nose can provide a number of advantages. Its readings can be consistent and objective; it can be used to detect gases which are hazardous or odorless to humans; and despite the high cost of electronic noses, human labor costs even more, and electronic noses are generally both cheaper and more easily deployable for on-site investigations than a panel of human sniffers [14].

2.3 Gas handling and delivery

An important factor in the reproducibility of electronic nose readings is the sampling procedure. Measurements are either taken by bringing the sensors into the atmosphere to be analyzed or by placing the sample of interest in an enclosed environment, and, after time for equilibration, transferring a fraction of the air around the sample (called headspace) to the sensor array. A fixed volume of the headspace can be transferred, or a constant stream of it can be circulated over the sensor during the measurement. Sensor responses are directly affected by the partial gas pressure of volatile compounds that the sensor is exposed to, and this partial gas pressure can be influenced by sample size, headspace volume, temperature, humidity, pressure, equilibrium time, and the type of ambient or carrier gas used. Often, preconcentrators are used to enhance the sensitivity of a sensor array, but care must be taken to maintain vapor concentrations below their saturated vapor pressure. This saturated vapor pressure, which varies with temperature and can change depending on the mixture of gases present, marks the point above which the vapor of interest will begin to condense into liquid drops [10].

Direct exposure of the sensor array to odors in an open system is often more practical in field implementations, or in systems where cost is a concern, as sample delivery systems can often be both unwieldy and expensive. Open systems are also preferred if the dynamics of rapid concentration change in the environment are of interest. However, such systems must often deal with strong fluctuations in environmental conditions, and the dynamics of sensor response must be considered in addition to the sensors array's steady state response [10].

2.4 Gas sensing elements

The heart of an electronic nose is its array of gas sensors. Individually, each sensor is a transducer capable of converting chemical interactions with ambient vapors into an electrical signal that in some way corresponds to the quantity and quality of the vapor constituents. Transduction mechanisms can vary widely, from conductometric to capacitive, potentiometric, calorimetric, gravimetric, optical, and amperometric. Gas sensor elements that have been used for commercial electronic nose systems are listed in Figure 2.3. Typically, two-terminal chemoresistor or three-terminal chemotransistor structures are preferred due to ease of signal processing. Gravimetric devices, which respond to vapors with a mass change that is then translated into an electrical signal, have also been used in commercial electronic nose systems. These include quartz crystal microbalance (QCM) and surface acoustic wave (SAW) sensors [13].

The classes of transistors differ in the complexity and quantity of the collected information, as well as the extent to which sensitivities can be tuned. Some electronic noses actually employ "heterogeneous" sensor arrays that include more than one class of sensors in order to increase the comprehensiveness of the collected data.

Sensor Type	*Fabrication*	*Sensitivity*	*Advantages*	*Disadvantages*
MOS chemoresistor	microfabricated, sputtering	5-500 ppm	Inexpensive	Requires high temperature operation, signal drifts over time.
Conducting polymer chemoresistor	microfabricated, electroplating, plasma chemical vapor deposition, solution processing	0.1-100 ppm	Room temperature operation	Signal drift and sensitivity to humidity
Polymer composite chemoresistor	Solution deposited	<0.1ppm	Room temperature operation	Signal drift and sensitivity to humidity
MOSFET chemotransistor	microfabricated	~few ppm	Integrated with CMOS	Gate is barrier to sensing
Quartz crystal microbalance (QCM)	microfabricated, solution processing	1.0 ng mass change	Transduction mechanism is well understood	Integration is difficult
Surface acoustic wave (SAW)	microfabricated, solution processing	1.0 ng mass change	Good selectivity and sensitivity	Integration is difficult, sensitive to humidity, drifts over time.

Figure 2.3: Table of chemosensors that have been used for commercial electronic nose systems.

2.4.1 Metal-oxide sensors

A number of metal oxides, including tin oxide, zinc oxide, iron oxide, and tungsten oxide, are n-type semiconductors. When used in two-terminal chemoresistor structures (Figure 2.4), the conductivity of metal oxide sensors (MOS) is proportional to the free electron concentration and the electron mobility in the material. At elevated temperatures (200-500ºC), certain odorant molecules, such as hydrogen, methane, carbon monoxide, or hydrogen sulfide, can be chemically reduced by oxygen species present at the surface of the metal oxide film. This reduction reaction results in increased free electron concentration and reduced barrier heights at grain boundaries, which increases the effective electron mobility within the material. The most widely used MOS devices are based on tin oxide resistors that have been doped with

different catalytic metal additives such as platinum or palladium in order to modulate its sensor response. P-type MOS devices are also available, based on materials such as copper oxide, nickel oxide, and cobalt oxide, which respond to oxidizable odorants like oxygen, nitrous oxide, and chlorine. Sensitivity of MOS devices depends on operating temperature and device geometry, and can be modified by catalytic dopants [15].

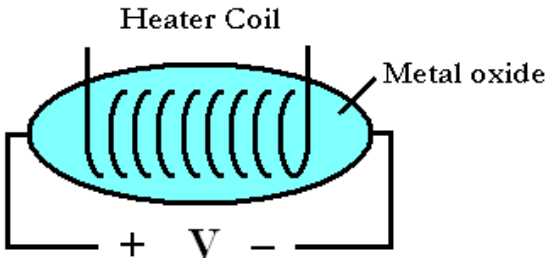

Figure 2.4: The basic construction of a metal oxide chemo-resistor gas sensing element.

Elevated operating temperatures are required for MOS devices for two main reasons. First, the oxidation and reduction reactions necessary for both sensor response and recovery are too slow for practical use at temperatures below 200ºC. Second, chemisorbed water on the metal oxide surface inhibits sensor-analyte reactions, and must be removed by operating at temperatures above 100ºC. The result of this high temperature operation is that power consumption of MOS based devices is very high, and, in cases where power supply is constrained or system portability is desired, care must be taken to reduce power consumption by minimizing device size and insulating the sensors to prevent heat loss[15].

MOS devices based on tin-oxide were first commercialized in the 1960s. Modern MOS devices are typically deposited through sputtering and patterned with microfabrication to minimize device size. However, integration of multiple metal oxides, or even the same metal oxide

containing different dopants, onto the same substrate is difficult and expensive using traditional microfabrication techniques, because it requires extensive subtractive processing, and yield drops quickly with each additional layer of material used. Overall, MOS devices offer the advantages of low cost, insensitivity to humidity, and an output signal which is easy to read and process. Disadvantages, however, include high operating temperatures, signal drift over time, limited selectivity, high power consumption, and only modest levels of sensitivity (5-500 ppm). They are also vulnerable to poisoning by certain odors such as silicones [13].

2.4.2 Conducting polymer sensors

In conducting polymer (CP) sensors, the metal oxide semiconductor is replaced with a semi-conducting polymer film that is either chemically engineered or coated to selectively absorb specific odorants (Figure 2.5). They can be used independently for detection of individual vapors or in arrays for handling of complex odors.

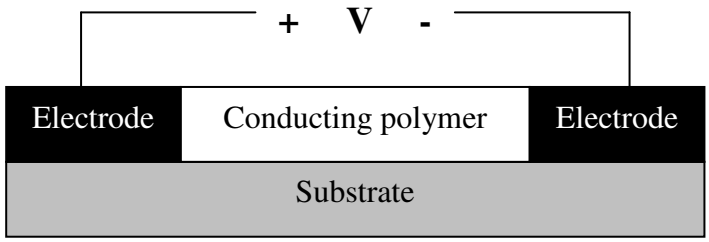

Figure 2.5: Cross-section of a conducting polymer chemoresistor gas sensing element.

The sensor response is produced when ambient vapors absorb into the polymer, inducing physical or chemical interactions that change the conductivity of the film, which is easily monitored. Depending on the strength and nature of interaction between the CP and the absorbent, this process is typically reversible, but hysteresis is common, especially when the

absorbent is present in high concentrations. The sensor response is correlated with the concentration of the odorant, and can be modified by chemically altering the CP or by varying the distance between electrodes [16].

Conducting polymers can be deposited in a variety of ways, depending on the chemistry of the specific polymer. Some of the CPs used for sensing are soluble, and can be easily deposited through solution processing methods such as spin-coating, screen printing, or drop-casting. Most often, however, the CPs used for sensing are insoluble, and are deposited using electrochemical polymerization across narrow electrode gaps. This allows selective deposition of the material, and provides good reproducibility as well as flexibility in control over film properties. CPs can also be deposited uniformly across an entire substrate through physical chemical vapor deposition, and then patterned using microfabrication techniques [17].

In contrast to MOS devices, which were used as stand-alone gas sensors for several decades before incorporation into electronic noses, CP chemoresistors were developed much later and are less commonly used as stand-alone sensors. However, several key advantages of CP gas sensors makes them more suitable than MOS devices for sensor array applications, and as a result, the first commercially available electronic noses were based on CP gas sensor arrays. These advantages include:

1. rapid, reversible responses at room temperature, which helps prolong lifetime and reduce power consumption;
2. a greater sensitivity to a wide range of organic vapors;
3. low-cost materials;
4. resilience to poisoning by many of the compounds inorganic sensors are typically inactivated by.

5. and the ease with which a wide variety of materials can be synthesized due to the flexibility of organic chemistry. This enables wide selectivity.

The biggest disadvantage of CP sensors is their sensitivity to humidity and their susceptibility to poisoning due to irreversible binding of vapor molecules to the sensing material[17].

2.4.3 Polymer composite sensors

While conducting polymers can be synthetically designed for solubility, the majority of conducting polymers used for sensing are not soluble. Polymer composites, however, are a related class of sensing materials that can typically be solution processed. This class of materials refers to mixtures of a conductive filler, usually either carbon black or polypyrrole, and a non-conductive, but chemically sensitive polymer [18]. When used in a chemoresistor structure (Figure 2.6), resistance in polymer composite films is well described by percolation theory, in which conduction occurs through the percolation of charge through sparsely connected clusters of conductive material. The ratio of conductive to insulating material is chosen to be near the percolation threshold, at which the density of conductive clusters is barely enough to support charge conduction. Upon exposure to analytes, the insulating polymer swells, causing the conductive network to be stretched, and changing the ability of charge to percolate through the thin film. The insulating polymer is chosen for its ability to selectively absorb vapors with good sensitivity and reversibility. Because these polymers do not need to be conductive, the pool of potential materials is much larger than that of conductive polymers [19]. In addition, modifying the polymers for sensitivity to specific odorants is easier. Using polymers custom designed for the purpose, carbon black composite sensors have been

demonstrated which exhibit sensitivity to amine analytes at concentrations as low as 2.7 parts per billion [20].

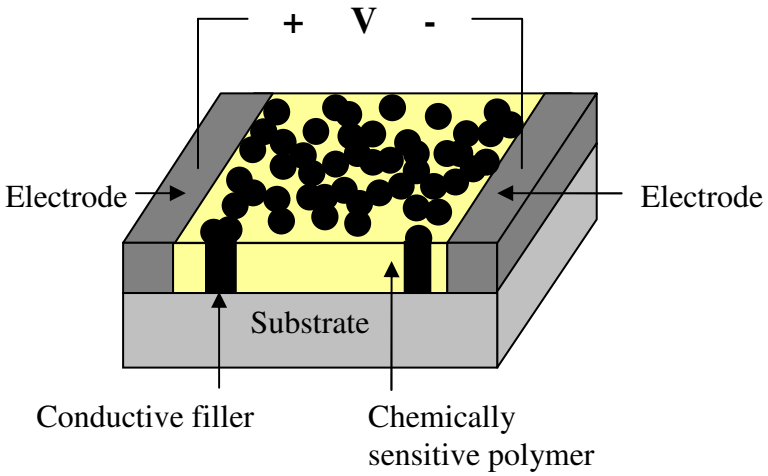

Figure 2.6: Cross-section of a polymer composite chemo-resistor gas sensing element.

Polymer composites offer many of the same advantages as conducting polymer chemoresistors, including low temperature operation, low-cost materials, and good sensitivity. They also suffer from the same reliability and lifetime issues. In addition, they offer the additional advantage of being solution-processable, and are deposited using techniques such as dip-casting and spin-casting. Also, the larger variety of polymers that can be used in composites is helpful for constructing sensor arrays with a properly tailored range of discrimination.

2.4.4 MOSFET sensors

Another type of gas sensor can be fabricated by replacing the polysilicon gate of traditional MISFET (metal insulator semiconductor field effect transistor) or MOSCAP (metal insulator semiconductor capacitor) with a gas-sensitive material (Figure 2.7).

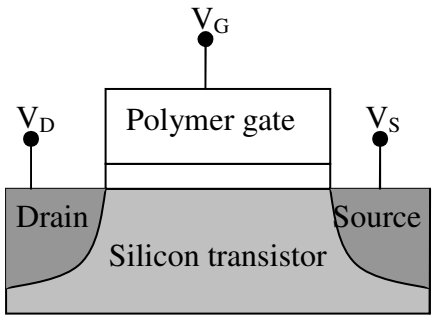

Figure 2.7: Cross-section of MOSFET gas sensor with a polymer gate.

Metals such as palladium or platinum show a work function shift when exposed to gases such as hydrogen, carbon monoxide, or hydrogen sulfide. This results in a threshold voltage shift. The sensitivity of these sensors is comparable to that of the MOS devices discussed in Section 2.4.1, but the range of gases that it can respond to are limited. The main advantage of this structure is its similarity to traditional MOSFETs used in silicon electronics, allowing for easy integration with signal processing circuitry [21]. Conducting polymer materials may also be used as gate electrodes for silicon MOSFETs. This offers the dual advantage of easy integration and low-temperature, low-power operation [22].

2.4.5 Gravimetric sensors

Gravimetric odor sensors rely on mass changes to detect vapors. The basic device structure includes a piezoelectric substrate like quartz or zinc oxide coated with a film of sorbent material. Sorption of vapor molecules into the film results in a mass change, which changes the wave velocity and resonant frequency of acoustic waves propagating through the piezoelectric substrate. Quartz crystal microbalance (QCM) sensors can detect changes in the resonant frequency, while surface acoustic wave (SAW) sensors detect changes in wave velocity. Differentiation and selectivity is achieved by modifying the coating film. Because SAW sensors can operate at higher frequencies, they can be more sensitive than QCMs. However, SAW sensors use zinc oxide or lithium niobate substrates rather than quartz, and are therefore more susceptible to long-term drift and more sensitive to humidity[13].

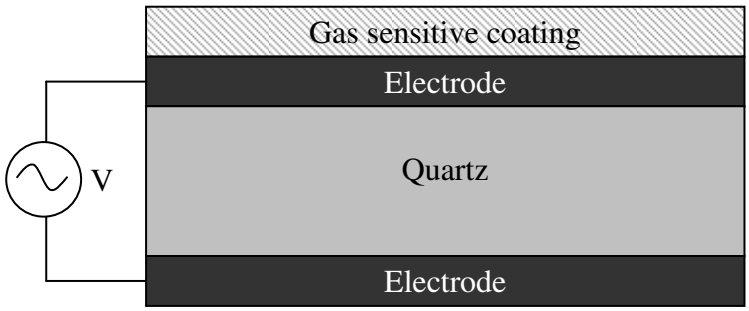

Figure 2.8: Cross-section of a quartz crystal microbalance gas sensing element.

2.5 Data analysis

Depending on the application, data processing for electronic noses can range from relatively straight-forward computation to extremely complex algorithms which push the envelope of modern day artificial intelligence research. The first step in signal processing involves converting the sensor property of interest, such as a resistance, drive current, or oscillation

frequency, into a voltage signal. This analog voltage is then amplified and converted into a digital signal that can then be fed into a processor equipped to perform the relevant computations.

2.5.1 Nearest neighbor method

Sensor array responses are typically normalized, and then stored and handled within the processor as a vector. The simplest pattern recognition strategy, known as the nearest-neighbor approach, is to subtract an unknown input vector from a series of stored reference vectors that correspond to known odors. The length of the difference vector is small if the response patterns are similar, and large if they are very different. After comparing each reference vector to the unknown, the closest one is selected as the identity of the unknown vapor. If no close match is found, then the electronic nose may conclude that the unknown is not in the library of reference vectors and cannot be identified [13].

2.5.2 Statistical analysis techniques

The information that can be gleaned from sensor readings compounds quickly with the size of the sensor array, provided that each sensor has been carefully designed to provide information that is as unique as possible. For each set of non-correlated sensor readings, the dimensionality of the data set is increased; the greater the diversity in the sensor array, the greater the dimensionality of the data set, which increases the range of odors an electronic nose can recognize, and enhances its ability to distinguish between subtle odors. The dimensionality of data sets is large for even small sensor arrays and large arrays can present a truly formidable maze of information. Therefore, it is helpful to reduce the dimensionality of a data set by

getting rid of redundant dimensions or combining multiple dimensions into a single dimension in which the most pertinent information has been concentrated [13].

One way of organizing a data set into a more useful form is to use models to sort experimental observations into different related groups. Cluster analysis, discriminant function analysis, or other more complex techniques can be used for this process of classification. Similarly to the nearest neighbor method, odor identification then proceeds by evaluating an unknown response vector's "closeness" to reference vector groups [13].

Principle component analysis is a mathematical technique for culling a dataset down to its most critical dimensions. When sensor array responses are plotted in these reduced dimensions, related data points become clustered, and identification of a data point due to its proximity to known data points in this space is both more powerful and more flexible than results given by the nearest neighbor method. For example, if a large number of reference data points for a particular odor have been taken, principle component analysis will tend to filter out the variations between different readings of the same odor, and similar noise in the unknown reading is also likely to be filtered out. Moreover, principle component analysis often tends to reveal trends in which similar odors cluster more closely together. For example, different alcohol vapors may produce distinct clusters of readings which are all in close proximity to each other and far away from the clusters produced by other classes of odors such as acids or esters. If an electronic nose encounters a reading from an unknown substance which produces a data point outside of any known cluster but which falls in close proximity to other alcohol readings, it may conclude that the odor sample is an unknown alcohol [13].

2.5.3 Artificial neural network

Due to the sheer complexity of gas sensor response patterns, many electronic nose systems have turned to more powerful information processing methods that can be dynamically "trained" to "learn" new odors. The most commonly used "intelligent" pattern analysis technique is the artificial neural network, a machine-learning algorithm inspired by current understanding of how the brain works. The brain is composed of an enormous mass of highly interconnected neurons, and learning is believed to be accomplished in part by dynamic manipulation of the strength of neuron interconnections based on positive or negative feedback. Artificial neural networks imitate this process by setting up a large array of neuron elements that receive inputs from multiple elements (either sensors or other neurons,) manipulate these inputs, and pass on the results to other elements (either other neurons or an output signal). During an extensive training phase, reference inputs are provided to the system and system parameters, such as the interconnections between neurons and the specific nature of the manipulation performed by each neuron, are dynamically manipulated until correct outputs are consistently achieved. Once trained, artificial networks are generally able to process information quickly, efficiently, and accurately. However, the training process is involved and can be labor intensive [10].

2.6 Current applications of electronic noses

Most odors that we encounter in daily life consist of a complex mixture of vapors. For example, volatile organic compounds play an important role in shaping the aroma and taste of most foods, and can act as a keen indicator of freshness and quality, but even the simplest foods may contain hundreds of these volatile flavor-contributing chemicals. Designing a chemical sensor-based instrument to quantify all the individual odor constituents in an attempt

to resolve flavor-related problems can be a frustrating exercise. In order to guarantee a certain standard of raw materials as well as final products, quality control must rely on approaches that analyze odors as a whole, the way human noses and electronic noses do. Thus, electronic noses are used commercially for a wide variety of odor and volatile compound applications, including:

1. Quality control in the food industry
2. Quality control of packaging material
3. Medical diagnostics
4. Environmental monitoring
5. Perfume and aroma industry
6. Control of beverages such as wine and beer
7. Tobacco industry
8. Coffee industry
9. Assessment of car interiors

Despite an impressive list of analytical capabilities, commercialization of electronic nose instruments has been somewhat rocky. Early users had to navigate through complex calibration and interpretation procedures, efforts that were often rewarded with readings which were undependable due to poor reproducibility and stability. Many of these problems still plague modern instruments, and continue to limit their popularity. Nevertheless, electronic noses remain unique in their ability to handle certain complex odor analysis, and in some applications, are the best available option regardless of cost [13].

2.7 References

[7] J.W. Gardner, P.N. Barlett, "A brief history of electronic noses," Sensors and Actuators B, 18, 211, 1994.

[8] G.A. Eiceman, Gas Chromatography, in R.A. Meyers (Ed.), Encyclopedia of Analytical Chemistry: Applications, Theory, and Instrumentation, pp. 10627. Wiley: Chichester, 2000.

[9] K Persaud and G.H. Dodd, "Analysis of discrimination mechanisms of the mammalian olfactory system using a model nose," Nature, 299, 352, 1982.

[10] J.W. Gardner and P.N. Bartlett, Electronic Noses Principles and Applications, Oxford University Press: New York, NY, 1999.

[11] C.D. Natale, F.A.M. Davide, A. D'Amico, G. Sberveglieri, P. Nelli, G. Faglia, C. Perego, "Complex chemical pattern recognition with sensor array: the discrimination of vintage years of wine," Sensors and Actuators B, 24, 801, 1995.

[12] J.W. Gardner, H.V. Shurmer, and T.T. Tan, "Application of an electronic nose to the discrimination of coffees," Sensors and Actuators B, 6, 71, 1992.

[13] T.C. Pearce, S.S. Schiffman, H.T. Nagle, and J.W. Gardner (Ed.), Handbook of Machine Olfaction Electronic Nose Technology, Wiley-VCH: Weinheim, Germany, 2003.

[14] H.T. Nagle, R.Gutierrez-Osuna, and S.S.Schiffman,"The how and why of electronic noses," IEEE Spectrum, 22, 1998.

[15] R.F. Taylor and J.S. Schultz, Handbook of Chemical and Biological Sensors, Institute of Physics Publishing: Philadelphia, PA, 1996.

[16] K.C. Persaud, "Polymers for chemical sensing,"Materials Today, 8, 38, 2005.

[17] J. Janata and M. Josowicz, "Conducting polymers in electronic chemical sensors," Nature, 2, 19, 2003.

[18] K.J. Albert, N.S. Lewis, C.L. Schauer, G.A. Sotzing, S.E. Stitzel, T.P. Vaid, and D.R. Walt, "Cross-Reactive Chemical Sensor Arrays," Chem. Rev., 100, 2595, 2000.

[19] E.J. Severin, Array-based vapor sensing using conductive carbon black-polymer composite thin film detectors, dissertation submitted to California Institute of Technology, 1999.

[20] T. Gao, E.S. Tillman, and N.S. Lewis, "Detection and Classification of Volatile Organic Amines and Carboxylic Acids Using Arrays of Carbon Black-Dendrimer Composite Vapor Detectors," Chem. Mater., 17, 2904, 2005

[21] B.J. Polk and J. Janata, "ChemFET Arrays for Chemical Sensing Microsystems" IEEE Sensors Conference, Orlando, Florida, 5.13, 2002.

[22] Covington, J. A., J.W. Gardner, P.N. Bartlett, and C-S. Toh, "Conductive polymer gate FET devices for vapour sensing," IEE Proc. Circuits Devices Syst. 151, 326, 2004.

Chapter 3: BACKGROUND ON ORGANIC ELECTRONICS

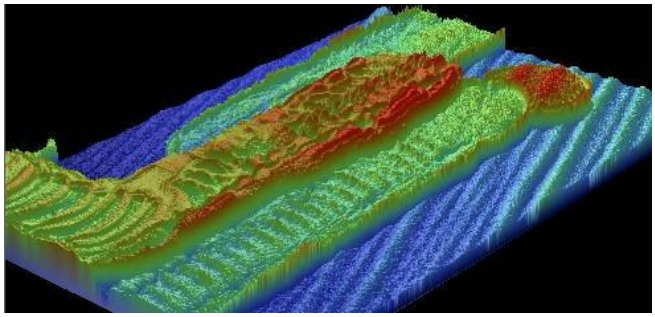

Courtesy: Daniel Soltman

Figure 3.1: All-printed pentacene OTFT on plastic

Organic electronics is uniquely poised to provide a monolithic low-cost electronic nose solution because it can potentially provide a complete sensing and signal processing solution that is compatible with ultra-low cost manufacturing. Organic materials are useful for electronic nose applications for several reasons. First and most importantly, the carbon backbones that make up organic semiconductors make them more chemically active than most of their relatively inert inorganic counterparts. Thus, electrical devices based on organic materials tend to have strong electrical responses to chemical exposures, a trait which translates into sensing devices with good sensitivity to a broad range of vapors. A side effect of this chemical reactivity is that organic electronics typically have problems with air stability and lifetime, but this is true of all organic electronic devices, not just sensors, and there are many on-going efforts to address these issues. Still, stability and lifetime issues are among the most serious present-day challenges to the commercial use of organic electronics.

A second advantage of organic electronic materials for electronic noses is the fact that they can be readily modified using synthetic chemistry, allowing their chemical sensitivities to be

controlled by careful engineering during the organic synthesis process. Chemical functionalization or other similar manipulation can be used to tuned and adjust the sensitivities and selectivities of organic semiconductor-based gas sensors. Finally, organic molecules tend to be soluble at room temperature in common solvents, thus making it easy to process and deposit these materials from solution. This is especially important for applications like the electronic nose, where the ability to place multiple sensing materials on the same substrate is necessary for the construction an integrated array of different chemical sensors.

3.1 Historical development

The idea that organic molecules could transport electronic charge was suggested as early as 1941, when it was proposed that certain biological processes could be explained by the movement of electrons over large distances along organic molecules. By 1948, charge transport in number of organic oligomers and other complexes had been observed [23]. The discovery of electroluminescence in organic molecular crystals in the 1960's triggered a sharp rise in research activity, and much of the basic theory for electronic processes in organic materials was worked out in this period. The next major advance came in the 1970's, with the development of an important new class of organic semiconductors based on conjugated polymers. Photovoltaic cells based on organic hetero-junctions, thin-film transistors with conjugated oligomer and polymer active materials, and high-efficiency electroluminescent organic diodes were demonstrated in the 1980's, eliciting both scientific and commercial interest. Organic light-emitting diode (OLED) technology progressed rapidly over the next decade, and made its debut in consumer applications in 1997 [24]. Today, judging from the present amount of research activity and industrial investment, logic circuits based on organic

thin film transistors (OTFTs) and organic photovoltaic cells are both expected to follow a similar path to commercialization in the near future.

3.2 Electrical characteristics of conjugated oligomers and polymers

Nearly all conducting organic materials are conjugated π-electron systems, meaning that they have a backbone of sp^2-hybridized carbon atoms. The molecular structures of a few prototypical organic semiconductors are given in Figure 3.2. Notice that all these molecules contain a pattern of alternating double and single bonds, a trademark characteristic of conjugated structures [24].

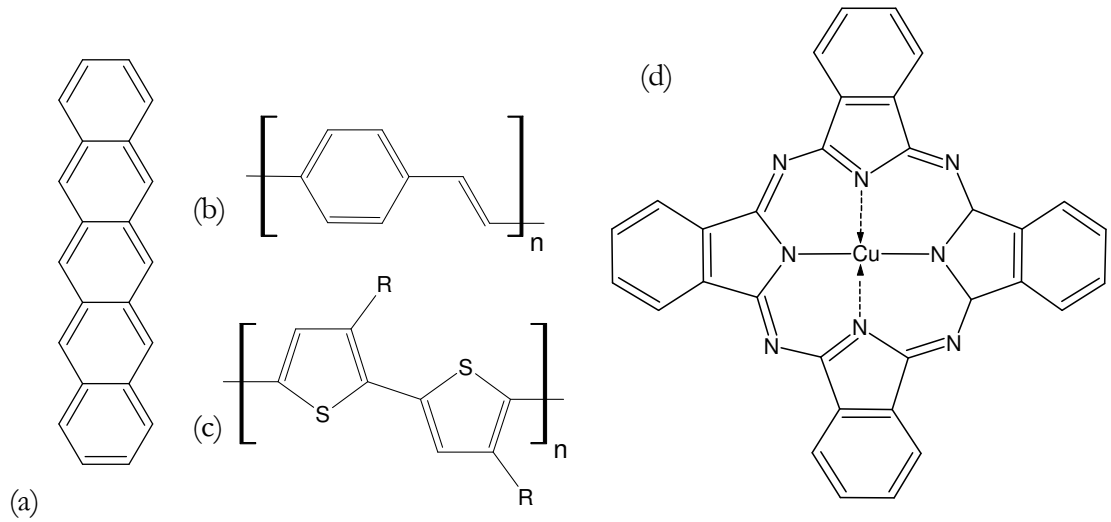

Figure 3.2: Molecular structure of commonly used organic semiconductors.
(a) pentacene (b) poly (p-phenylene-vinylene) (PPV) (c) poly (3-alkylthiophene) (P3AT) and (d) copper-phthalocyanine (CuPc).

Electrons in an sp^2-hybridized carbon atom can either occupy a directional σ-orbital, where it can participate in a σ-bond with one of its nearest neighbors, or a π-orbital, where it can be

shared with the overlapping π-orbitals of neighboring atoms. A chain of atoms with interacting π-orbitals can form a continuous π-electron cloud within which electrons can become delocalized. While the wave function of a σ-electron is localized to one particular bond, delocalized π-electrons have wave functions are that are spread across a distance of many atoms. The orbital structure of ethene, the simplest example of a conjugated π-electron structure, is illustrated in Figure 3.3. Non-carbon substituents may also be introduced into conducting organic molecules, and as long as they also contain a π-orbital, π-conjugation within the system can be preserved [24].

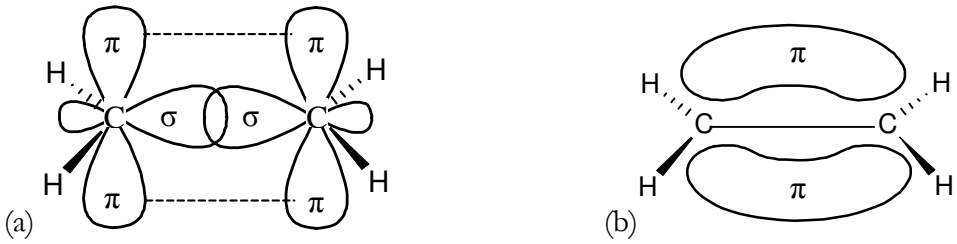

Figure 3.3: Orbital structure of conjugated sp^2 hybridized carbon atoms.
(a) Ethene is composed a pair of double bonded carbon atoms. The first bond is formed by overlapping σ-orbitals, while the second bond is formed by interacting π-orbitals. (b) π-electrons can then delocalize across the π-orbitals of adjacent molecules.

For small oligomers, the distance over which charge delocalization extends has been shown to be approximately correlated with the length of molecule, but for longer molecules such as polymers, chemical or physical defects cause the π-electron cloud to be broken up into smaller segments, and electrons cannot delocalize across the entire length of the molecule. In this case, the molecule is treated as a string of independent, conjugated segments, and the average length of these conjugated segments is known as the conjugation length. During charge transport,

this conjugation length is the average distance over which a charge can travel before it is trapped or before it must hop over an energy barrier [25].

Unlike σ-bonds, which are in-plane with the atoms, π-bonds are out-of-plane, meaning that the conjugated π-electron cloud from one molecular chain can interact with π-electron clouds on neighboring molecules. This sort of interaction can be easily disrupted by steric hindrances such as side chains or bent chains which keep neighboring molecules far from each other or prevent them from aligning. However, when present, this interaction promotes intermolecular alignment and long-range ordering which enables the formation of ordered grains or even molecular crystals. Interaction between π-orbitals of neighboring molecules is also important for the intermolecular transport of charge [25].

Because π-bonds are much weaker than σ-bonds, the lowest excited state of a conjugated system involves the transition of an electron from a bonding to an antibonding π-orbital. The delocalization of electrons across many π-orbitals results in a splitting of molecular orbital energy levels to form a spread of energy levels comparable to the energy bands in inorganic materials [24]. The gap between the highest occupied molecular orbital (HOMO) energy band and the lowest unoccupied molecular orbit (LUMO) energy band provides the equivalent of an energy bandgap (E_g) in organic molecules. However, the energy bands in organic materials arise from the interactions of a handful of molecules, rather than a large crystalline lattice of atoms, and the resulting band is narrower and contains a lower density of states than the energy bands in inorganic semiconductors such as silicon. Materials with overlapping HOMO and LUMO bands or very small E_g can be doped and used as conductors, while materials with larger E_g (typically in the range of 2-3 eV) are used as semiconductors. E_g is affected by the nature of π-bonding within the system, the immediate environment of the molecule, and its

conjugation length. In a film, molecules exhibit a random distribution of defects, molecular orientations, and grain structure. This results in conjugated segments with variable lengths, as well as inhomogeneities in the immediate environments of different conjugated segments. Therefore, organic semiconductors exhibit density-of-states profiles with gradual band edges, in contrast to the sharp band edges typically seen in the more perfectly ordered crystalline inorganic semiconductors (see Figure 3.4) [24].

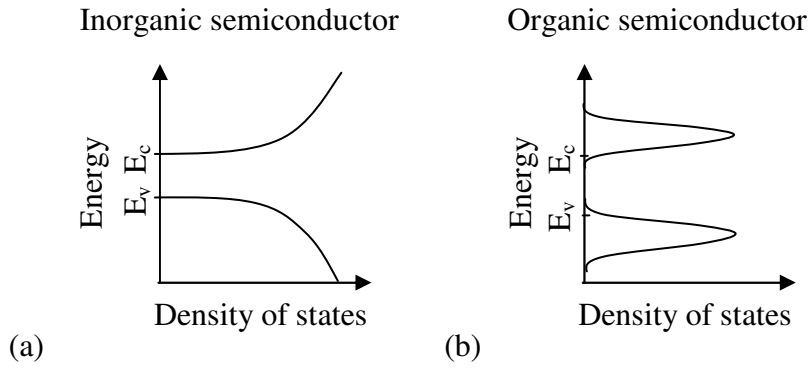

Figure 3.4: Comparison of the ideal energy band structure of inorganic and organic semiconductors.
Qualitatively, organic semiconductors have more gradual band edges, and more narrow bands with less energy states.

The physics of electron transport in organic semiconductors is predominately modeled using Gaussian or exponential bandtail profiles [26], and many parallels are drawn to inorganic materials in order to draw upon the large body of understanding developed for inorganic electronics, namely silicon-based systems. However, key differences between organic and inorganic systems should be kept in mind when using these band-theory based analyses. Most significantly, band theory assumes that mobile charge carriers moving within an energy band are able to freely redistribute in response to the average field emanating from other mobile charges. In other words, electron-electron correlations are negligible. This assumption holds

true in conventional metals and semiconductors, where strong covalent bonds between atoms results in large overlaps between neighboring orbitals, and charge transfer from atom to atom is quick. In inorganic materials, however, neighboring molecules are held together by van der Waals forces, which are orders of magnitude weaker than covalent bonds. The amount of overlap between π-orbitals of neighboring molecules is weak, meaning that charge transfer between organic molecules takes much longer. In fact, the kinetic energy associated with charge transfer between organic molecules is almost always small compared to the energy from the Coulomb repulsion of nearby charges. Consequently, the behavior of charge carriers is more heavily influenced by the instantaneous configuration of neighboring charges (which is different for every carrier) than by the average distribution of charge (which would be the same for every carrier) [25].

At the physical level, then, charge transport in organics is often better understood in terms of correlated electrons, holes, and/or particle pairs rather than individual free carriers. Unlike free charge carriers in silicon, "free" charge carriers in organics are often weakly bound to the dopant or ionized molecule from which it was excited, or to the mobile hole that was generated simultaneously. In some systems, the pair may be separated thermally, and the energy required to achieve this separation has important consequences on the nature of conduction. In other cases, a high density of other carriers in the immediate vicinity of the pair can screen the attraction between the pair, allowing independent motion of the mobile carriers. Another common possibility is for conduction to occur via the movement of bound particle-hole pairs known as excitons [25].

Semiconductors are referred to as being either "n-type" or "p-type." In inorganic systems, these terms are used to refer to materials which have been doped with either electron

acceptors or donors so as to have an abundance of either positive or negative mobile charge carriers. The meaning of these terms in organic systems refers to an entirely different set of concepts. In many organic materials, the carrier mobility of one charge polarity is orders of magnitude greater than that of the other. Hole transport materials are thus considered p-type, while electron transport materials are considered n-type. In others cases, the preferred polarity of mobile charge is determined by the alignment of the energy band levels of the organic semiconductor and the contact material from which charge is injected. Because organic semiconductors tend to have large bandgaps, it is impractical to use the same source/drain contact material for injection of carriers into both the HOMO and LUMO bands. Rather, the contact material is chosen to align with either one or the other of these bands, and the n- or p-type nature of the film is thus dictated by the work function of the contact electrode. Because the work functions of stable materials suitable for contacting organic semiconductors only span a limited range, most organic semiconductors are limited to one polarity of operation in practical devices. Therefore, n-type materials are characterized by high electron affinity (high LUMO levels) and p-type materials by low ionization potentials (low HOMO levels) [27].

3.3 Organic thin film transistors (OTFTs)

The thin-film transistor is the device structure of choice for logic based on organic electronics, as organic semiconductors do not easily form crystalline structures suitable for the construction of bulk devices.

3.3.1 Device structure and fabrication

Organic electronic devices are typically built using thin-film deposition techniques such as evaporation, sputtering, chemical vapor deposition, and spin-coating. There is usually no body

contact, so OTFTs are three-terminal field-effect transistors in which charge conduction between two terminals, the source and the drain, is controlled by modulating the electrical potential of a third terminal—the gate. The structure of an organic thin film transistor can take on a number of variations, the most common of which are illustrated below in Figure 3.5.

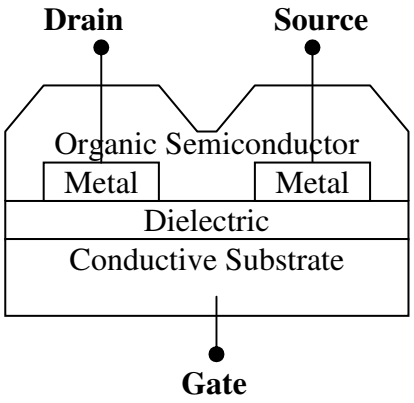

(a) Substrate-gated bottom contact OTFT

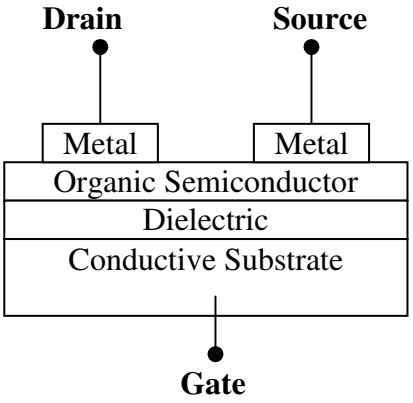

(b) Substrate-gated top contact OTFT

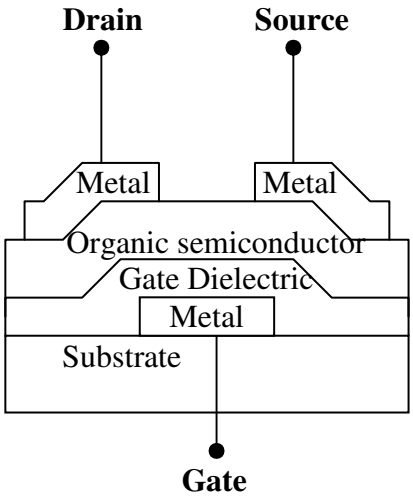

(c) Top-contact OTFT with patterned back-gate

Figure 3.5. Variations on the OTFT device structure

In bottom-contact substrate-gated devices (Figure 3.5a), a conductive substrate such as heavily doped silicon acts as a common gate for all devices. This substrate is then insulated with a gate dielectric such as thermally grown silicon dioxide. Next, metal is deposited onto the insulated substrate and patterned to form source and drain contact electrodes. Finally, the organic semiconductor is deposited on top of the structure. Conduction between the source and the drain occurs through a channel formed in the semiconductor layer, which is why this layer is often referred to as the 'active' layer.

The bottom-contact substrate-gated structure is commonly used in the field of organic electronics to characterize new materials due to ease of fabrication. The entire structure except for the active layer can be built and patterned using standard photolithography and microfabrication techniques, which, while not compatible with low-cost manufacturing, are mature and readily available to many research laboratories. The microfabricated structures can then serve as ready-made structures on top of which various organic semiconductors can be deposited. However, one disadvantage of depositing organic materials on preformed structures is that the organization of the organic thin film is often disrupted by the nonuniformity of the substrate. The differences in surface energy and surface roughness between the electrodes and the dielectric cause the organic film to adapt different microstructures, resulting in regions of disorder at the source/drain contacts. As a result, bottom-contact structures typically suffer from larger source and drain contact barriers and contact resistance.

A variation on this structure is the substrate-gated top-contact TFT (Figure 3.5b), in which the organic semiconductor is deposited directly onto a uniform substrate such as an oxidized silicon wafer. The formation of the organic film on a uniform substrate can be advantageous for obtaining well-ordered films. Source and drain electrodes are then deposited on top of the

organic semiconductor, typically through a shadow mask, because the organic layer tends to be sensitive to the photolithographic patterning and chemical etching techniques usually used to pattern metal contacts.

Though useful for materials characterization, substrate-gated devices are impractical for several reasons. First, the use of silicon substrates and microfabrication techniques are not compatible with the low-cost, roll-to-roll manufacturing goals of organic electronics. More importantly, the construction of OTFT-based circuits requires that devices be individually gated. For this, transistors with a patterned gate are required. The patterned back-gate structure (Figure 3.5c) also places the gate and dielectric below the active layer, but the use of an insulating substrate and individually patterned gates allows devices to be independently controlled. These structures have been fabricated on a number of substrates including silicon, glass, and plastic.

3.3.2 Current-voltage characteristics

The band tail in organic semiconductors and the frequent presence of energy states within the band gap due to impurities and defects result in a high density of traps within the band gap, making it difficult to invert organic semiconductors. Therefore, OTFTs are run in accumulation. For a p-type organic semiconductor, a negative charge applied to the gate electrode stimulates the accumulation of positive charge carriers within the active layer near the dielectric interface. When enough charge carriers have been accumulated, the conductivity of the accumulated region increases dramatically, providing a conductive channel running through the organic semiconductor between the source and drain. The current-voltage (I-V) characteristics of a representative substrate gated, bottom contact, pentacene are given in Figure 3.6.

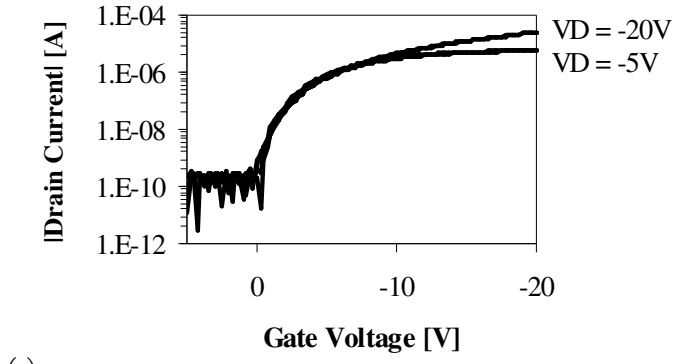

(a)

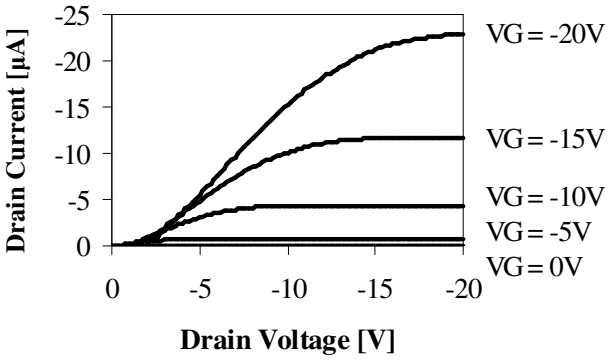

(b)

Figure 3.6: I-V characteristics of a representative OTFT.
(a) transfer characteristics and (b) output characteristics of a substrate-gated, bottom contact 500µm X 20µm pentacene OTFT with 950Å of SiO_2.

To a first approximation, OTFT I-V curves look very similar to those of inorganic FETs [28]. Cutoff, subthreshold, linear, and saturation regimes of operation are all discernable. In addition, drain current scales as expected with device width, length, and gate dielectric thickness. Because of this, OTFTs are characterized with many of the same metrics as inorganic FETs: field-effect mobility (μ_{FET}), threshold voltage (V_T), on-off ratio (I_{on}/I_{off}), transconductance (g_m), output resistance (R_o), series resistance (R_S and R_D). However, standard square-law MOSFET equations do not provide a good quantitative fit for OTFT behavior. Because OTFTs often suffer from significant non-idealities at contacts, addressing contact

resistance and contact injection barriers using standard MOSFET theory for Schottky contacts improves the accuracy of these models, but not completely. In particular, several aspects of OTFT behavior cannot be explained by direct adaptation of bulk silicon MOSFET theory, including gate-bias-dependent mobility, thermally activated transport, and gradual turn-on characteristics.

3.3.3 Field-effect mobility

Perhaps the most technologically interesting measure of transport in organic semiconductors is the field effect mobility (μ_{FET}), measured using OTFTs. For convenience, the standard extraction of μ_{FET} assumes square law behavior, which is known to be an invalid assumption for OTFTs. Consequently, μ_{FET} is not a good measure of the intrinstic charge mobility in the organic thin-film semiconductor, which is a measure of the velocity of charge carriers under applied electric field (Equation 3.1).

$$\mu = \frac{\mathbf{v}}{\mathbf{E}} \qquad \text{Equation 3.1}$$

μ = charge carrier mobility
v = velocity of charge carrier
E = applied electric field

Rather, μ_{FET} is useful because it provides a metric for quantifying OTFT device performance that is normalized for device dimensions (channel width, channel length, and gate capacitance). Reported values of μ_{FET} are rarely normalized for non-idealities such as series resistance or contact barriers. Therefore, this value is a convolution of various factors including the intrinsic mobility (μ_o) of the semiconductor, the quality of the semiconductor film (grain structure, purity, and ordering, for example), and the quality of the contact between the semiconductor and the source-drain electrodes.

When the threshold voltage (V_T) is known, μ_{FET} can be calculated using Equations 3.2a and 3.1b, which are derived from standard FET square-law equations. However, ambiguities in OTFT turn-on characteristics (see Section 3.3.4) render accurate estimation of V_T difficult.

$$\mu_{FET} = \begin{cases} \dfrac{-I_{DS}}{\frac{W}{L} C_{ins}\left[(V_{GS} - V_T)\, V_{DS} - \frac{V_{DS}^2}{2}\right]} & \textit{Linear regime} \\ \dfrac{I_{DS}}{\frac{W}{L} C_{ins}\,(V_{GS} - V_T)^2} & \textit{Saturation regime} \end{cases}$$

Equation 3.2a

Equation 3.2b

μ_{FET} = field-effect mobility [cm^2/V-s]
I_{DS} = drain-to-source current [A]
W/L = width-to-length ratio of OTFT active area
C_{ins} = capacitance per area of gate dielectric [F/cm^2]
V_{GS} = applied gate bias relative to source bias [V]
V_{DS} = applied drain bias relative to source bias [V]
V_T = device threshold voltage [V]

In order to avoid ambiguity, some groups choose to arbitrarily assume a zero threshold voltage [29]. More commonly, mobility is extracted from the slope of the transfer curve (Equation 3.3), which eliminates the V_T dependency, but assumes that mobility is independent of gate bias.

$$\mu_{FET} = \frac{\frac{\partial I_{DS}}{\partial V_{GS}}}{\left(\frac{W}{L} C_{ins} V_{DS}\right)}$$

Equation 3.3

In OFETs, gate-bias-independent mobility is an invalid assumption since the error introduced is often as large as the calculated mobility itself [26]. This can be seen clearly from the example given in Figure 3.7, where the extracted mobility values change significantly with gate bias.

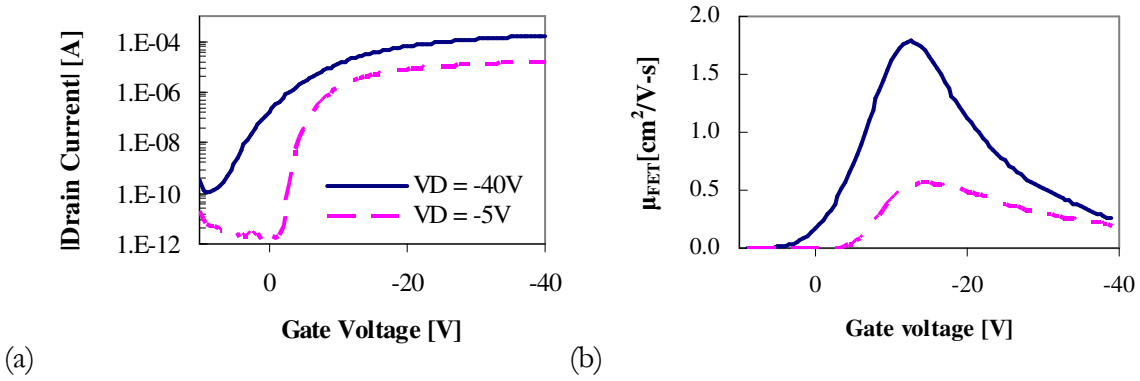

Figure 3.7: Extraction of μ_{FET} from the transfer characteristics of an OTFT.
(a) Linear and saturation transfer characteristics of a substrate-gated, top contact 500μm X 50μm pentacene OTFT with 1250Å of SiO_2 (b) μ_{FET} values extracted using Equation 3.3.

The increase in μ_{FET} with increasing negative gate bias seen here is regularly observed in OTFTs, and any charge transport model for OTFTs is expected to account for gate-potential-activated mobility. A more detailed discussion of charge transport models for OTFTs can be found in Section 8.1. At highly negative gate biases in Figure 3.7b, μ_{FET} reverses directions, and begins to decrease. This affect is not always observed, and occurs at relatively high current levels. It is due to the increasing dominance of series resistance at high drain currents, which results in smaller extracted μ_{FET}. In practice, the maximum value of the curves in Figure 3.7b is the value that is reported as μ_{FET}. Typically only the saturation value is reported (μ_{FETsat}), but μ_{FETlin} is also useful, because discrepancies between the two are a good indicator of series resistance.

The performance of OTFTs, gauged predominantly by μ_{FET}, is comparable to that of amorphous silicon TFTs, especially amorphous silicon TFTs processed within the temperature

range allowable for low-cost, flexible substrates (<200ºC). μ_{FET} values as high as 5 cm^2/V-s have been reported for top contact, silicon substrate-gated, evaporated pentacene TFTs [30], though these numbers have not yet been matched or even approached in OTFTs with the patterned gates necessary for use in circuits. The use of low cost fabrication methods such as printing and low cost substrates such as plastic further degrades performance. In most electronic devices, both organic and inorganic, μ_{FET} is an important metric because it is directly related to the performance of a transistor in nearly all its forms of application. These include the raw amount of current a device can drive at a given voltage supply, the speed at which digital circuits can operate, and the amount of gain a device can provide in analog circuits. Sensors are an exception to this generalization. Relevant performance metrics for gas sensors include sensitivity, discriminatory power, and stability, none of which are closely related to μ_{FET}. Still, increased μ_{FET} can be an advantage for sensors if the sensitivity of a system is limited by the signal-to-noise ratio. This is especially true if the dominant source of noise is extrinsic to the sensor devices, a situation which is quite likely if signal processing is implemented using OTFT circuitry.

3.3.4 Turn-on characteristics

The transition from a non-conductive to conductive channel involves a build-up of mobile charge carriers as gate bias potential is increased. The channel conductivity increases with the charge carrier concentration, as the filling of traps and screening effects help to expedite charge transport. This transition region is known as the subthreshold region; it begins at the onset voltage (V_{on}), the gate potential at which exponential increase of drain current begins, and ends at the threshold voltage (V_T), the gate potential where the channel is considered "on."

In an ideal device, V_{on} is determined by C_{ins}, the doping level within the semiconductor, the band structures of the semiconductor and gate electrode, and the amount of fixed charge in the gate dielectric and semiconductor. In real devices, contact effects between the semiconductor and source and drain electrodes also play a large role in determining V_{on}. Any phenomenon that shifts V_{on} should shift V_T by an equal amount. In addition, traps in the gate dielectric or semiconductor which charge and discharge within the range of operation of the device can shift V_T without shifting V_{on}. In an ideal device, the subthreshold region is very steep, and the separation between V_T and V_{on} is small, typically less than one volt. Organic devices, however, tend to have an extended subthreshold region that usually extends over a significant portion of the range of operation.

In devices with low off-currents, V_{on} can usually be readily identified with reasonable precision by inspection of a semi-log plot of a device's transfer characteristics. V_T, on the other hand presents more of a challenge. In inorganic semiconductors, V_T is clearly defined as the point at which the channel has been completely "inverted," that is, when the concentration of inversion charge in the channel equals the equilibrium majority charge carrier concentration in the bulk. The meaning of V_T in organic semiconductors does not have such a crisp conceptualization. Currently, the most commonly used definition for the V_T of an OTFT is derived from the ideal square law model. V_T is extracted either from Equation 3.2a, by extrapolating the linear portion of the I_{DS} vs. V_{GS} curve to $I_{DS}=0$ and setting that value to $V_T + V_{DS}/2$, or from Equation 3.2b, by plotting the square root of I_{DS} vs. V_{GS} and extrapolating the V_G-intercept from the linear (high V_G) portion of the curve. V_{on} extraction and both methods for V_T extraction are illustrated in Figure 3.8.

Both methods for V_T extraction assume a region of square-law behavior (a linear region in the former case, and a quadratic region in the latter) exists in the transfer curves, which is often not the case. Rather, gate-bias dependent mobility, extended subthreshold regions, contact resistance effects, and a host of other non-idealities often mean that the V_T extraction will involve trying to extrapolate a line out of data points that obviously do not lie in a straight line. This is not surprising, as this V_T extraction method assumes ideal square-law behavior, an assumption that does not hold for OTFTs. As a result, interpretation and use of this parameter involves significant ambiguities.

For example, Figure 3.8 shows significant separation between V_T and V_{on}, and subthreshold behavior which extends over a 5 V range in linear operation and a 10 V range in saturation. The traditional explanation for this extended turn-on behavior invokes the high density of traps present in organic materials [31]. As in inorganic FETs, interface trap states can degrade subthreshold slope by gradually shifting the effective V_T as traps are filled. While a fixed interface charge will tend to shift both V_{on} and V_T in the same direction, and not affect subthreshold slope, a steep, shallow distribution of traps near the valence band will predominantly affect the V_T. Conversely, a wider, deeper trap distribution will predominately affect V_{on}. In both cases, donor-type traps will cause a shift in the negative direction, and acceptor-type traps will cause a positive shift. [32].

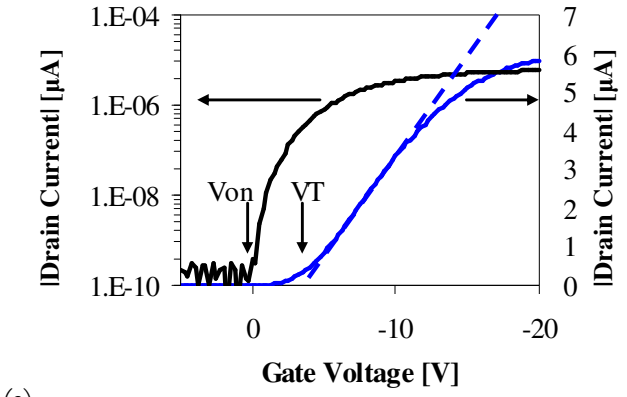

(a)

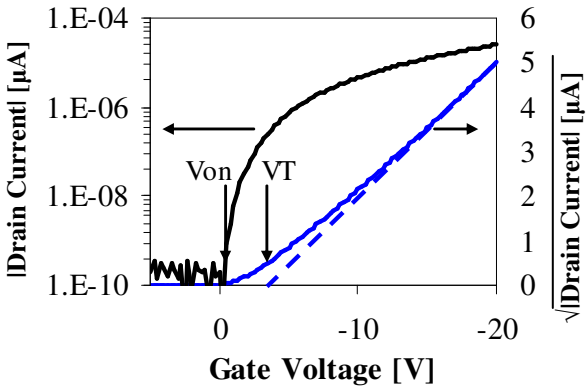

(b)

Figure 3.8: V_T extraction using ideal square law model. Extraction from OTFT transfer characteristics in (a) linear (V_{DS}=-5V) and (b) saturation (V_{DS}=-20V) operating regimes. Data is from the same OTFT as Figure 3.6.

An alternate explanation for the extended subthreshold region is that charge mobility is gate-bias dependent. If charge mobility is assumed, as it often is, to have a power-law dependence on V_{GS} (see Section 8.1) then OTFTs are no longer square-law devices, and the use of square-law equations to extract a number for V_T will result in an artificially enlarged subthreshold region. It should be noted that the exponential and Gaussian band-tail formalisms often used to model the trap distributions discussed in the previous paragraph also predict a V_{GS}-dependent mobility [26][32][33].

Because of this ambiguity, the use of V_T in this work was restricted largely to comparative tasks, as a quantitative measure for shifts in the transfer characteristics of a device. When two transfer curves look identical (or similar, at least) except for a constant shift along the V_{GS} axis, V_T is a convenient metric for this shift that can be easily extracted. An example of an unambiguous V_T shift caused by bias stress is illustrated in Figure 3.9 (see section 4.1.1 for more information about bias stress).

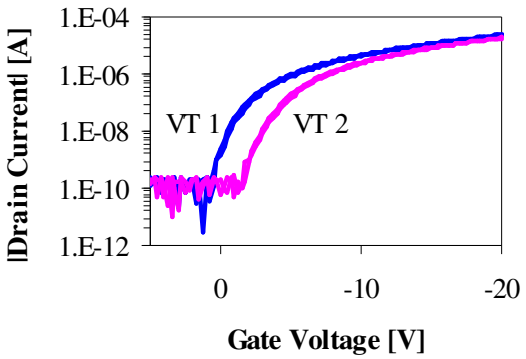

Figure 3.9: The effect of a V_T shift an OTFT transfer curve. I-V characteristics are measured on a substrate-gated, bottom contact 500μm X 20μm pentacene OTFT with 950Å of SiO_2, before and after 15 minutes of bias stress.

The ability to control V_T and achieve device-to-device and run-to-run consistency in OTFT V_T's is important for both digital and analog logic. In silicon technology, V_T can be tuned precisely by adjusting doping levels. Unfortunately, no equivalent methodology exists for organic semiconductors, where V_T is determined primarily by the relative work-functions of the gate, source/drain contacts, and organic semiconductor, as well as the fixed charge and trap distributions in the organic semiconductor. None of these parameters offer fine adjustment, and worse, random and run-to-run variations in the fixed charge and trap distributions in the organic semiconductor can be difficult to suppress. In addition, OTFTs

exhibit strong, reversible V_T shifts during operation (see section 4.1.1), making the V_T of a device dependent on its operational history. Thus, V_T control is an important hurdle to commercialization of OTFTs.

3.4 Applications of OTFTs

Currently, OTFTs are not yet used in any commercial applications, but two applications are being heavily pursued for commercialization. The first is as pixel drivers for flexible active matrix displays. The second is for the digital and analog logic needed for radio frequency identification tags (RFID). Though the needs of these two applications are different from those of sensor applications, many of the challenges faced in using OTFTs are similar. In particular, environmental and operational stability are a major concern in all cases.

3.4.1 Displays

In a display, individual pixels are laid out in a grid along metal row and column selector lines. Each pixel resides at the crossing point of a row and column selector. In passive addressing, a voltage is applied across one row and one column, and the brunt of this voltage is dropped across the pixel at their intersection, activating it. However, large capacitances, parasitic voltage drops and leakage currents along the selector lines degrade refresh speed and display contrast, making it advantageous to include active transistor elements in each pixel. These active elements amplify the signals from the selector lines, enabling larger displays with faster refresh rates and better contrast. In flexible displays, these active elements can be made of either amorphous silicon TFTs or OTFTs. At the low processing temperatures necessary for flexible substrates (typically <200ºC), the current drive and amplification power of these two technologies is comparable.

Amorphous silicon is already widely used in the display industry, and is thus the entrenched technology. OTFTs can be potentially much cheaper, since amorphous silicon deposition techniques are less compatible with low cost roll-to-roll fabrication. An OTFT-OLED pairing would be especially attractive due the similarities in materials and fabrication requirements between the two technologies. However, it is still a challenge for OTFTs to supply the high current densities required by OLEDs, and improvements in μ_{FET} are necessary before OTFTs can be used to drive OLED displays. For systems with lower current drive requirements, such as liquid crystal, electrochromic, or electrophoretic displays, OTFTs with adequate current drive are already available, though higher μ_{FET} would increase the maximum display size and refresh rate of the system.

Aside from μ_{FET} enhancement, the main hurdles for use of OTFTs in displays concern I_{on}/I_{off} and stability issues. When a pixel is activated, all devices along the same row will experience the same applied V_{DS}. While I_{on} flows in the activated device, I_{off} flows in all other devices along the row, and the contrast in the display is thus limited by I_{on}/I_{off}.. To fabricate devices with consistently good I_{on}/I_{off}, a steep subthreshold region is desirable. Unfortunately high trap densities and gradual band edge characteristics result in slow turn-on characteristics, meaning that higher supply voltages must be used to achieve adequate I_{on}/I_{off}. Good I_{on}/I_{off} also requires that V_T variation be well-controlled, especially in OTFTs with V_T's close to 0V. However, as discussed in Section 3.3.4, V_T control is a difficult undertaking. In certain monochrome systems such as liquid crystal displays, OTFT V_T variation also limits the number of grayscale levels that can be resolved in each pixel.

Maintenance of adequate I_{on}/I_{off} throughout the operational lifetime is also a concern. Generally, oxygen and humidity tend to simultaneously increase doping levels and decrease μ_o

in organic semiconductors. Increased doping results in enhanced I_{off}, while degraded μ_o reduces I_{on}. A similar problem with environmental stability in OLEDs was addressed through the use of protective encapsulation layers, and this is currently the dominant approach to stability in OTFTs as well. Efforts to improve environmental and operational stability through materials engineering are also on-going, and are discussed in Section 4.5.1.

3.4.2 Radio frequency tag identification (RFID)

The term RFID refers to a system in which passive "RFID" tags, when activated by a nearby reader, can be triggered to broadcast identifying information that is then collected by the reader. This is the technology used by key cards and automatic toll-collectors. Because RFID tags are powered remotely by the reader, the tags themselves require no power source. In fact, the required components—inductors, diodes, capacitors, and transistors—are all elements that could conceivably be fabricated on low-cost substrates with an ultra-low-cost roll-to-roll manufacturing process based on organic electronics. At a cost of a few pennies per tag, the potential market for RFID as a replacement for barcodes in supermarkets would be huge, and the use of OTFTs for ultra-low-cost RFID tags has thus been the focus of intense commercial and academic research activity in recent years.

While roll-to-roll manufacturing is generally accepted as the most direct route to ultra-low-cost RFID tags, it is unclear whether organic electronics or some other printable technology will be the best solution. For OTFTs to be useful in RFID tags, a number of challenges remain to be addressed. Currently, the main challenge is arguably improving μ_{FET}. By governmental regulation, RFID must operate within certain frequency ranges, meaning that the electronics in an RFID tag must operate at a minimum speed. In addition, low-cost fabrication methods can

offer only a certain level of precision in their patterning and alignment of different layers. These two considerations, when taken together, present a minimum constraint on μ_{FET}, one which is currently still higher than what has been demonstrated in OTFTs fabricated on low-cost substrates with methods compatible with roll-to-roll manufacturing.

Another major challenge in using OTFTs for RFID is environmental and operational stability. As in displays, performance degradation due to exposure to ambient conditions must be addressed either with encapsulation or materials engineering. Because of the extremely low cost margins predicted for this application, materials engineering is the strongly preferred solution. See Section 4.5.1 for a discussion of strategies for modifying organic semiconductors to improve air stability.

3.5 References

[23] E. Riande and R. Díaz-Calleja, Electrical Properties of Polymers, Marcel Dekker, Inc.: New York, NY, 2004.

[24] W. Brütting (Ed.), Physics of Organic Semiconductors, Wiley-VCH: Winheim, Germany, 2005.

[25] J.-P. Farges (Ed.), Organic Conductors Fundamentals and Applications, Marcel Dekker, Inc.: New York, NY, 1994.

[26] Y. Roichman, Y. Preezant, and N. Tessler, "Analysis and modeling of organic devices," Phys. Stat. Sol., 201, 1246, 2004.

[27] G. Horowitz, "Organic thin film transistors: From theory to real devices," J. Mater. Res., 19, 1946, 2004.

[28] R. S. Muller, T. I. Kamins, and M. Chan, Device Electronics for Integrated Circuits, John Wiley & Sons: New York, NY, 2003

[29] A. Salleo, T.W. Chen, and A. R. Völkel, "Intrinsic hole mobility and trapping in a regioregular poly(thiophene)," Phys. Rev. B, vol. 70, 115311, 2004.

[30] T.W. Kelley, D.V. Muyres, P.F. Baude, T.P. Smith, and T.D. Jones, "High Performance Organic Thin Film Transistors," Mat. Res. Soc. Symp. Proc. Vol. 771, L6.5.1, 2003.

[31] T. Lindner, G. Paasch, and S. Scheinert, "Influence of distributed trap states on the characteristics of top and bottom contact organic field-effect transistors," J. Mater. Res., 19, 2014, 2004.

[32] A. R. Völkel, R. A. Street, and D. Knipp, "Carrier transport and density of state distributions in pentacene transistors," Phys. Rev. B, 66, 195336, 2002.

[33] Y. Roichman and N. Tessler, "Generalized Einstein relation for disordered semiconductors—implications for device performance," Appl. Phys. Lett., 80, 1948, 2002.

Chapter 4: LIFETIME AND RELIABILITY

Stability is one of the greatest challenges that must be addressed for OTFTs to become a commercially viable technology. The chemically sensitive carbon backbones of organic materials interact readily with both oxygen and water vapor, causing both immediate and gradual shifts in electrical characteristics. For some applications, encapsulation of OTFTs is a feasible approach to avoiding degradation by air, but this solution has but a limited potential for gas sensors, since encapsulation would inhibit or prevent interaction between the sensitive material and analyte vapors in the ambient.

Furthermore, even if degradation by air can be satisfactorily addressed, shifts during operation due to bias stress effects will still be a concern. Even when used in inert environments, the simple act of operating an OTFT causes shifts in the device characteristics. This type of drift, known as bias stress, can be reduced through careful choice of fabrication method, materials, and operating conditions, but cannot be completely avoided. Consequently, it is important to understand the kinetics behind bias stress.

Sensing applications are potentially more tolerant of device aging, since they rely on signal modulation rather than absolute signal values. As long as a detectable sensor response is retained and that response can be interpreted properly, drain current or switching speed requirements are fairly lax. At the same time, though, drift behavior overlays on top of signal response, and may influence the sensor response itself. Therefore, it is essential that baseline shift in OTFTs be well-characterized.

In this section, the sources of signal drift are discussed, and results from experimental investigations of signal drift are presented. Baseline drift in different materials is compared, and effect of active layer thickness is investigated for pentacene OTFTs. Finally, strategies for dealing with signal drift are discussed.

4.1 Causes of signal drift

Drift in an OTFT's electrical behavior can be fairly well characterized by cataloguing shifts in its V_T, μ_{FET}, I_{on}, I_{off}, and subthreshold slope. Bias stress effects mainly affect V_T, and are particularly important to study because they are unavoidable. Unintentional environmental doping, usually from water vapor or oxygen, can cause changes in any or all of the device parameters listed above. Finally, physical degradation of the organic semiconductor typically manifests as a drop in μ_{FET}.

4.1.1 Bias stress effect

Even when encapsulated or operated in inert environments, OTFTs exhibit a bias stress effect (BSE) in which the threshold voltage (V_T) shifts under continuous bias. The shift is logarithmic in nature. It begins immediately upon application of bias, and can be observed at time scales of under a second. Upon removal of the bias stress, recovery also begins immediately, in a logarithmic fashion. It is not an exclusively short-term effect, however. While the rate of shift decelerates over time with continual applied bias, V_T continues to decay indefinitely, and even a relatively short-term removal of the bias prompts a strong recovery and then a period of accelerated decay upon reapplication of the bias. Examples of BSE dynamics are illustrated in Figure 4.1.

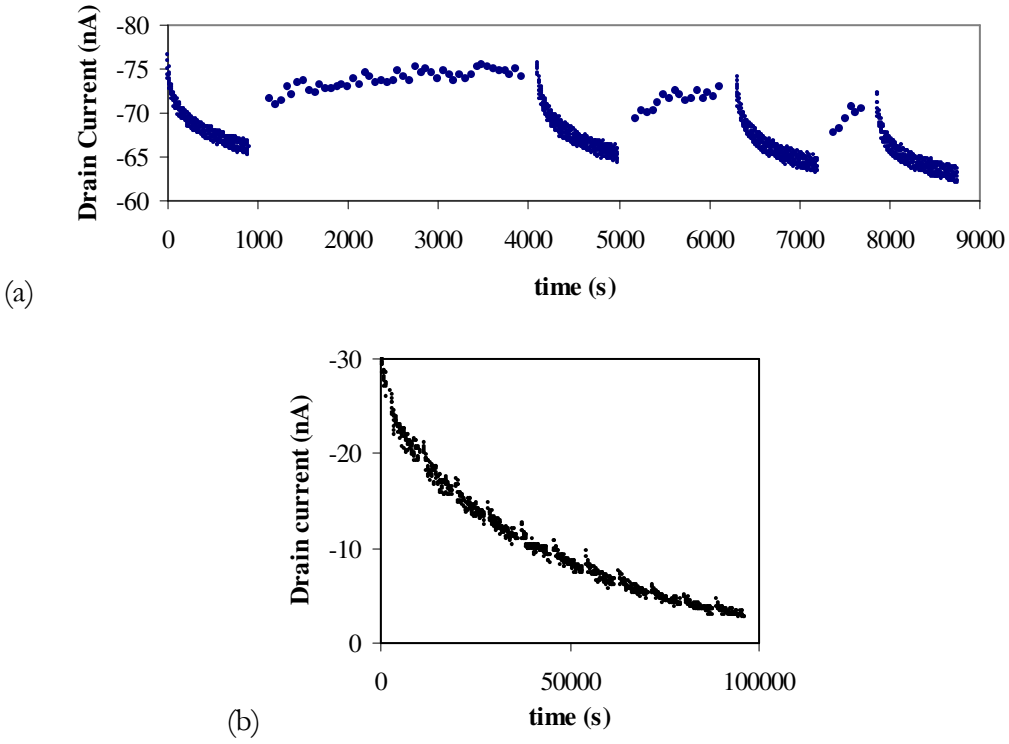

Figure 4.1: Examples of BSE kinetics observed in OTFTs. Data is taken from a substrate-gated, bottom-contact (a)poly-3-hexylthiophene and (b)α-sexithiophene OTFTs with W/L=500μm/20μm. Bias (V_{GS}=V_{DS}=-20V) was alternately applied and released to illustrate kinetics of current decay and recovery.

Such bias instability has been observed in OTFTs with a wide range of different active materials, including pentacene [34]-[36], various thiophene derivatives [36]-[38], polyfluorene [39], polythienylene vinylene [40], and polyarylamines [41]. Recently, some groups have achieved enhanced stability through processing steps [34] or material engineering [41], but BSE remains a significant issue to be addressed before organic electronics can become commercially viable.

A few mechanisms have been proposed to explain this instability, including defect generation [37], the formation of bound hole pairs[42][43], charge trapping [39][44], and migration of

mobile ions[35][38]. A number of groups have shown that BSE is reversible after long relaxation [40], and that this reversibility can be accelerated with opposite polarity biasing [42] or exposure to light [39], suggesting that BSE is an electronic phenomenon, rather than a physical degradation or a chemical interaction. Charge trapped near the dielectric-semiconductor interface is usually believed to be responsible for V_T shifts in the direction of applied bias [34][39][44], though in some cases, mobile ions in the dielectric or active material [35][38]have been reported to have a dominant effect. Due to weak intermolecular interactions, grain boundaries, imperfect ordering, interface states, and chemical impurities, organic semiconductors are known to contain a high density of traps. Shallow traps with short time constants are probably involved in charge transport [45][46]. BSE, which causes a shift in V_T but not μ_{FET}, is therefore often believed to be caused by deep traps with long discharge time constants, since shallow traps would affect μ_{FET}. Such traps have been observed in pentacene by several groups [47][48].

Generally, however, neither trapping nor BSE in OTFTs is well-understood, and both can vary significantly depending on the active and dielectric materials used [34][36], device processing conditions [34], biasing conditions[35][42], and operating temperature[42]. Partly due to this sensitivity to many different variables, not many systematic studies have been published concerning the effect of processing conditions on OTFT bias stability.

4.1.2 Sensor response to oxygen and humidity

For non-sensor applications, the chemical sensitivity of organic semiconductors is not a desirable property. In particular, the sensor response of OTFTs to varying ambient working conditions can be detrimental to proper functioning, operational stability, and lifetime of

OTFT-based electronics. Due to these concerns, the OTFT sensor response to oxygen and humidity has been studied carefully.

Jurchescu *et al* [51] studied the affect of air exposure on the electrical properties of crystalline pentacene. By monitoring both the mass uptake during exposure and the affect of light on the sensor response, they convincingly deduced that absorbed oxygen introduces holes near the valance band, which increases conductivity, while absorbed water molecules generate defect states which trap mobile charges, lowering μ_{FET}.

In thin-film structures, Li *et al* [52] found that grain boundaries also play an important role in the oxygen and humidity sensor responses, which include degraded μ_{FET} and a positive shift in V_T. Bottom-contact structures, with finer grain structures, exhibited an enhanced sensor response compared to top-contact structures. They postulated three possible mechanisms for the μ_{FET} response: (1) water molecules localize to grain boundaries, where their polar structure causes interactions with charge carriers that reduce carrier mobility; (2) water molecules affect the intermolecular interactions in grain boundaries, causing an increased energy barrier to intergrain transport of charge carriers; or (3) ions dissolved in the absorbed water screen the electric field seen by the channel, resulting in a lower concentration of accumulated mobile carriers.

For polythiophene thin films, Hoshino *et al* [53] found that O_2 acts as a p-type dopant which increased conductivity and decreased μ_{FET}. H_2O produces a similar, but pronouncedly stronger effect, despite the fact that the diffusion of water into polythiophene should be more hindered due to its larger size. In addition, H_2O in polythiophene films interferes with gate control over conduction, resulting in large off-state currents and lack of saturation in the output

characteristics. Hoshina *et al* attributed this behavior to the generation of holes in the film in the vicinity of adsorbed H_2O due to the molecule's large dipole. H_2O is expected to adsorb only at the surface and grain boundaries, and so the holes induced by H_2O provide conduction paths different from the accumulated channel induced by the gate.

4.1.3 Material Degradation

Organic electronic materials are generally more susceptible to physical degradation than their inorganic counterparts. Degradation processes vary widely, and are especially important to consider when organic electronics are to be operated in stressful conditions. Relevant degradation mechanisms include [50]:

1. Thermal. Elevated temperatures can induce or accelerate oxidation or other degradation of chemical structure.

2. Mechanical. The application of force or stress or sheer strain can induce crack propagation or cause scission of polymer chains.

3. Ultrasonic: The application of ultrasonic sound waves is a popular method for cleaning substrates and accelerating dissolution processes. However, the violent vibrations induced by sound waves of certain frequencies can cause polymers chains to split.

4. Hydrolytic: For materials functionalized with water-sensitive groups, chemical degradation can be caused by hydrolytic decomposition. De-esterification, resulting in a break down of the molecule into acids and glycol is a common example.

5. Chemical: Corrosion by aggressive agents such as ozone can attack the basic structural integrity of organic material.

6. Radiation: Organic materials or the impurities that are mixed in with them can absorb photons from sunlight or other sources of energetic radiation. This absorbed power can instigate decomposition reactions or directly cause the splitting of polymer chains.

The material degradation of organic materials by these mechanisms can be a gradual process. For example, organic electronics can be operated at elevated temperatures or in the presence of water vapor or radiation, but their operational lifetimes will be reduced. The ideal operating conditions for organic devices are in inert environments such as nitrogen or argon, in the dark, and at medium temperatures, low enough to avoid thermal degradation, but high enough to support charge conduction. However, if the price tag of organic electronics is lowered enough to support disposable or short-term use applications, decreased lifetime may be an acceptable tradeoff for operating at non-ideal conditions.

4.2 Experimental setup

Substrate-gated, bottom-contact OTFTs were fabricated on n+ silicon substrates. For a dielectric, SiO_2 was thermally grown at 900 °C in the presence of water vapor, and then annealed at 900 °C in N_2 for 20 minutes. To create source and drain contacts, 50 nm thick gold pads, thermally evaporated with a chrome adhesion layer, were patterned onto the SiO_2 using lift-off. Device dimensions were W=500 μm, L=20 μm. On top of these preformed structures, various organic semiconductors were deposited, including pentacene, poly-3-hexylthiophene (P3HT), and several air-stabilized polythiophene derivatives. The air-stable polymer poly(didodecyl-2,2'-bithiophene-4,4'dicarboxylate-co-2,2'-bithiophene) (P1) has ester

functional groups attached to alternating thiophene rings along the polymer chain. Details of molecular chemistry and synthesis as well as electrical characteristics are provided in ref [54]. Two other air-stable commercially produced polythiophene derivatives were used as well [55],[56]. In these polymers, a fraction of the thiophene rings were replaced with either thieno[2,3-b]thiophene (M1) or selenophene (M2) groups.

Pentacene was obtained commercially, zone purified, and stored at high vacuum before use. It was deposited using thermal evaporation at high vacuum (~10^{-7} torr) at 1 nm/minute onto the preformed substrates, which were held at 70ºC. Film thickness was measured using a quartz crystal monitor, whose readings were calibrated against atomic force microscopy measurements of pentacene film thicknesses. The resulting pentacene OTFTs had saturation mobilities (μ_{FETsat}) ranging from 0.05~0.5 cm^2/V-s, starting turn-on voltages (V_{on}) close to 0V, and I_{on}/I_{off} ratios > 10^3, without active layer isolation.

All other materials were solution-processed and deposited using spin-casting. P3HT was dissolved in chloroform at 0.8 wt%, P1 was dissolved in chloroform at a concentration of 4 mg/mL, and M1 and M2 were dissolved in either chloroform or dichlorobenzene for solution deposition. Mild heating and sonication were used to accelerate dissolution, and resulting solutions were passed through a 0.45 μm filter and spun-cast onto the preformed structures an N_2 environment. P3HT was spun at 6000 rpm, P1 at 4500 rpm, and M1 and M2 at 3000 rpm. Before spinning, the substrates were dehydrated by heating for 2 minutes at 120ºC, and then cooled to room temperature before spinning. After spinning, samples were annealed at 120ºC for 20 minutes in N_2.

All electrical measurements were taken at room temperature, in the dark, in nitrogen. Up to four devices could be probed at once, and so, where possible, devices to be compared were measured simultaneously. Whenever possible, drain current (I_D) was used to monitor BSE kinetics because it can be measured directly and continuously during bias stress and requires no extraction. In this work, the term on-current (I_{on}) is used to refer to the I_D measured at $V_{DS}=V_{GS}=V_{DD}=-20V$. However, measuring I_{on} alone leaves the exact nature of degradation under bias stress unclear. By continuously sweeping the gate bias (V_G) through a short range of voltages (-18 V to -20 V) while holding the drain bias (V_D) constant and monitoring I_D, the time evolution of μ_{FETsat} and V_T could be extracted as well, with μ_{FETsat} calculated from the linear slope of I_D vs. V_G (Equation 3.3) and V_T extrapolated from the x-intercept of the $\sqrt{I_D}$ vs. V_G (Figure 3.8b). Bias stress measurements obtained in this way are less repeatable from measurement to measurement because the rate of parameter analyzer sweeps varies depending on noise and signal levels, but they are useful for observing qualitative trends. The bias stress degradation of a representative pentacene OTFT, depicted in Figure 4.2a, indicates that the decrease in I_{on} is caused predominately by a V_T shift, and that charge mobility remains relatively unchanged. This is consistent with the observations of other groups [37][40][43], and allows the analysis of bias stress degradation of I_{on} solely in terms of V_T shifts.

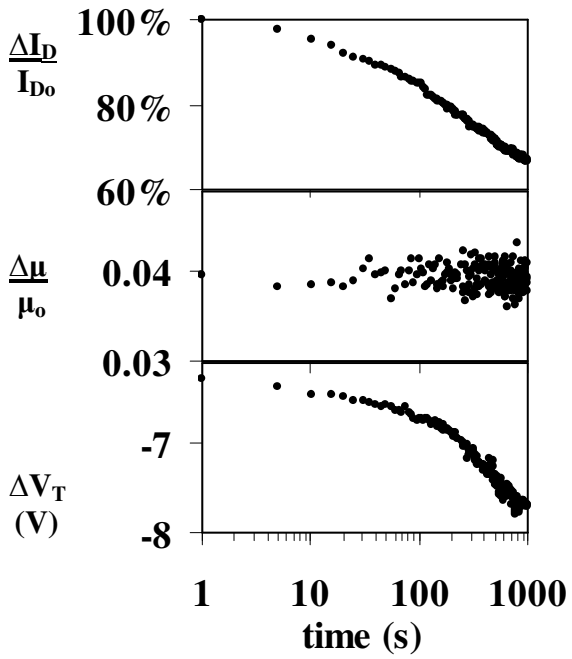

Figure 4.2: Evolution of device characteristics under bias stress.
Data is measured in continuous short sweeps (V_G=-18V to -20V, V_D=-20V), allowing I_{DS}, mobility, and V_T to be simultaneously monitored. (30 nm pentacene, 90 nm oxide).

4.3 Results

The effects of both active layer material and active layer thickness on signal drift are investigated, with an emphasis on bias stress effect. Qualitatively different baseline drift behavior is seen in the various materials, indicating a difference in underlying mechanisms responsible for signal drift. Active layer thickness is observed to have a strong quantitative affect on the rate of signal drift in pentacene OTFTs, which is attributed to a volume charge trapping bias stress effect.

4.3.1 Active layer material dependence

The baseline drift in pentacene, P3HT, P1, M1, and M2, is plotted in Figure 4.3. The on-current decay characteristics of these five materials exhibit a remarkably wide range of behavior, from superlogarithmic (pentacene, P1, and M1) to logarithmic (M2) to sublogarithmic (P3HT). Notably, the initial decay rate (during the first 10 seconds of operation) is not a good predictor of the decay rate after several minutes of operation (t>100s), in absolute or relative terms. For example, though the I_{on} of P3HT decays more rapidly than all of the other materials at first, its long-term decay rate is slower than all but M2. This behavior is consistent with previous reports that different processes may dominate in the short term versus long term decay of on-current in OTFTs.

When operating in air rather than in nitrogen, both oxidative doping and oxidative degradation are of concern. Oxidation of the active layer of an OTFT, accelerated by the application of large fields to the material while in the presence of oxygen, degrades the charge mobility and thus the on-current of the OTFT. Oxidative doping, on the other hand tends to increase on-current, but may also drastically lower I_{on}/I_{off} ratio because increased dopants in the body of the active layer make it more difficult for the gate to fully control the entire thickness of the active material, and leakage through the parasitic bulk depletion device increases. From Figure 4.3b, it is clear that oxidative degradation is the dominant effect for all materials when operation is shifted from an inert nitrogen environment to ambient conditions, since the decay rate becomes steeper for all materials.

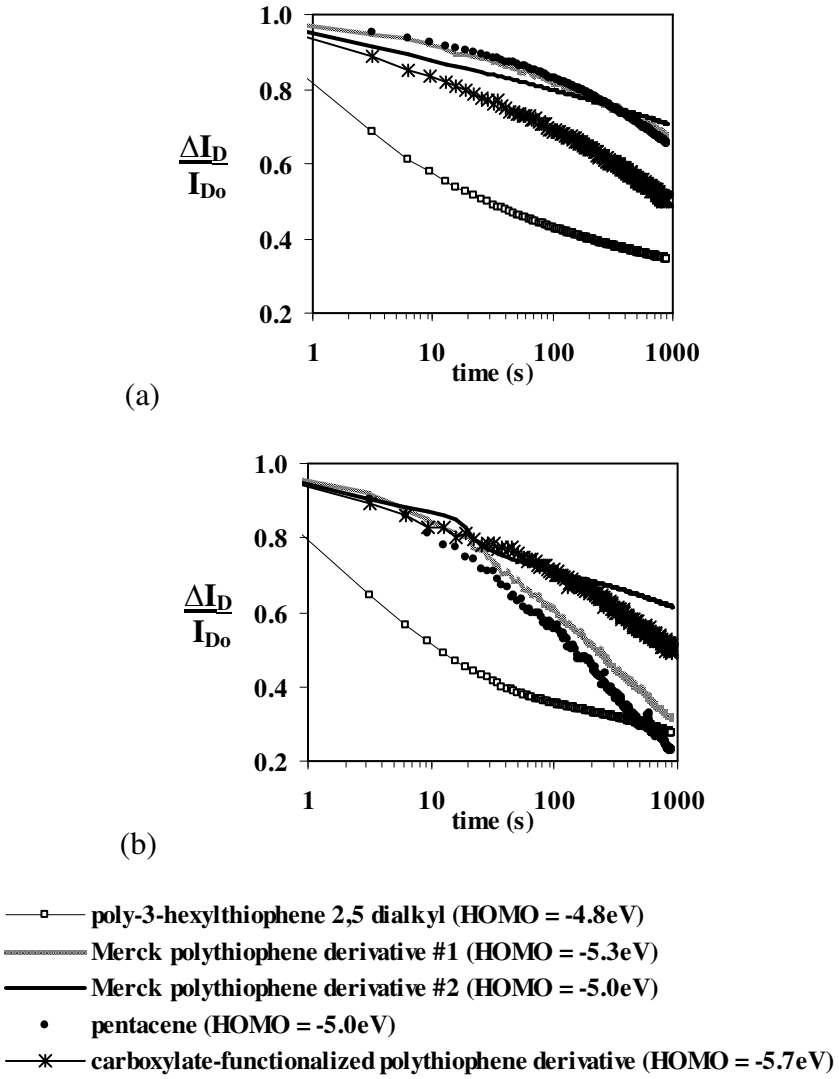

Figure 4.3: Baseline drift in OTFTs with different active materials during operation in (a) nitrogen and (b) air.

4.3.2 Active layer thickness dependence

When studying how processing parameters affect BSE, it is important to establish the extent to which bias stress measurements taken from different devices can be compared. This is a particularly pertinent question as, despite nominally identical processing, the performance of

transistors fabricated in different runs often show significant scatter. The time evolution of I_{on} in four different pentacene OTFTs as the drain and gate are held at -20 V is plotted in Figure 4.4.

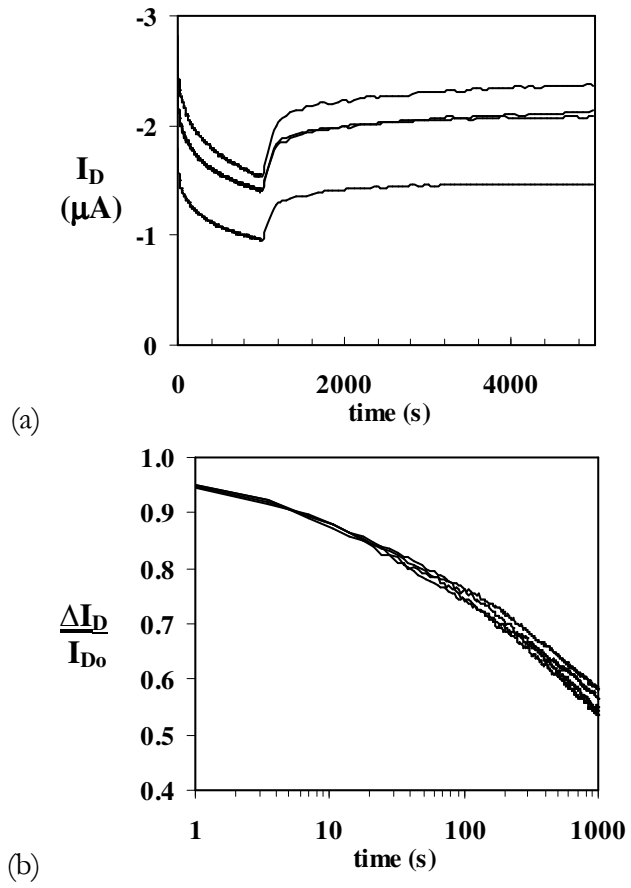

Figure 4.4: Repeatability of bias stress measurements. BSE (V_G=V_D=-20V, t<1000 s) and recovery (no applied bias, in the dark, t>1000 s) of four different pentacene devices. (a) Devices show a significant scatter in starting performance values, but the normalized current (b) reveals a consistent degradation pattern. (20 nm pentacene, 60 nm oxide).

Despite a relatively large scatter in initial current levels, the degradation kinetics for all four devices are similar once normalized to starting values. This repeatability was confirmed for several different processing conditions, including different pentacene thicknesses, dielectric

thicknesses, and surface treatments. The width of the distribution in Figure 4.4b qualitatively suggests the extent to which observed differences in BSE kinetics can be attributed to processing differences rather than device scatter or uncontrolled variables. Figure 4.4a also shows the recovery of the four devices after bias stress. This recovery behavior is consistent with observations of other groups and with the assumption that BSE mechanisms are nondestructive and electrical in nature [40].

After establishing comparability of data taken from different devices, the measurement illustrated in Figure 4.4 was repeated for devices in which active layer thickness and oxide thicknesses were varied. The time evolution under bias of I_{on} in four devices with pentacene thicknesses of 10 nm, 20 nm, 40 nm, and 80 nm, and otherwise nominally identical processing, is plotted in Figure 4.5. Dots represent experimental data, while the superimposed solid lines are curves fit using the stretched hyperbola formalism that will be discussed later in this section [37]. Superlogarithmic decay is observed for all devices, but the rate of decay increases monotonically with active layer thickness. After 1000 s of continuous bias at $V_G=V_D=-20V$, the I_{on} in the device with 80 nm thick pentacene drops by 60%, while in the device with 10 nm thick pentacene, I_{on} only drops by 35%. As in Figure 4.4, this current decay was reversed upon removal of bias. Transfer characteristics for these four devices before and after bias stress are given in Figure 4.6 and Figure 4.7 respectively.

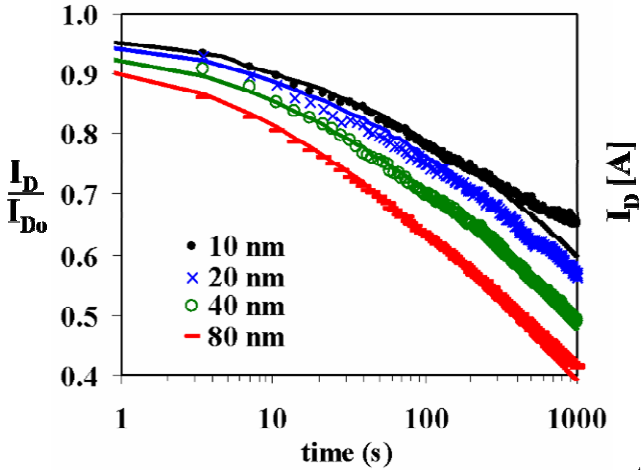

Figure 4.5: Effect of varying pentacene thickness on bias stress effect in OTFTs.
(a) Devices with thicker pentacene exhibit accelerated BSE (VG=VD=-20V, 90 nm oxide). Individual points represent experimental data, while superimposed lines are simulated using the bandtail defect generation model, with different trap creation activation energies for each thickness [37].

Before stressing, all four devices have similar V_{on} and V_T, suggesting similar initial doping levels, trap densities, and fixed charge distributions. I_{on}, on the other hand, varies by over an order of magnitude, indicating differing μ_{FET} values for the different thicknesses. It should be noted, however, that μ_{FET} and I_{on} do not vary monotonically with active layer thickness, while the rate of bias stress degradation does. Device stability is thus correlated best to pentacene thickness, rather than I_{on} or initial charge distribution. This qualitative trend was observed in multiple runs and remained consistent even when oxide thickness was varied.

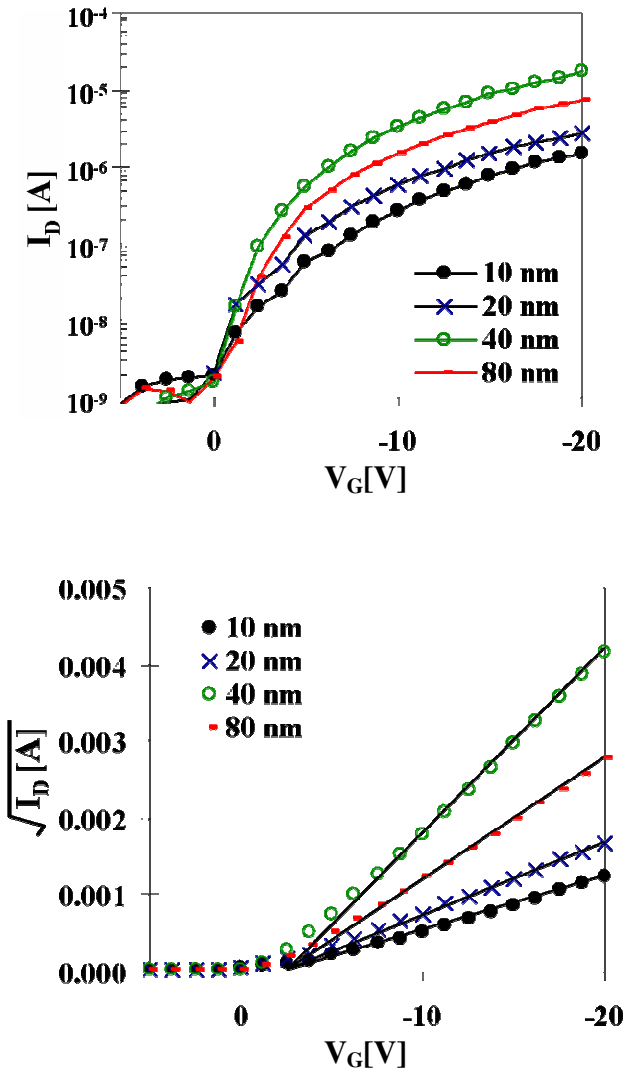

Figure 4.6: Device transfer characteristics of OTFTs from Figure 4.5 before bias stress.
The four devices have the similar starting V_T and V_{on} values, but μ_{FETsat} and I_{on} span a range of over an order of magnitude, and do not vary monotonically with pentacene thickness.

Extracted values of μ_{FETsat} from the device transfer curves after stressing (Figure 4.7) are within 5% of the original μ_{FETsat} values (Figure 4.6), indicating that the observed drop in I_D in the devices is due predominately to V_T shifts, an observation that is consistent with a bias stress degradation mechanism.

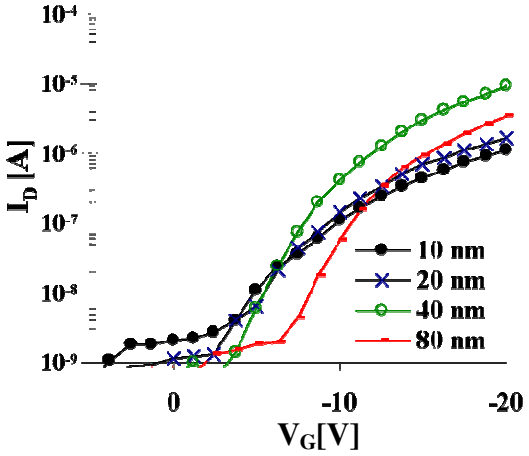

Figure 4.7: Device transfer characteristics of OTFTs from Figure 4.5 after 1000s of bias stress.
Comparison of these curves to their corresponding curves before stressing (Figure 4.6) reveals that μ_{FETsat} does not shift during the stressing, indicating that the observed drops in I_D are due to V_T shifts. Furthermore, the accelerated shift of the devices with thicker pentacene correlates to neither I_D nor original V_{on} or V_T.

Since the BSE observed here is not correlated with current, it is reasonable to guess that the responsible processes are field-activated. To investigate the field dependence of BSE, a single pentacene OTFT was repeatedly stressed at different gate and drain bias conditions. Between each stress event, the device was allowed to recover to within 99% of its original I_{on} (>5000 s) before being subject to the next set of stress conditions. The rate of bias stress degradation at different V_{DS} values was similar (Figure 4.8a), but increasing V_{GS} resulted in accelerated degradation (Figure 4.8b). This is consistent with both a field-dependent and carrier density-dependent mechanism for BSE.

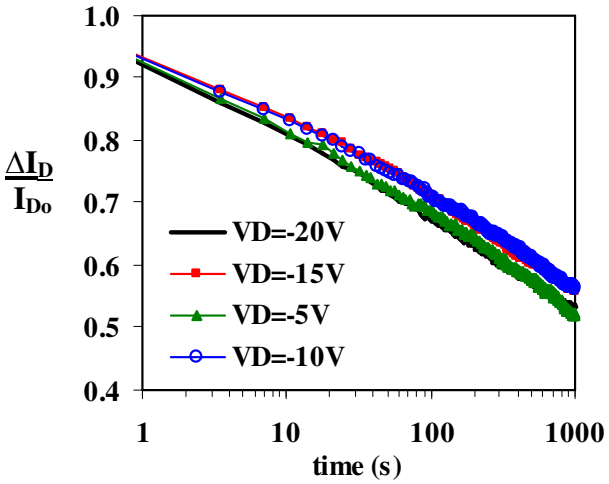

(a)

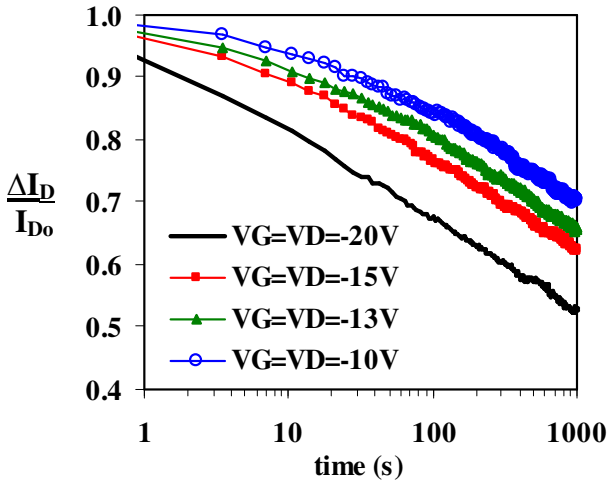

(b)

Figure 4.8: Effect of bias conditions on bias stress effect. (a) Varying V_D as V_G is held constant at -20V has little effect on the BSE, while (b) varying V_G and V_D together significantly modulates BSE. Curves were taken from a single device, with measurements separated by long (>5000 s) recovery times (20 nm pentacene, 60 nm oxide).

The observed thickness dependence of BSE is difficult to explain using the bipolaron mechanism, as the concentration of mobile charge carriers in an accumulated OTFT channel is unlikely to increase with increasing pentacene thickness under the same biasing conditions.

Rather, the most direct interpretation of this result is a volume trapping effect, in which charge trapping and trap creation under bias stress occur not only within the channel, but throughout the entire semiconductor film. As the volume of active material increases, the amount of initial traps and traps created during bias stress both increase proportionally. The magnitude of V_T shift caused by such trapped charge is given by Equation 4.1,

$$\Delta V_T = \int_0^{x_d} \left(\frac{1}{C_{ox}} + \frac{x}{\varepsilon_{pent}\varepsilon_o} \right) \rho(x) dx \qquad \text{Equation 4.1}$$

x_d = width of band bending
C_{ox} = gate dielectric capacitance
$\varrho(x)$ = distribution of trapped charge within the active layer
ε_{pent} =relative dielectric constant of pentacene

Charge must be integrated over the entire region of band-bending within the active layer, starting from the dielectric interface (x=0) and ending at the depth x_d at which the potential is no longer influenced by the gate bias.

T. Li *et al* [57] have reported results from two-dimensional electrostatic simulations of pentacene OTFTs, including a bottom contact device very similar to that used in the present study: gold contacts, a 100 nm thick silicon dioxide dielectric, and a 50 nm thick pentacene film. In their simulations, Li *et al* found that valence energy band profile of the pentacene layer showed significant curvature near the dielectric interface, where the channel charge is accumulated, and that this region of band bending extended throughout the entire semiconductor film. Moreover, surface potential profiling techniques have revealed that gate bias affects the surface potential of the active layer in an OTFT even in the presence of an accumulated channel [58]-[60], confirming again that band bending extends through the entire

film, and that bulk trapped charge in an OTFT can contribute to V_T. Also, the field outside the accumulation layer in the bulk of the pentacene does not go to zero. This field can trigger trap creation. Because of the low concentration of free carriers outside of the accumulation channel, however, the creation of traps throughout the bulk of the active layer requires a mechanism in which trap creation is triggered by applied electric field, rather than high carrier concentration. Therefore, the volume trapping effect proposed here is not consistent with the bipolaron theory proposed by Street *et al* [42][43].

As mentioned earlier, the prevailing belief is that BSE is caused by charges trapped at the dielectric interface, rather than throughout the volume of the active layer [34][39][44]. An alternative explanation of the results in Figure 4.5 which is consistent with this theory of trapped interface charge is that the activation energy for creation of traps within the channel decreases with increased pentacene thickness. In this case, the set of curves in Figure 4.5 may be interpreted with the stretched-hyperbola formalism, as proposed by Gomes *et al* [37] for OTFTs. This theory was originally intended to describe BSE in amorphous silicon TFTs due to the creation of trap states [61]. The stability of a material is quantified by the mean activation energy for trap creation (E_A). Though the equations governing threshold shift under this formalism has too many degrees of freedom to provide quantitative insight, it is interesting to note that all four curves in Figure 4.5 can be fit reasonably well with the same equation by varying only E_A. BSE is simulated using the method outlined in ref [37], with the following parameter values: $\nu=10^5$ Hz, $\alpha=1.5$, $k_BT_o=70$ meV, and $E_A= 0.565$, 0.555, 0.535, 0.515 eV for pentacene thicknesses of 10 nm, 20 nm, 40 nm, and 80 nm respectively. Results are plotted as solid lines in Figure 4.5. A smaller E_A (corresponding to lower stability) is required for a good fit as pentacene thickness is increased. Possible mechanisms for a decrease of E_A with

increased pentacene thickness include a build-up of stress within the active layer, an increase in trap capture cross-section, as well as changes in film morphology, grain boundaries, or microstructure. Some studies have claimed a dependence of mobility on thickness in OTFTs, though it is unclear whether these results reflect a true modulation of the intrinsic mobility within the film or just the influence of external factors such as contact resistance which often complicate the extraction of μ_{FETsat} values [62][63]. If charge mobility does, indeed, depend on thickness, it is reasonable to assume that the change in film structure responsible for variations mobility are also responsible for altered bias stress responses.

4.4 Dealing with bias stress

Baseline drift in OTFTs is of particular concern for gas sensor applications. Because encapsulation is not an option for sensors, minimization of drift must be achieved through materials development, process control, signal processing or operational conditions. Furthermore, the detailed characteristics of baseline drift for each sensor material must be well-modeled before circuits for OTFTs can be designed and fabricated.

4.4.1 Pulsed operation

OTFTs have been shown to recover much more quickly from short-term (<10s) bias stress effects than from longer term biasing. In agreement with this observation, we have found that the use of pulsed measurements is effective at reducing the magnitude of signal degradation in cases where non-reversible mobility degradation is not significant. In Figure 4.9, I_{on} is seen to shift less for smaller duty cycle operations, due to a reduction of V_T shift. μ_{FET}, on the other hand, is relatively insensitive to duty cycle, and remains constant to within 5% even at 100%

duty cycle. The increased noise of the μ_{FET} data at the 100% duty cycle measurements in Figure 4.9 is due to the increased difficulty of extracting μ_{FET} when operating continuously.

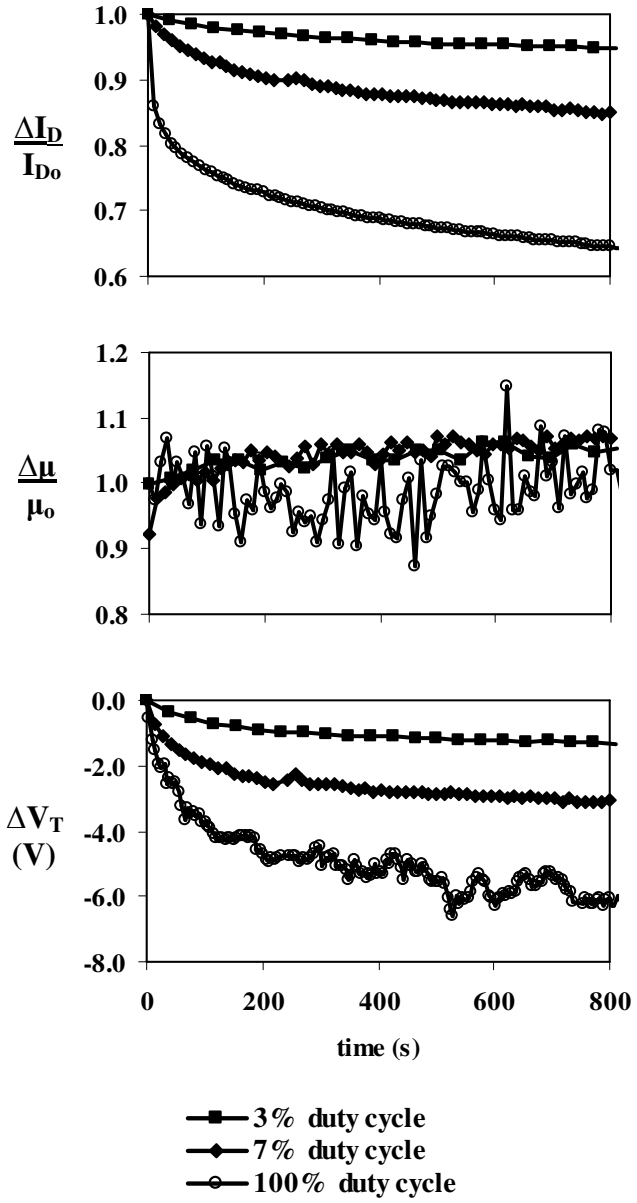

Figure 4.9: Baseline drift of an M2 TFT measured in air.
The use of pulsed measurements (<100% duty cycle) can reduce the magnitude of signal degradation.

For all experimental work on OTFT gas sensors described in Chapters 5, 6, and 8, a 3% duty cycle was used, and sensors were operated for a warm-up period of at least 15 minutes before sensing measurements were collected. With a measurement time of approximately 1 second, a time resolution of 30 seconds was achieved, which is adequate for most sensor applications. Using this operational scheme, sensors could be run for up to 5 hours with a signal drift of less than 5% (relative to the signal at the end of the warm-up period) allowing bias stress to be ignored during data analysis. In a real sensor system, however, continuous operation may be desired for a period of days, weeks, or even months, and pulsed operation will only mitigate, not eliminate, the problem.

Crone *et al* [64] demonstrated that reverse biasing of the gate between measurements could accelerate reversal of BSE shifts, resulting in complete recovery of the signal to within 2% in 1 minute. Using this technique, Crone *et al* were able to demonstrate a stable sensor response over 13 hours of operation and 420 repeated exposures. With careful choice of timing and duty cycle, the operation of OTFTs with an oscillating bias may also be able to completely eliminate some aspects of baseline drift.

4.4.2 Signal processing

For operation in inert environments, the fact that V_T shifts while charge mobility remains constant in many materials may allow the isolation of sensor responses through charge mobility. For example, Figure 4.10a shows the time response of I_{on}, extracted μ_{FET}, and V_T of two M2 OTFT devices as they are operated in nitrogen and exposed to varying levels of hexanol. Baseline drift is evident in the I_{on} and V_T responses, but the μ_{FET} response shows complete recoverability. Unfortunately, the extraction of μ_{FET} introduces a significant amount

of noise, which degrades the sensitivity. Sensor circuits which can distinguish shifts in mobility from shifts in V_T could be designed to take advantage of this behavior. However, this scheme only works if μ_{FET} degradation due to air exposure and material degradation are not a concern. In other words, use of relatively air-stable materials is still crucial.

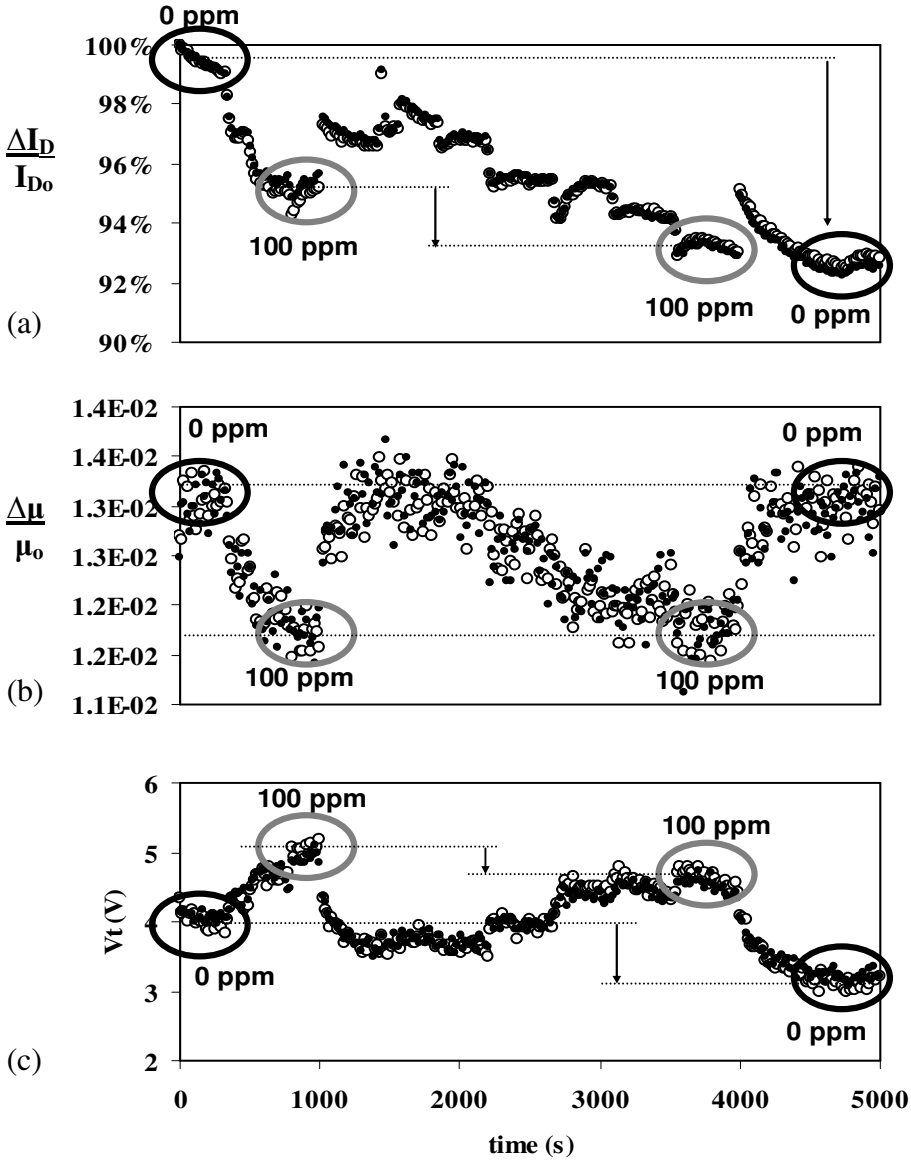

Figure 4.10: Time response of M2 sensors to hexanol.
The I_{on}, μ_{FET}, and V_T in two M2 TFT devices are plotted as they are exposed to varying levels of hexanol. Baseline drift is evident in the Ion and V_T responses, but not in the μ_{FET} response.

4.4.3 Encapsulation

Another approach to dealing with baseline drift is to use a differential circuit structure with a reference device that exhibits only baseline drift, but no sensor response. For subtracting out bias stress effects, such a reference device could be obtained by using an encapsulated sensor. Since encapsulated devices will necessarily be isolated from the ambient to which the sensor device is exposed to, it will not be useful for distinguishing sensor responses from responses to changes in ambient condition, such as humidity. The initial I-V characteristics and the time evolution of baseline drift in reference devices must be well-matched to that of sensor devices. This is a difficult requirement to meet, as the processing involved in encapsulating an OTFT may affect the bias stress degradation of reference devices by introducing a different charge or trap distribution into the system. Moreover, unlike silicon systems, proximity of two devices is not an automatic guarantee of good V_T matching in most OTFT fabrication methods.

4.5 Dealing with environment-induced instabilities

The task of distinguishing between sensor responses to analytes of interest and responses to background elements such as oxygen or water vapor is no different from the task of differentiating between mixtures of odors. A sensor array can either be engineered for sensitivity and discrimination of background vapors as well as odors of interest, or it can be engineered to be completely insensitive to those elements of the ambient which are not of interest. Given the tendency of most organic electronic materials to interact strongly with water vapor and oxygen, the former approach is more realistic, and well-aligned with the strengths and abilities of electronic noses.

4.5.1 Material engineering

If there were a way to engineer sensor materials which are insensitive to water vapor and oxygen, but still sensitive to other odors of interest, use of such materials would be advantageous since it would reduce the complexity of the sensor array. There is, indeed, much on-going work in synthesizing organic semiconductors which operate stably in air, and for the reasons just listed, these efforts are of interest to the sensors community.

Chemists have followed two different approaches for the development of air stable organic semiconductors. The first, advocated predominantly by researchers at Avecia, Ltd. (now a part of Merck Chemicals, Inc.) [41], is to start with materials such as polyarylamines which exhibit good air stability but poor electrical performance, and then progressively optimize these materials for better electrical performance.

The second is to start with an organic semiconductor that works well in inert environments, and modify it to make it air stable. P1, M1, and M2 are examples of this approach. All three materials are modifications of the traditional poly-alkyl-thiophene class of materials that are known to work well in OTFTs, but are air-sensitive. Poly-alkyl-thiophenes owe their high charge carrier mobility to an extended conjugated thiophene system which is planar and electron-rich. This extended conjugation also gives poly-alkyl-thiophenes a low HOMO level and thus a low ionization potential in the range of 4.5 to 5 eV. Materials with ionization potentials in this range are prone to oxidative doping, resulting in air sensitivity. Strategies for reducing air sensitivity thus typically revolve around increasing the HOMO energy level by limiting the delocalization length or electron density of π-conjugation systems along the polymer chain. Conjugation lengths can be lowered by introducing twists or kinks into the polymer chains [65]. For example, the bulky carboxylate side group introduced in P1 [54]

lowers the conjugation length along the polythiophene backbone by sterically forcing the chain to twist. Similarily, the thieno[2,3-b]thiophene substituents in M1 and the selenophene groups in M2 cause an out-of-plane bend in the polymer chain.

Lowering the ionization potential of a material will affect its charge transfer interactions from analytes to the conjugated π-system, but will not prevent such interactions between analytes and functional groups on the polymer. This ability to achieve both air stability and enhanced sensor response in a sensor material is demonstrated in Chapter 5.

4.5.2 Controlled gas delivery systems

A third approach to dealing with interfering background elements is to carefully control the gas inflow to the sensors, always using one chosen carrier gas to carry only the odor of interest to the sensor array. This is the solution employed by many commercial electronic noses systems today. It is feasible due to the high price tags of these systems, and is appropriate for many of the laboratory and research environments in which these systems are used. For the low cost applications which motivate this work, however, sophisticated gas flow systems are not a viable option.

4.5.3 Physical degradation

The problem of material degradation is a separate issue from the non-degradative sensor responses to air. If exposed to harsh environments such as caustic chemicals, excessive radiation, or high temperatures, physical deterioration of the components that make up an OTFT will, at some point, inevitably lead to sensor failure, and there is not much that can be done about it. For nearly all practical purposes, organic-based electronics are simply not as

hardy as their inorganic counterparts, and will have more difficulty operating in harsh conditions. However, OTFTs are meant to be part of a low cost solution, and for extreme conditions or situations where reliability and lifetime must be guaranteed, a low cost solution is not the best option.

4.6 Conclusion

This chapter surveyed the issues affecting operational lifetime and signal reliability in OTFT gas sensors. Among the mechanisms responsible for baseline drift, bias stress effect was highlighted due to its unavoidability in organic semiconductors. In order to optimize lifetime and reliability, the effect of active layer chemical composition and physical thickness on bias stress effect was investigated. In addition, strategies for dealing with baseline drift were discussed, including pulsed operation, separation of μ_{FET} and V_T responses, and encapsulation of reference devices.

4.7 References

[34] T. Sekitani, S. Iba, Y. Kato, Y. Noguchi, T. Someya, and T. Sakurai, "Suppression of DC bias stress-induced degradation of organic field-effect transistors using postannealing effects," Appl. Phys. Lett. 87, 073505 (2005).

[35] S. J. Zilker, C. Detcheverry, E. Cantatore, and D. M. del Leeuw, "Bias stress in organic thin-film transistors and logic gates," Appl. Phys. Lett. 79, 1124 , 2001.

[36] J. B. Lee, M . Heeney, S. Tierney, I. McCulloch, A. Murphy, J. Liu, J. M. J. Fréchet, and V. Subramanian, "Stability in OTFT gas sensors," Mater. Res. Soc. Symp. Proc. 871E, I1.5., Warrendale, PA, 2005.

[37] H. L. Gomes, P. Stallinga, F. Dinelli, M. Murgia, F. Biscarini, D. M. de Leeuw, T. Muco, J. Geurts, L.W. Molenkamp, and V. Wagner, "Bias-induced threshold voltages shifts in thin-film organic transistors," Appl. Phys. Lett. 84, 3184, 2004.

[38] D. B. A. Rep, A. F. Morpurgo, W. G. Sloof,and T. M. Klapwijk, "Mobile ionic impurities in organic semiconductors," J. Appl. Phys. 93, 2082, 2003.

[39] Salleo and R. A. Street, "Light-induced bias stress reversal in polyfluorene thin-film transistors," J. Appl. Phys. 94, 471, 2003.

[40] M. Matters, D. M. de Leeuw, P. T. Herwig, and A. R. Brown, "Bias induced instability of organic thin film transistors," Synth. Met. 102, 998, 1999.

[41] T. McLean, "Barriers to the implementation of plastic electronics," Cintelliq Conference, Cambridge, UK OSC-04, 2004.

[42] R. A. Street, A. Salleo, and M. L. Chabinyc, "Bipolaron mechanism for bias-stress effects in polymer transistors," Phys. Rev. B 68, 085316, 2003.

[43] A. Salleo and R.A. Street, "Kinetics of bias stress and bipolaron formation in polythiophene," Phys. Rev. B, 70, 235324, 2004.
[44] Torres, D. M. Taylor, and E. Itoh, "Interface states and depletion-induced threshold voltage instability in organic metal-insulator-semiconductor structures," Appl. Phys. Lett. 85, 314, 2004.
[45] A. Salleo, T.W. Chen, A.R. Völkel, Y. Wu, P. Liu, B.S. Ong, R.A. Street, "Intrinsic hole mobility and trapping in a regioregular poly(thiophene)," Phys. Rev. B 70, 115311, 2004.
[46] G. Horowitz, M. E. Hajlaoui, "Grain size dependent mobility in polycrystalline organic field-effect transistors," Synth. Met. 122, 185, 2001.
[47] R. A. Street, J. E. Northrup, and A. Salleo, "Transport in polycrystalline polymer thin-film transistors," Phys. Rev. B 71, 165202, 2005.
[48] E. M. Muller and J. A. Marohn, "Microscopic Evidence for Spatially Inhomogeneous Charge Trapping in Pentacene," Adv. Mat. 17, 1410 (2005).
[49] D. V. Lang, X. Chi, T. Siegrist, A. M. Sergent, and A.P. Ramirez, "Bias-Dependent Generation and Quenching of Defects in Pentacene," Phys. Rev. Lett. 93, 076601, 2004.
[50] N. S. Allen and M. Edge, Fundamentals of Polymer Degradation and Stabilization, Elsevier Applied Science: New York, NY, 1992.
[51] O.D. Jurchescu, J. Baas, and T.T.M. Palstra, "Electronic transport properties of pentacene single crystals upon exposure to air," Appl. Phys. Lett., 87, 052102, 2005.
[52] D. Li, E.-J. Borkent, R. Nortrup, H. Moon, H. Katz, and Z. Bao, "Humidity effect on electrical performance of organic thin-film transistors," Appl. Phys. Lett., 86, 042105, 2005.
[53] S. Hoshino, M. Yoshida, S. Uemura, T. Kodzasa, N. Takada, T. Kamata, and K. Yase, "Influence of moisture on device characteristics of polythiophene-based field-effect transistors," J. Appl. Phys., 95, 5088, 2004.
[54] A.R. Murphy, J. Liu, C. Luscombe, D. Kavulak, J.M.J. Fréchet, J.R. Kline, M.D. McGehee, "Synthesis, characterization, and field-effect transistor performance of carboxylate-functionalized polythiophenes with increased air stability," Chem. Mater., 17, 4892, 2005.
[55] M. Heeney, C. Bailey, K. Genevicius, M. Shkunov, D. Sparrowe, S. Tierney, and I. McCulloch, "Stable Polythiophene Semiconductors Incorporating Thieno[2,3-b]thiophene," J. Am. Chem. Soc., 127, 1078, 2005.
[56] S. Tierney, C. Bailey, K. Genevicius, M. Heeney, I. MacDonald, R. Rawcliffe, R. Simms, D. Sparrowe, M. Shkunov, W. Zhang and I. McCulloch, "Fused thiophene semiconducting polymers for OFETs: Solutions to high mobility and stability," Mat. Res. Soc. Fall Symposium, Boston, MA, M7.9, 2005.
[57] T. Li, J. W. Balk, P. P. Ruden, I. H. Campbell, and D. L. Smith, "Channel formation in organic field-effect transistors," J. Appl. Phys. 91, 4312, 2002.
[58] L. Burgi, H. Sirringhaus, and R. H. Friend, Appl. Phys. Lett. "Noncontact potentiometry of polymer field-effect transistors," 80, 2913, 2002.
[59] T. Li, P. Ruden, I. H. Campbell, and D. L. Smith, "Investigation of bottom-contact organic field effect transistors by two-dimensional device modeling," J. Appl. Phys. 93, 4017, 2003.
[60] K. P. Puntambekar, P. V. Pesavento, and C. D. Frisbie, "Surface potential profiling and contact resistance measurements on operating pentacene thin-film transistors by Kelvin probe force microscopy," Appl. Phys. Lett. 83, 5539, 2003.
[61] R. B. Wehrspohn, M. J. Powel, and S. C. Deane, "Kinetics of defect creation in amorphous silicon thin film transistors," J. Appl. Phys. 93, 5780, 2003.
[62] R. Schroeder, L. Majewski, and M. Grell, "A study of the threshold voltage in pentacene organic field-effect transistors," Appl. Phys. Lett. 83, 3201, 2003.
[63] O. Marinov, M. J. Deen and B. Iniguez, "Charge transport in organic and polymer thin-film transistors: recent issues," IEE Proc.-Circuits Devices Syst., 152, 189 (2005).
[64] B. Crone, A. Dodabalapur, A. Gelperin, L. Torsi, H. E. Katz, A. J. Lovinger, and Z. Bao, "Electronic sensing of vapors with organic transistors," Appl. Phys. Lett., 78, 2229, 2001.
[65] I. McCulloch, C. Bailey, M. Giles, M. Heeney, I. Love, M. Shkunov, D. Sparrowe, and S. Tierney, "Influence of Molecular Design on the Field-Effect Transistor Characteristics of Terthiophene Polymers," Chem. Mater. 17, 1381, 2005.

Chapter 5: OTFT GAS SENSORS

The goal of making a low-cost sensor array requires the development of a library of printable sensor materials which show good sensitivity and discrimination as well as stable operation in ambient environments over an adequate lifetime. Stability to air and variations in humidity would be of especial interest for sensors, but chemical reactiveness is part of what makes organic semiconductors good for sensing in the first place. Reducing this reactivity may interfere with the sensor response. One of the motivating questions for the work presented in this chapter was whether a trade-off between air stability and chemical sensitivity must be considered when designing sensor materials. Results indicate that there is not a direct trade-off between the two, and that the complexity of the chemistry of gas sensing yields many separate knobs which can allow sensitivity to different elements to be adjusted separately. Before describing the experimental work, a review of the current understanding of how OTFT gas sensors work is presented, and motivation is given for the choice of polythiophene OTFTs as a model system.

5.1 Basic principles

Electronic noses based on conducting polymer chemoresistor sensors have been commercially available for over a decade. Due the chemical activeness of their carbon backbone, conducting polymers are sensitive to a wide range of analytes, including oxygen, humidity, and a host of volatile organic compounds [66]. Using a three-terminal OTFT structure instead of the two-terminal chemoresistor construction introduces additional process complexity and complicates signal processing, but judicious use of the gate bias can enhance sensitivity, discrimination, and

measurement repeatability[67]-[71]. The extraction of multiple parameters such as μ_{FET}, V_T, and bulk resistivity also allows the partial deconvolution of various analyte-sensor interactions, which is not possible in the single-parameter chemoresistor devices.

The use of OTFTs as gas sensors requires a sensor device structure in which a chemically sensitive, electrically active material is accessible to ambient analyte vapors. Typically, the sensing material is the organic semiconductor, though field-effect transistor sensors have also been demonstrated in which an organic gate materials [72],[73] or even organic gate dielectric [74] produces the sensor response. Use of the semiconductor as the sensing material offers a number of advantages. First, OTFT device structures in which the semiconductor is on top are easier to fabricate (see section 3.3.1). Also, sensing within the semiconductor enables field-effect-enhancement of the sensor response [68] and can cause a greater variety of changes in the OTFT I-V characteristics. Gate electrode sensing, for example, is based on work function shifts, and dielectric sensing is based on shifts in dielectric constant or fixed charge distribution. All of these effects show up in the OTFT I-V characteristics predominately as a V_T shift. Sensing interactions within the semiconductor, on the other hand, can affect V_T as well as μ_{FET} and bulk resistivity. A final advantage of using organic semiconductors as the sensing material is that there exist many organic semiconductors which are suitable for sensing.

An example of an OTFT gas sensor device structure appropriate for an organic semiconductor sensing material is illustrated in Figure 5.1. This bottom-gated, bottom contact structure leaves the active material on top, where it is easily accessible to ambient vapors. Odors flowing across the surface of the OTFT can either be adsorbed onto the surface of the active material or absorbed into the film through dissolution and diffusion. Once sorbed, the analyte can alter

the electrical characteristics of the semiconductor film through either mechanical or chemical interactions.

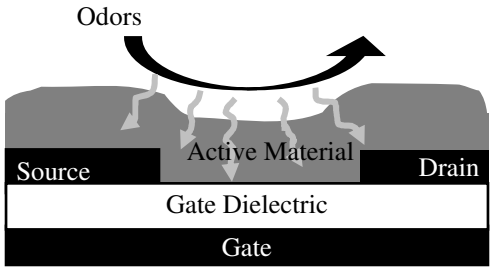

Figure 5.1: Cross-section of an OTFT gas sensor.

5.1.1 Partitioning of analyte into active layer

The first step in generating a sensor response is sorption of analyte molecules into the active material. The sorption process is described by a partition coefficient, K, which defines the thermodynamic equilibrium between the gas and sorbent phases of the vapor. K, defined below, depends on the saturated vapor pressure of the analyte and its solubility in the sensor material, and changes with temperature and pressure. It is also affected by the presence of other vapors.

$$K = \frac{C_S}{C_V}$$

Equation 5.1

C_S = concentration of sorbent phase in the polymer film
C_V = concentration of vapor phase in the ambient

In an idealized system, induced sensor response (R) is linearly related to C_S, and K is constant over the range of operation conditions. Assuming that amount of analyte sorbed into the

sensor is negligible compared to the amount present in the ambient, C_V remains constant throughout the sensing process, and R is simply linearly proportional to C_V [75].

$$R \propto C_S = KC_V \qquad \text{Equation 5.1}$$

In fact, a linear correlation between sensor response and analyte concentration is often observed at low concentrations. By building poly(pyrrole) chemoresistors on a piezoelectric microbalances, Charlesworth *et al* [76] simultaneously measured the change in the mass and resistivity of the conducting polymer thin films as they were exposed to different concentrations of various volatile organic compounds. They found that the resistance response correlated linearly with mass uptake up to a sorbed mass of 5 weight percent. They also investigated the kinetics of mass sorption into the films, and discovered that sorption and diffusion of vapors into this conducting polymer differed with molecular size and chemical properties of both the vapor and the organic material. Smaller vapor molecules followed Fick's law of diffusion for planar surfaces, while larger molecules displayed non-Fickian behavior. Also, some vapors sorbed more readily than others, making them easier to detect at lower concentrations.

Upon removal of the vapor from the ambient, the analyte will desorb completely from the sensor film unless interactions between the analyte and sensor molecules are strong enough to either prevent desorption or kinetically hinder the process. Complete desorption allows recovery of the original electrical characteristics, while incomplete desorption results in either signal drift or poisoning of the sensor. Because strong interaction between the analyte and

sensor molecule is a characteristic of both good sensitivity and an irreversible sensor response, there is a trade-off between optimizing sensor systems for good sensitivity and reusability [75].

5.1.2 Sensor response transduction

The mechanisms behind the electrical response of conducting polymers to gas analytes has been the subject of much on-going investigation [77], and many details remain unclear. Early studies on polypyrrole films suggested that a small but reversible charge transfer between the analyte and sensor molecule results in a work function shift [78]. Electrical doping and de-doping effects are commonly cited as well. For vapors with Lewis acid or base characteristics, the idea is that electron donation or withdrawal by the analyte can lead to a change in charge carrier concentration. The direction of conductivity change should in theory be predictable given the polarity of majority charge carriers and the relative magnitudes of the vapor and polymer electronegativities [79]. Observed sensor responses do not always bear out the predictions of this theory. Many of its qualitative predictions are reliable (whether conductivity will go up or down), but a larger electronegativity difference does not consistently translate into a stronger shift in conductivity.

Another proposed mechanism is the modulation of electron hopping due to changes in the dielectric property of the film when analyte vapors are present. Most models of charge transport in organic semiconductors assume that effective charge mobility is limited by the need for electrons to hop across barriers, and equations for hopping rate predict a dependence on the dielectric property of the film [76].

A final popular mechanism cites the physical effect of vapor sorption into the film. Configurational changes due to polymer swelling by the analyte vapors may result in modified

electrical behavior. In many polymers, charge flow is believed to percolate through a network of "good" connections between molecules. In this case, swelling could have a strong affect on the percolation dynamics [80].

A comprehensive study by Bissell *et al.* [81] addressed the sensor response of polypyrroles and polythiophenes to several classes of volatile organic compounds, including alcohols, esters, alkanes, and aromatics. They found that the different classes of analytes elicited responses of different strengths, but that, within each class of analytes, sensor response was linearly related to saturated vapor concentration, regardless of the specific size or shape of the analyte molecule. This method of analysis is fruitful for determining if differences in a sensor response to various vapors are due to analyte-specific interactions.

One problem with many mechanistic studies is that interface effects are often ignored due to their complexity. However, the fact that most conducting polymers are used in thin-film form for sensing means that interfaces have a strong influence on both the electrical and chemical characteristics of the film and on the transduction of the sensor response. The same is true in OTFT structures, where conduction flows primarily along the surface of the organic semiconductor along its gate dielectric interface. Tanese *et al* [68] found that the electronic character of the gate dielectric, and its similarity or dissimilarity to that of the organic semiconductor, strongly influenced the sensor behavior of OTFTs. They attributed this to differences in the organic semiconductor – gate dielectric interface. Torsi *et al* [82] established that, in many analyte-sensor systems, film swelling does not occur, indicating that material incompatibilities (such as a hydrophilic/ hydrophobic mismatch) prevent absorption of the analyte into the sensor film. In these cases, the sensor response is elicited entirely by adsorption of the analyte at the surface or along grain boundaries in the film.

5.1.3 Multiparameter OTFT sensor response

In chemoresistors, all of the mechanisms mentioned in the previous section will affect the one measured parameter, resistivity, in different ways, and the resulting sensor response is thus an average of all effects. In an OTFT, however, these mechanisms will affect different parameters in different ways.

When no bias is applied to the gate electrode, an OTFT operates simply as a chemoresistor, and can be used to monitor the bulk conductivity of the film. This property is strongly affected by electrical doping and de-doping, and shifts in bulk conductivity typically indicate changes in the free carrier concentration in the material. Because bulk conductivity changes approximately linearly with mass uptake, but at a different rate for different vapors, this indicator can provide both qualitative and quantitative information about the vapors. Direction of change (more or less conductive) as well as patterns in these changes (which materials get more conductive, and which ones get less so) can help to identify the substance. Once the vapor is identified, the amount of change in conductivity can be used to quantify the concentration of the vapor in the air. Taking advantage of the information already available from studies on chemoresistors, this indicator can provide significant sensing resolution even when used alone, allowing test arrays to sense and distinguish between a many of different vapors. However, in many OTFTs, bulk conductivity is low, and its measurement can be easily obscured by noise.

When a non-zero gate bias is applied to an OTFT, the device changes from a chemoresistor to a field-effect transistor. There is some evidence that the application of gate bias can be used to enhance sensitivity or improve repeatability and recoverability of the sensor response [68]. Electrical measurements taken in this mode can be analyzed to extract μ_{FET}, V_T, and I_{on} (defined as the drain current when both V_{DS} and I_{DS} are biased to their maximum negative

value). As discussed in section 3.3.3, μ_{FET} is influenced by many factors which have nothing to do with the intrinsic mobility (μ_o) of the organic semiconductor. Still, changes in μ_o are expected to show up most strongly as a shift in extracted μ_{FET} values. In organic semiconductors, charge conduction is limited mostly by hopping across potential barriers at grain boundaries. Charge trapping and de-trapping at grain boundaries is thought to modify the potential barriers at these points, modulating the carrier charge mobility. Supporting this hypothesis are studies that show that sensing in OTFTs occurs predominately at grain boundaries [82].

Threshold voltage (V_T) is sensitive to the work function of the material, as well as fixed charge and trap density within the organic semiconductor film. Because carrier concentration in organic semiconductors is low, band bending during accumulation mode operation typically extends through the entire thickness of the film. Evidence of this is the fact that surface potential measurements in OTFTs have been found to closely follow channel potential profiles [83]. Thus, even analytes adsorbed along the top surface of the film can affect V_T. However, the effect of charges on V_T become stronger as they move closer to the dielectric interface, and new traps are more likely to capture charge as they move closer to the channel where free charge is accumulated. Because the gate dielectric interface is at the bottom of the active later, opposite the surface that is exposed to chemical vapors, V_T response is highly dependent on thickness and continuity of the active layer. In thick, continuous films, few or no vapor molecules can diffuse to the dielectric surface, and V_T response is weak. In thinner films, however, or in films with a high density of grain boundaries, vapor molecules can diffuse easily to the bottom of the organic active layer, and large changes in V_T may be observed. V_T response is expected to increase linearly with amount of vapor adsorbed, much like bulk

conductivity. Thus, bulk conductivity and threshold voltage are weakly correlated. Differences in the behavior of these two indicators arise largely from the fact that V_T is also strongly dependent on the ability of the vapor molecules to diffuse effectively into and out of the organic material. Also, these two indicators show different recovery behavior, since adsorbed molecules at the surface, which affect bulk conductivity most, can desorb most quickly, while molecules at the dielectric interface, which affect V_T, are more kinetically hindered.

Due to a low intrinsic conductivity, measurements of bulk conductivity are more sensitive to noise, and V_T is thus the metric that is used in this work. Unfortunately, V_T is difficult to control in OTFTs, and device-to-device variation in V_T makes it difficult to design analog circuits capable of monitoring V_T shifts within individual devices, since these usually require a reference device with a matching V_T. Despite concentrated efforts to model and control V_T in OTFTs over the past decade, most research groups still routinely observe run-to-run variations in this value. More troubling is the gate bias effect, in which a continuous gate bias on a device causes a slow shift in its V_T over the course of minutes or hours. Changes in V_T have been shown to asymptote to a stable value after many hours—sometimes days, but is reversible upon relaxation, and this reversal can be accelerated by applying light or a gate bias of the opposite charge. Thus, burn-in strategies used in silicon technology are not applicable.

A final parameter, the drive current of a FET device, depends on the threshold voltage, charge mobility, and carrier concentration, which is related to bulk conductivity. Thus, this indicator provides a good integration of the various indicators described above. Because this is an easy value to measure, saturation current is usually favored as the ultimate indicator of electrical response. Because parameters such as μ_{FET} and V_T require mathematical extraction that is difficult to implement using analog circuitry, saturation current may be the only parameter that

can be monitored practically if complexity in signal processing circuitry is to be minimized, as is desired in low-cost applications. However, because drive current is sensitive to so many factors, it is difficult to decouple the exact effects being observed. Therefore, it is useful to monitor at least one other indicator, and preferably two, along with drive current in order to shed light on the mechanisms behind the response.

5.2 Experimental setup

A schematic cross-section of an OTFT gas sensor is shown in Figure 5.1. For convenience, a standard substrate-gated architecture was used. A 95 nm layer of wet oxide was grown on heavily n-doped silicon substrates, and 50 nm thick gold pads with a 2.5 nm chrome adhesion layer were thermally evaporated to form source/drain contacts. The contact electrodes were patterned using lift-off. Two polythiophenes were chosen for use as the OTFT active material: regioregular poly-3-hexylthiophene (P3HT) and poly (didodecyl-2,2'-bithiophene-4,4'dicarboxy-late-co-2,2'-bithiophene) (P1). The chemical structures of both are illustrated in Figure 5.2.

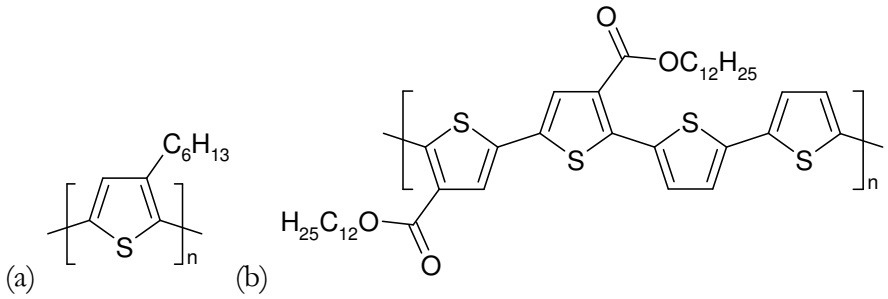

Figure 5.2 Polythiophene organic semiconductors used for OTFT gas sensor devices.
(a) Regioregular poly-3-hexylthiophene (P3HT) (b) Poly (didodecyl-2,2'-bithiophene-4,4'dicarboxy-late-co-2,2'-bithiophene) (P1)

P3HT was obtained commercially and used as-received. For deposition, it was dissolved in chloroform at 0.8 wt%. As described in Section 4.2, P1 is a polythiophene derivative which has been air-stabilized through the attachment of ester functional groups. Details of molecule design and synthesis as well as electrical characteristics are provided in ref [84]. For processing, P1 was dissolved in chloroform at a concentration of 4mg/mL.

For both P3HT and P1, mild heating and sonication were used to accelerate dissolution. The dissolved polythiophene solutions were then passed through a 0.45μm filter and spun-cast onto bottom-gate, bottom contact, silicon substrate structures in a nitrogen environment. P3HT was spun at 6000 rpm, while P1 was spun at 4500 rpm. Before spinning, the substrates were dehydrated by heating for 2 minutes at 120ºC, and then cooled to room temperature. After spinning, samples were annealed at 120ºC for 20 minutes in nitrogen.

We chose to base our OTFT gas sensors on polythiophene materials for several reasons. Used as a chemoresistor, polythiophenes have been shown to provide good sensor response to a range of gases, with sensitivities in the low ppm level, good repeatability, and stable operation in an air ambient environment [85]-[87]. Polythiophenes can be solubilized through functionalization with alkane chains, and derivatives such as P3HT have been extensively studied for use in OTFTs. The suitability of soluble polythiophenes as inks for inkjet printing has been demonstrated by several groups [88]-[90]. The use of P3HT as a sensor for biological molecules, and the tuning of its sensitivity through functionalization, has also been demonstrated [91]. Note that we have previously demonstrated a process to fabricate all-printed transistors on plastic that is generally compatible with the sensor technology described here [92]. It is worth mentioning, however, that the fabrication of such sensors on silicon platforms is potentially advantageous, since underlying silicon circuitry may be used to process

the complex signatures collected from the gas sensor array. Also, the use of inorganic substrates rather than low-cost substrates helps to avoid problems with degraded device performance, stability, and noise. Since the processes used herein are all compatible with silicon backend-processes, such sensors may potentially be post-processed over completed silicon-based signal processing circuitry.

Sensors were operated at room temperature in the dark, in an isolated chamber with controlled gas flow and probed remotely with an HP 4145 parameter analyzer (Figure 5.3). A fan within the chamber ensured swift, even distribution of gas analytes. Purging was performed using compressed air, which provided consistent ambient humidity. To avoid bias stress, devices were operated at a 3% duty cycle, which allowed a measurement time resolution of approximately 30 s.

(a)  (b) 

Figure 5.3: Chamber used for sensor experiments.
(a) There is an inlet at the top for analyte introduction, an outlet at the bottom for purging, and multiple connectors for the simultaneous monitoring of multiple sensor chips. (b) Signals are probed remotely with an HP4145 and an opaque cover blocks light during measurements.

During sensor experiments, the time-response of I_{on}, μ_{FET}, and V_T were monitored and correlated with calculated gas concentration. I_{on} is the drain current when $V_{GS}=V_{DS}=-20V$. μ_{FET} and V_T were both extracted from the high-$|V_{GS}|$ portion of the saturation transfer curves. μ_{FET} was calculated from the slope of the transfer curve using Equation 3.3; V_T was calculated from the x-intercept of $\sqrt{I_{DS}}$ plotted vs. V_{GS} using the method illustrated in Figure 3.7b.

5.3 Results

A typical OTFT sensor response is illustrated in Figure 5.4. The saturation transfer curve of a P3HT OTFT taken before and during exposure to 50 ppm acetic acid, and again after purging with air, reveals that acetic acid exposure causes a reversible decrease in μ_{FET} and I_{on} as well as a positive V_T shift.

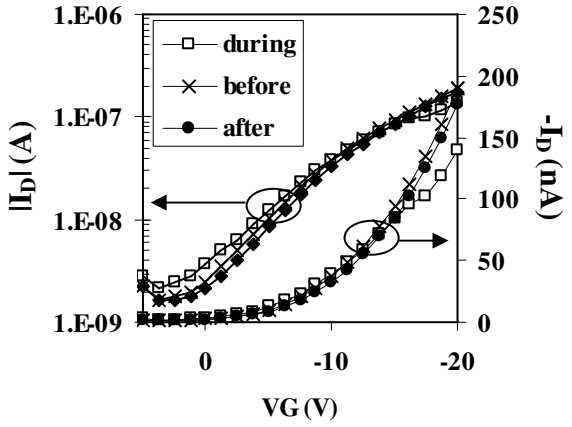

Figure 5.4: Transfer curve of a P3HT OTFT gas sensor before, during, and after acetic acid exposure.
50 ppm acetic acid exposure causes a decrease in μ_{FET} and I_{on} as well as a positive V_T shift which is reversible upon purging with compressed air.

During sensor experiments, only the high-$|V_{GS}|$ portion of the transfer curve is measured in order to avoid bias stress effects. The sensors were swept from -15 to -20 V V_{DD} once every 30 s with a 3% duty. From these sweeps, the multiple parameter time response of an array of OTFTs can be monitored as gas analyte concentrations are changed

To better understand and manipulate the sensor response of polythiophene materials, the effect of varying analyte functionalization was explored. P3HT and P1 polymers were exposed to a range of different organic vapors, including hexane, hexanol, hexanethiol, hexylamine, and hydrochloric acid, at gas phase concentrations ranging from 10-500 ppm. By monitoring both extracted parameters such as μ_{FET} and V_T as well as I_{on}, different forms of analyte-sensor interactions could be distinguished.

Sensor response was found to depend strongly on analyte functionalization. Accordingly, saturated alkane chains such as hexane produced no sensor response even at their saturated vapor pressure. From these results, it is unclear whether this lack of response is due to the inability of saturated hydrocarbons to sorb into the sensor materials or to a lack of interaction between sorbed analyte and the sensor film.

In comparison, as little as 10 ppm of hexanol produced a detectable response in both materials (Figure 5.5). P3HT exhibited a positive V_T shift and a degradation of extracted μ_{FET}. Interestingly, P1 exhibited a stronger I_{on} response even though its μ_{FET} response was weaker, because it did not undergo a V_T shift. One possible explanation for the P3HT response is the introduction of fixed negative charge into the polymer backbone through charge transfer between hexanol and polythiophene. This fixed charge would trap mobile carriers but simultaneously make it easier for the gate to accumulate charge in the channel. Physical

swelling of the film could also induce a similar affect by interfering with π-orbital overlap and simultaneously increasing the thickness of the film that must be depleted for the device to be turned off. In P1, on the other hand, it appears that hexanol either reduced carrier concentration or interfered with charge transport, but did not introduce extra charge into the film. The alcohol response for both materials was found to be quickly reversible upon removal of the hexanol, indicating that the desorption of hexanol from polythiophene is not hindered

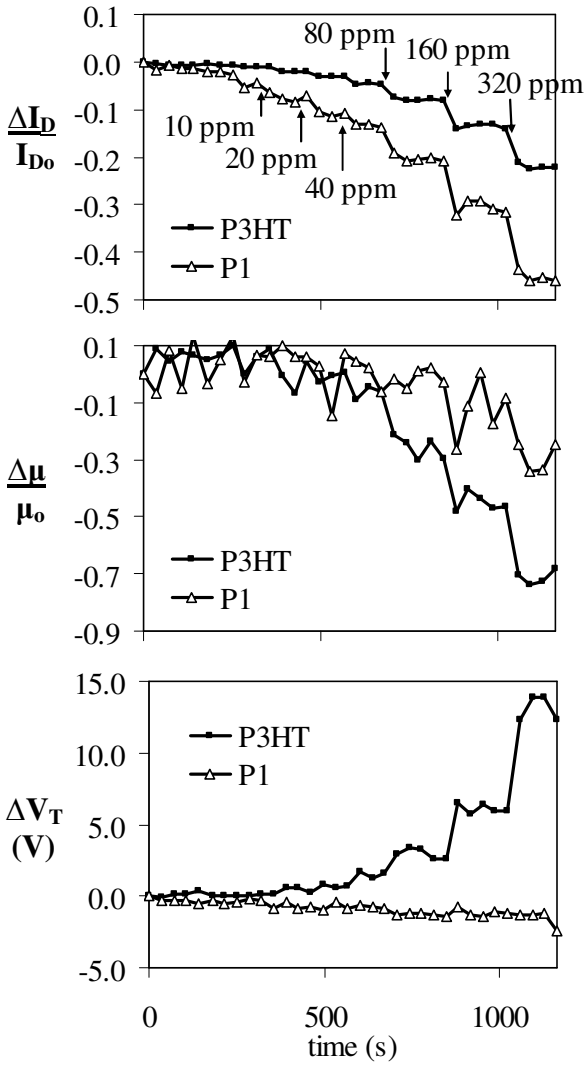

Figure 5.5: Response of P3HT and P1 to hexanol.
The OTFT sensors undergo a fast, reversible on-current degradation accompanied by a decrease in mobility and a positive threshold voltage shift.

by the interactions responsible for the sensor response. Notably, many inorganic sensors tend to be sensitive to alcohol poisoning, so this repeatable, reversible response to alcohol may be a significant advantage of organic gas sensors.

Hexanethiol produced a slow degradation of both V_T and μ_{FET} (Figure 5.6). In the presence of more than 10ppm of hexanethiol, shifts in the both polythiophene materials continued slowly over the course of more than an hour, until the material finally became non-conductive. At analyte concentrations above 10 ppm, the rate of this shift did not correlate strongly with analyte concentration. Removal of the hexanethiol stabilized the electrical characteristics, preventing further shifts in the OTFT I-V curves, but did not reverse any shifts that had already occurred, suggesting that the thiol functional group diffuses slowly in polythiophenes, but interacts strongly with the material, preventing desorption. The opposite directions of V_T shift induced by the hexanethiol compared to hexanol in P3HT indicate that they probably introduce opposite interface or bulk charges within the active layer.

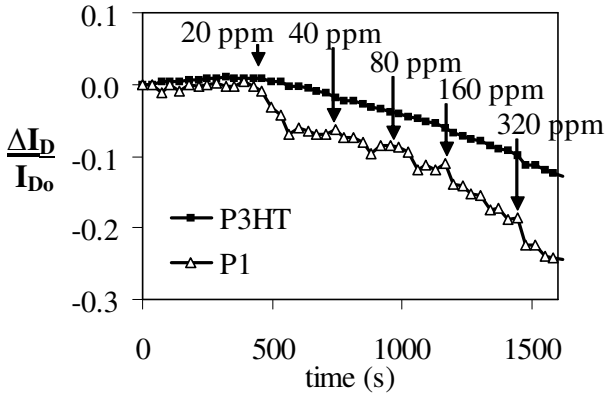

Figure 5.6: Response of P3HT and P1 to hexanethiol.
The OTFT sensors undergo a slow, irreversible I_{on} degradation accompanied by a negative threshold voltage shift.

Amine functional groups are nucleophilic, due to the lone electron pair of the nitrogen. Thus an analyte such as hexylamine could be expected to de-dope polythiophene, as illustrated in Figure 5.7b. Indeed, both P3HT and P1 quickly became non-conductive upon exposure to 10 ppm of hexylamine (Figure 5.7a). This response was not reversed upon removal of the analyte, likely due to a strong interaction between polythiophene and the amine functional group. Amines are commonly released during decomposition of proteins; a good sensitivity to amines is thus an advantage for food spoilage sensing applications.

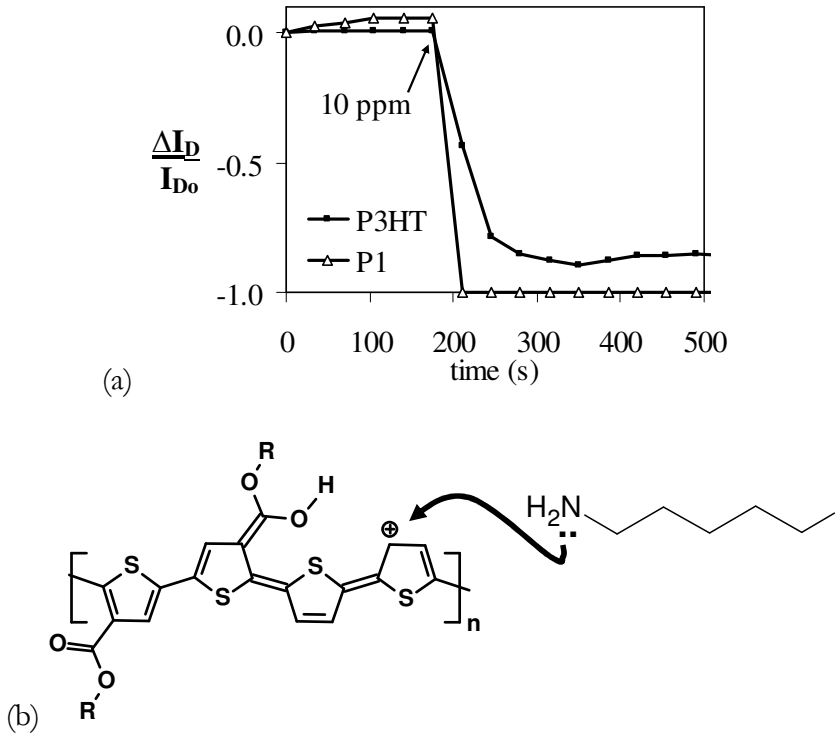

Figure 5.7: Response of P3HT and P1 to hexylamine.
(a) Both OTFT sensors become nonconductive after exposure to 10 ppm of the analyte, probably due to the dedoping effect illustrated in (b).

Hydrochloric acid (HCl) should be proton-donating, and increase doping polythiophenes. P1 does, in fact, show a strong increase in on-current upon exposure to small concentrations of HCl, though P3HT does not (Figure 5.8a). Both materials quickly become non-conductive at

higher concentrations. The enhanced P1 response suggests that the ester side chains present on P1 enhance the effect of HCl doping. Indeed, protonation of the carbonyl group would leave the oxygen with a positive charge, which would then be rapidly transferred to the thiophene backbone (Figure 5.8b).

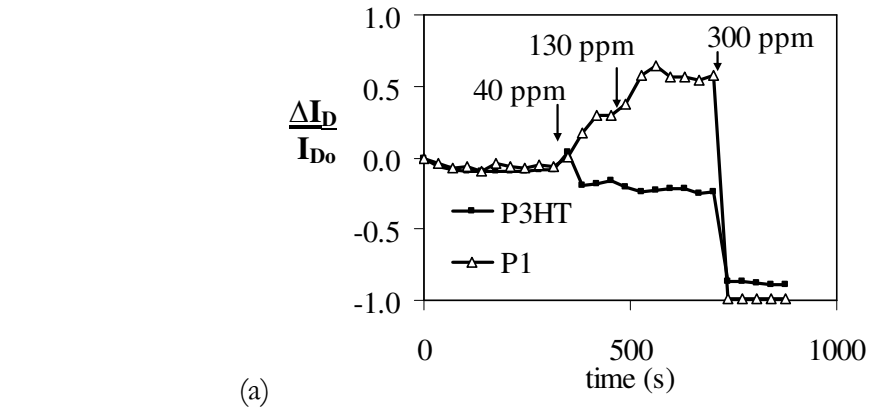

(a)

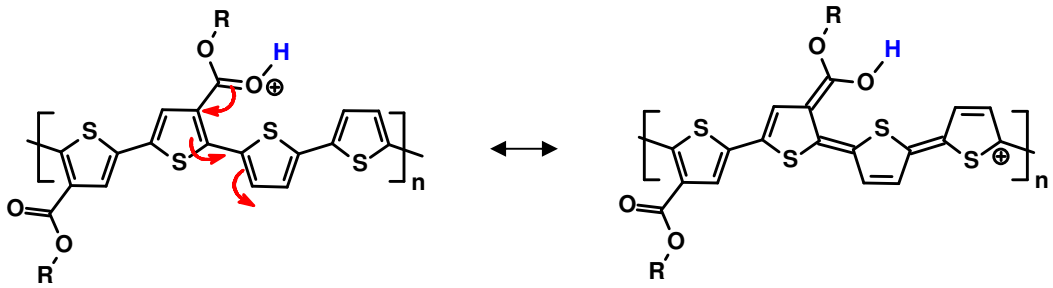

(b)

Figure 5.8: Response of P3HT and P1 to hydrochloric acid. (a) The functionalized P1 sensor appears to be doped by the acid, while P3HT remains relatively unaffected. Both sensors become nonconductive at high acid concentrations. (b) A possible mechanism for the doping effect of hydrochloric acid on P1.

This HCl sensor response is particularly interesting because P3HT and P1 showed the type of differential response necessary for discrimination in sensor arrays. In addition, P1 which has been modified for air stability, actually showed a stronger response than P3HT, indicating that

reduced sensitivity to oxygen and water do not necessarily translate into a weaker sensor response to other analytes of interest.

5.4 Discussion

The polythiophene response to alcohols is interesting because of its repeatability and reversibility, and because many inorganic sensors are poisoned by alcohol. Therefore, to further understand the alcohol response, P3HT and P1 sensors were exposed to a series of alcohols with varying alkane chain lengths (Figure 5.9).

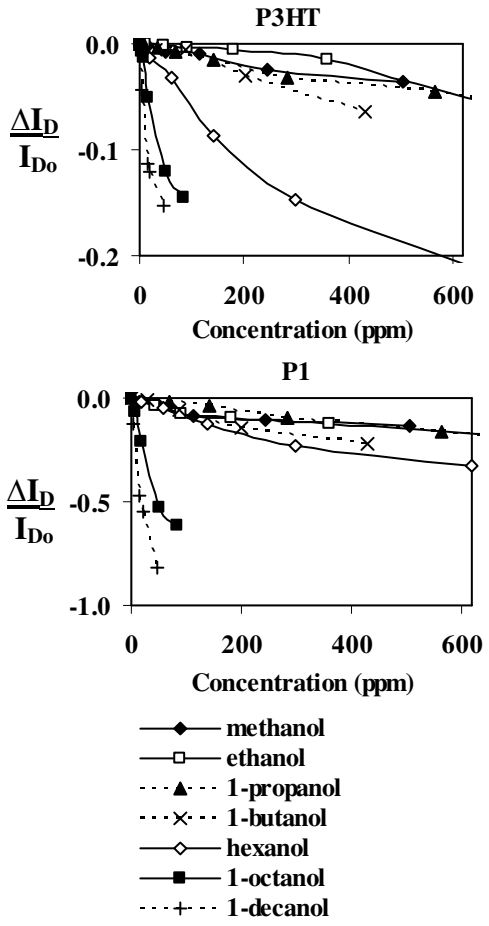

Figure 5.9: On-current response of polythiophene OTFT gas sensors to alcohols with varying chain lengths.
As the alkane chain is increased, the I_{on} degradation increases for both materials.

Bissell, *et al* [81] demonstrated that the response of conductive polymer chemoresistor sensors is strongly correlated with volatility, indicating that the initial diffusion of analytes into the sensor is the dominant step, and that the actual sensor transduction mechanism may often be nonspecific. This is consistent with physical transduction mechanisms such as mechanical swelling of the film due to absorption of analytes. Following the methodology outlined by Bissel, *et al*, the gas-phase concentration required to produce a 2.5% drop in I_D (C_g) was plotted against the saturated vapor pressure of the analyte at room temperature (SVP) in a $\log(1/C_g)$ vs. log (1/SVP) plot, revealing a linear relationship for the longer-chained alcohols (Figure 5.10).

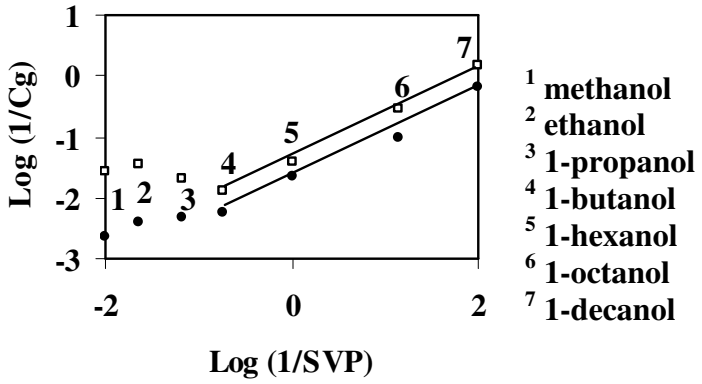

Figure 5.10: Nonspecific partitioning of alcohols into P3HT and P1.
Response of P3HT (●) and P1 (□) to primary alcohols is diffusion-controlled for the longer chained alcohols. The sensor response at the $\Delta I_D/I_{Do}$=2.5% level is used.

The linear relationship observed in this analysis indicates that while P3HT and P1 show good sensitivity and reversible sensor responses to alcohols, they are not sensitive to variations in size or shape for alcohols longer than butanol. For the shorter alcohol chains on the other hand, the P3HT and P1 responses flatten out, and the magnitude of the sensor response

becomes less sensitive to saturated vapor pressure. The fact that a lower C_g of ethanol is required to elicit the same response in P1 as a higher C_g of 1-butanol is surprising, since, at the same C_g, more butanol than ethanol is expected to sorb into the active layer (i.e. the solid phase concentration, C_v, of butanol would be higher than that of ethanol). This indicates that P1 experiences a stronger interaction with ethanol than butanol, either due to the higher concentration of -OH groups in a given C_v, or due to the fact that the -OH group in ethanol is less sterically hindered.

5.5 Conclusion

Polythiophene OTFT gas sensors were observed to show sensor response to a variety of volatile organic compounds down to an analyte concentration of 10 ppm. The air stable P1 did not show degraded sensor responses relative to the non-air-stabilized P3HT, negating a direct tradeoff between air stability and sensitivity. Rather, sensor response to HCl seemed to be more strongly influenced to functionality of the sensor molecule, encouraging the efforts to tune sensor responses through the functionalization described in Chapter 6.

5.6 References

[66] J. Janata and M. Josowicz, "Conducting polymers in electronic chemical sensors," Nature Materials, 2, 19, 2003.

[67] F. Liao, C. Chen, V. Subramanian, "Organic TFTs as gas sensors for electronic nose applications," Sensors and Actuators B, 17, 849, 2005.

[68] M.C. Tanese, D. Fine, A. Dodabalapur, L. Torsi, "Interface and gate bias dependence responses of sensing organic thin-film transistors," Biosensors and Bioelectronics, 21, 782, 2005.

[69] B. Crone, A. Dodabalapur, A. Gelperin, L. Torsi, H. E. Katz, A. J. Lovinger, and Z. Bao "Electronic sensing of vapors with organic transistors," Appl. Phys. Lett., 78, 3965, 2001.

[70] L. Torsi, A. Dodabalapur, L. Sabbatini, P.G. Zambonin, "Multi-parameter gas sensors based on organic thin-film-transistors" Sensors and Actuators B, 67, 312, 2000.

[71] L. Torsi, M.C. Tanese, N. Cioffia, M.C. Gallazzi,L. Sabbatini, and P.G. Zambonin, "Alkoxy-substituted polyterthiophene thin-film-transistors as alcohol sensors," Sensors and Actuators B, 98, 204, 2004.

[72] B.J. Polk and J. Janata, "ChemFET Arrays for Chemical Sensing Microsystems" IEEE Sensors Conference, Orlando, Florida, 5.13, 2002.

[73] Covington, J. A., J.W. Gardner, P.N. Bartlett, and C-S. Toh, "Conductive polymer gate FET devices for vapour sensing," IEE Proc. Circuits Devices Syst. 151, 326, 2004.
[74] T. G. Bäcklund, R. Österbacka, H. Stubb J. Bobacka, and A. Ivaska, "Operating principle of polymer insulator organic thin-film transistors exposed to moisture," Journal of Appl. Phys., 98, 074504, 2005.
[75] K.C. Persaud and P.J. Travers, Arrays of broad specificity films for sensing volatile chemicals, CRC Press, Inc.: New York, NY, 1997.
[76] J. M. Charlesworth, A. C. Partridge, and N Garrard, "Mechanistic Studies on the Interactions between Poly(pyrro1e) and Organic Vapors,", J. Phys. Chem., 97, 5418, 1993.
[77] B. Adhikari and S. Majumdar, "Polymers in sensor applications," Prog. Polym. Sci., 29, 699, 2004.
[78] Topart, P., and Josowicz, M., "Transient effects in the interaction between polypyrrole and methanol vapor," J. Phys. Chem., 96, 8662, 1992.
[79] J. Janata, and M. Josowicz, "Conducting polymers in electronic chemical sensors," Nat. Mater. 2, 19, 2003.
[80] K.C. Persaud, "Polymers for chemical sensing,"Materials Today, 8, 38, 2005.
[81] R.A. Bissell, K. C. Persaud and P. Travers, "The influence of non-specific molecular partitioning of analytes on the electrical responses of conducting organic polymer gas sensors," Phys. Chem. Chem. Phys., 4, 3482, 2002.
[82] L. Torsi, A. J. Lovinger, B. Crone, T. Someya, A. Dodabalapur, H. E. Katz, and A. Gelperin, "Correlation between Oligothiophene Thin Film Transistor Morphology and Vapor Response," J. Phys. Chem. B, 106, 12563, 2002.
[83] K. P. Puntambekar, P. V. Pesavento, and C. D. Frisbie, "Surface potential profiling and contact resistance measurements on operating pentacene thin-film transistors by Kelvin probe force microscopy," Appl. Phys. Lett. 83, 5539 (2003).
[84] A.R. Murphy, J. Liu, C. Luscombe, D. Kavulak, J.M.J. Fréchet, J.R. Kline, M.D. McGehee, "Synthesis, characterization, and field-effect transistor performance of carboxylate-functionalized polythiophenes with increased air stability," Chem. Mater., 17, 4892, 2005.
[85] J.J. Miasik, A. Hooper, B.C. Tofield, "Conducting polymer gas sensors", J. Chem. Soc., Faraday Trans. 1 82, 1117, 1986.
[86] K. Yoshino, H.S. Nalwa, J.G. Rabe, W.F. Schmidt, "The influence of nitric oxide, nitrous oxide and carbon monoxide on the electrical conductivity of polythiophene," Polym. Commun., vol. 26, pp. 103–104, 1985.
[87] T. Hanawa, S. Kuwabata, H. Hashimoto, H. Yoneyama, "Gas sensitivities of electropolymerized polythiophene films," Synth. Met., vol. 30, pp. 173–181, 1989.
[88] H. Sirringhaus, T. Kawase, R. H. Friend, T. Shimoda, M. Inbasekaran, W. Wu, E. P. Woo, "High-resolution inkjet printing of all-polymer transistor circuits," Science, 290, 2123, 2000.
[89] C. Arias, S. E. Ready, R. Lujan, W. S. Wong, K. E. Paul, A. Salleo, M. L. Chabinyc, R. Apte, Robert A. Street, Y. Wu, P. Liu, and B. Ong, "All jet-printed polymer thin-film transistor active-matrix backplanes," Appl. Phys. Lett., 85, 3304, 2004.
[90] W. Clemens, W. Fix, J. Ficker, A. Knobloch, and A. Ullmann, "From polymer transistors toward printed electronics," J. Mater. Res., 19, 1963, 2004.
[91] S.J. Higgins, F. Mouffouk, S.J. Brown, N. Sedghi, B. Eccleston, and S. Reeman, "Functionalized regioregular polyalkylthiophene for biosensing Applications," Organic Thin-Film Electronics, edited by A.C. Arias, N. Tessler, L. Burgi, and J.A. Emerson (Mater. Res. Soc. Symp. Proc. 871E, Warrendale, PA), I1.3, 2005.
[92] S.E. Molesa, A. de la Fuente Vornbrock, P.C. Chang, V. Subramanian, "Low-Voltage Inkjetted Organic Transistors for Printed RFID and Display Applications," Int. Electron Devices Meeting, Sec. 5.4, 2005.

Chapter 6: SENSOR ARRAY ENGINEERING

The gas sensor array is the core element of an electronic nose. Careful engineering of the sensitivity and specificity of individual sensing elements, as well as the collective range and discrimination of the sensor array as a whole, is thus the most crucial part of designing an electronic nose system. The ideal number of sensing elements to include in an array varies depending on the application, the specificity and range of each sensor, and the amount of correlation between sensor responses. It has been shown that the fundamental variances in analyte-sensor interactions can be summed up fairly well with as few as five molecular descriptors. Theoretically, then, five carefully chosen sensor materials should be enough for most applications. It is worth noting, however, that the human nose employs over 1000 olfactory sensors, and a canine's nose contains as many as 100 million olfactory cells. In practice, it is difficult to find sensors whose responses are perfectly orthogonal in the odor space of interest. Rather, correlation amongst sensors will necessitate an array size much greater than five. In practical systems, the redundant information provided by overlap in sensor responses is useful for robust operation in noisy situations as a safeguard against faulty readings [93].

The assembly of a suitable array typically involves a scavenger hunt for materials adequately similar to be fabricated, implemented, and read in the same way, but chemically different enough to provide a unique set of information about incoming vapors. The introduction of different dopants or other impurities into the same material is one simple method of differentiating sensor responses, though the range of discrimination achievable with this method is limited. With the advent of organic sensing materials, the use of synthetic chemistry

to generate new sensor materials has become a feasible tool as well, though synthesizing new molecules and predicting their chemical properties can often be a difficult proposition.

In this chapter, various strategies for diversifying sensor responses are reviewed. Then, a route for the generation of a library of functionalized polythiophene-based sensor materials is introduced, and used to synthesize four differently functionalized polythiophenes. These materials are soluble and can be solution processed, making them compatible with printed electronics. All materials are shown to exhibit good sensor responses to a range of volatile organic compounds, and differentiation of sensor responses is demonstrated. The process of functionalization retains the semiconducting properties of polythiophenes, but causes changes in sensor responses that can be easily detected using the OTFT structure.

6.1 Diversifying sensor response

For gas sensor arrays composed of conducting polymer chemoresistors, a variety of strategies for obtaining different sensor response have been employed. First, the starting materials for the polymer backbone can be chosen from a number of standard monomer building blocks, including single-ring heterocycles such as pyrrole, thiophene, or aniline as well as multiring fused or unfused heterocycles such as indole, and carbazole (see Figure 6.1). These starting monomers can be further diversified by attaching side groups [93]. Side groups can have a strong affect on molecular shape, energy band levels, charge transfer characteristics, packing, and intermolecular interactions in the final material. They have been extensively exploited to impart properties such as solubility, air stability, or self-organization. The response of the air stable polymer P1 to HCl (see Section 5.3) is a good example of how the functionality of side groups can affect sensor response. However, side groups can also interfere with the

polymerization process or have a disrupting effect on those electrical characteristics which are important to proper device functioning.

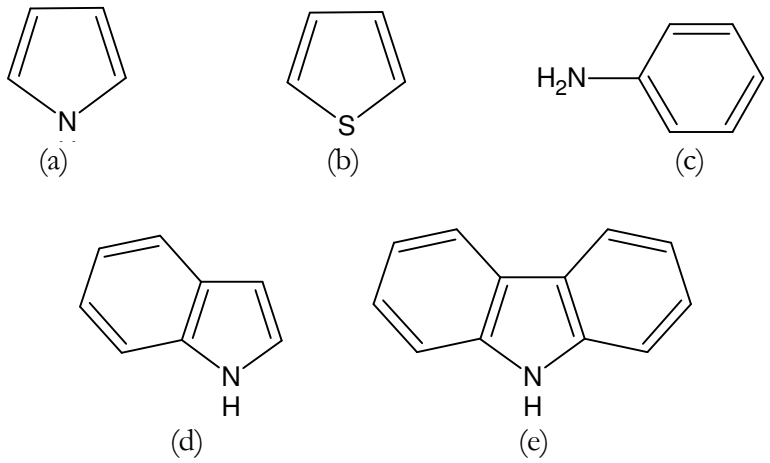

Figure 6.1: Different monomers that can be polymerized into conducting polymers.
(a) pyrrole, (b) thiophene, (c) aniline, (d) indole, and (e) carbazole

In conducting polymers which are deposited through electrochemical deposition, the introduction of different counterions during deposition and variation of polymerization conditions such as oxidation potential, temperature, solvent oxidant, and electrolyte or monomer concentrations can also have a drastic effect on final material properties [93].

6.2 Functionalization of polythiophenes

Though synthetic organic chemistry offers almost limitless possibilities for designing molecular structures, radically new structures are often difficult to make, and successfully synthesizing a new structure can take months or even years. Furthermore, the electrical and chemical properties of even the simplest electronic organic materials are enormously complex and difficult to model or predict. Even if a new molecule can be synthesized to order, its

functionality is not guaranteed, and will rarely be exactly as predicted. A better approach to tailoring the chemical sensitivity of organic sensor materials is to start with a material that is known to work as a sensor, and add different functional groups to it, preferably in locations which can modulate, but not disrupt, its ability to transport charge. Functional groups that interact strongly with specific vapors would be expected to cause a stronger electrical response to that specific vapor than to other ones, thus giving the material chemical specificity.

In this work, polythiophene has been chosen as a starting material due to its proven suitability both for gas sensors and printed electronics. To design an effective library of sensing materials, a systematic method of altering the P3HT sensor response is desirable. Adding side chains can be tricky, because this often requires significant changes in synthetic route, and may disrupt packing of the polymers, resulting in non-semi-conducting films. In contrast, adding functionalized end-capping groups is a fairly reliable way of altering sensor response without destroying the polymer functionality. This approach has been successfully used by Higgins, *et al* [94] to make polythiophene biosensors.

To create materials with different sensor responses, functional groups were attached onto end-capping groups.[1] The starting material, regioregular P3HT, was synthesized using a modified McCullough route [95]. This synthesis yields bromine groups on one end of 90% of the polymer chains. This bromine group provides an ideal reagent for Stille cross-coupling chemistry, which was used to attach aromatic compounds with protected functional groups to regioregular P3HT chains. The precursors were then converted to their respective active forms using appropriate deprotection methods revealing either carboxylic acid or amine

[1] All materials discussed in this chapter, including P3HT, were synthesized by Kevin Sivula and Christine Luscombe, chemists in Dr. Jean M. J. Fréchet's research group in the University of California Department of Chemistry. The details of the chemical synthesis routes are provided courtesy of Kevin Sivula.

functionalities (Figure 6.3 b-e). The general scheme for end-functionalizing P3HT is as follows:

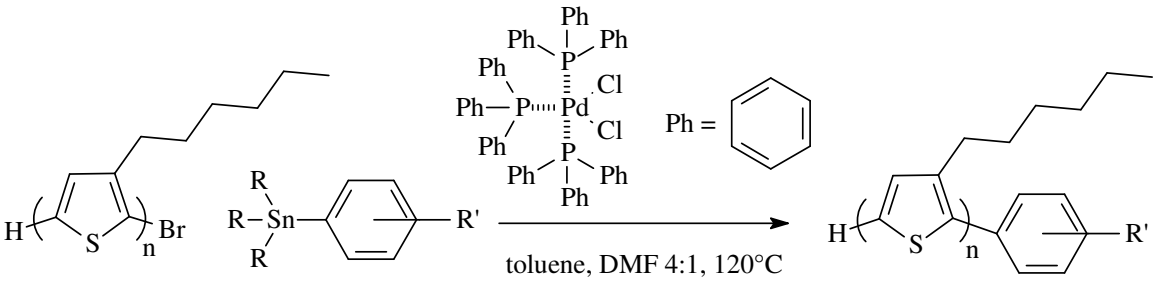

Figure 6.2: General pathway for the synthesis of end-functionalized P3HT.
R is either methane or butane, and R' is the desired functionality, with protecting groups where necessary.

Carboxylate and amine groups were appended onto the ends of P3HT (Figure 6.3a) chains with an end-group-to-monomer ratio of approximately 1:20 (Figure 6.3b,c) [96]. The difference in sensor response between the acidic carboxylic acid and basic amine groups were expected be most pronounced for polar analytes such as acids, bases, or alcohols. The effect of functional group placement on the sensor response was also investigated. Moving the NH_2 group one carbon out from the benzene ring to form P3HT-benzylamine (Figure 6.3d) increased the overall basicity of the molecule, and placing groups at the meta positions to form P3HT-benzyldiamine (Figure 6.3e) effectively doubled the concentration of functional groups. The resulting materials exhibited semiconducting properties and were soluble in organic solvents such as chloroform and dichlorobenzene.

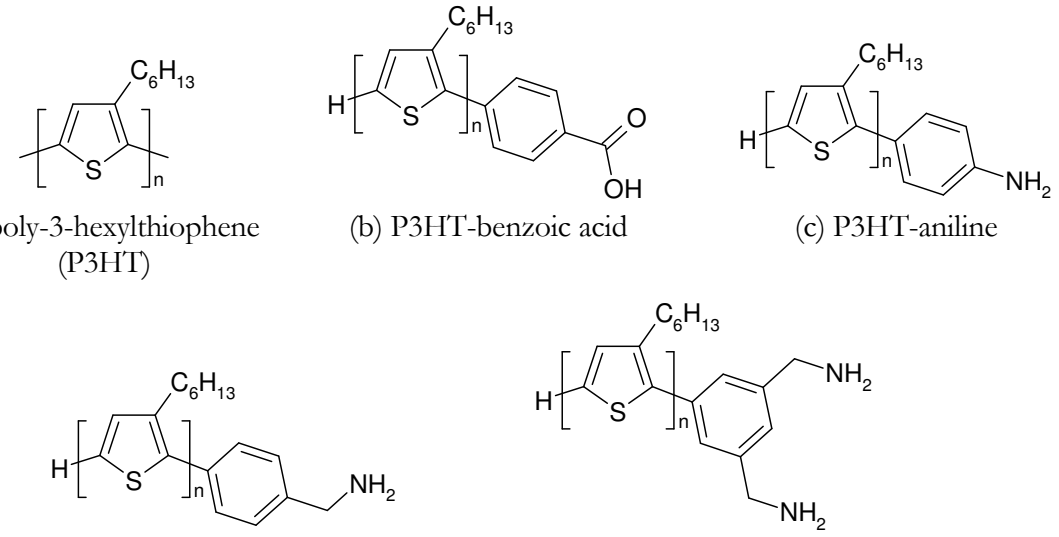

(a) poly-3-hexylthiophene (P3HT) (b) P3HT-benzoic acid (c) P3HT-aniline

(d) P3HT-benzylamine (e) P3HT- benzyldiamine

Figure 6.3: Functionalized P3HT sensor materials.
(a) Regioregular poly-3-hexylthiophene (P3HT) (b) P3HT-benzoic acid (c) P3HT-aniline (d) P3HT-benzylamine (e) P3HT- benzyldiamine.

6.3 Experimental setup

The polythiophene sensor inks were used as the active layer of substrated-gated, bottom contact OTFTs. A schematic cross section of the sensor devices is shown in Figure 5.1. A heavily doped silicon wafer with 65 nm of thermally grown wet oxide was used as a starting substrate. Source and drain electrodes were defined in photoresist using photolithography, and the pattern transferred to a metal layer using lift-off techniques. The contact metal layer consists of 2.5 nm of chrome evaporated at 0.5 nm/s at high vacuum ($\sim 10^{-7}$) , followed immediately by 100 nm of gold, also evaporated at 0.5 nm/s at high vacuum. These prepared substrates were then cleaned using acetone and isopropyl alcohol and stored for later use.

The active materials were dissolved in anhydrous chloroform at concentrations of 4-5mg/mL, with slight heating used to accelerate dissolution. They were then passed through a 0.45μm

filter and spun-cast at 4500 rpm onto the prepared substrates. Before spinning, the substrates were baked on a hot plate for 2 minutes at 120ºC, and then cooled to room temperature. After spinning, samples were annealed on a hot plate at 120ºC for 20. Devices were spun, annealed, and stored in a nitrogen environment, but exposed to and stored in air for at least 1 hour before sensor experiments.

Sensors were operated at room temperature in an isolated chamber with controlled gas flow (Figure 5.3), probed remotely with an HP 4145 parameter analyzer, and analyzed using custom Matlab scripts. These scripts allowed the real-time extraction of I_{on}, μ_{FET}, and V_T from the high-$|V_{GS}|$ portion of the saturation transfer curves. Devices were probed at a 3% duty cycle to avoid bias stress. A fan within the chamber ensured swift distribution of gas analytes, and purging was performed using compressed air, which provided consistent ambient humidity.

6.4 Results

OTFTs formed from all materials had starting μ_{FET} values in the 10^{-4} to 10^{-3}cm^2/V-s range, including P3HT. This is much lower than the μ_{FET} values of 10^{-1} cm^2/V-s that are typically reported in literature, probably due to a lack of structure or material optimization. In these structures, current (and thus extracted μ_{FET}) are probably limited by non-idealities such as contact resistance or disorder in the semiconductor film. Careful optimization studies to determine the maximum μ_{FET} of the new sensor materials were not performed, so it is not possible to say whether the end group functionalization had an impact on charge transport properties. However, their suitability for sensing applications was confirmed. Figure 6.4 shows a typical time response of an array of functionalized polythiophene OTFTs to increasing concentrations of acetic acid.

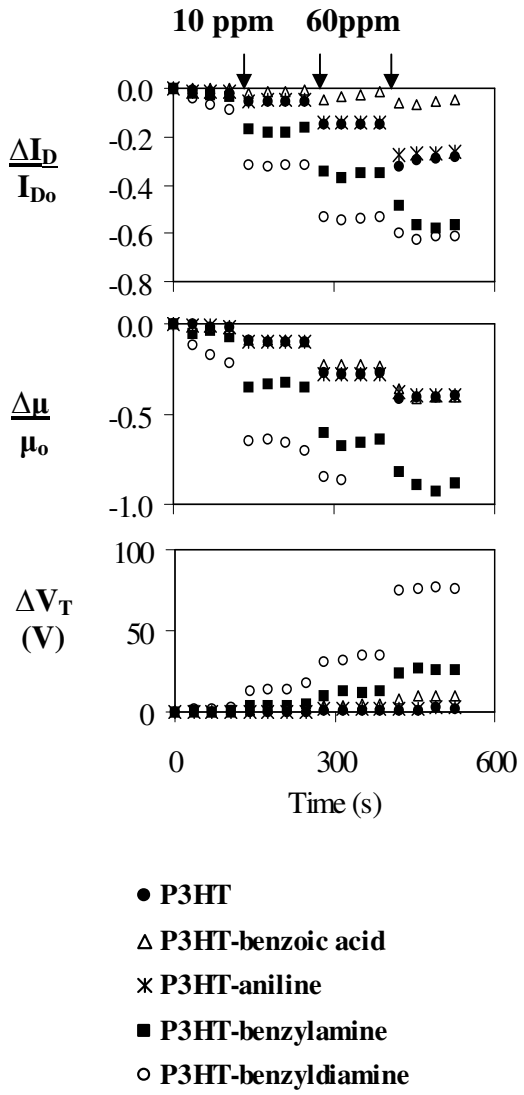

Figure 6.4: Time response of polythiophene OTFTs to increasing concentrations of acetic acid.
Relative ΔI_D at $V_{GS}=V_{DS}=-20V$, extracted charge mobility, and threshold voltage, are shown.

By correlating these plots with known concentrations of gas analytes, calibration curves matching sensor response to analyte concentration can be constructed. An example is shown in Figure 6.5. These calibration curves are stored in a reference library, and used for identification of unknown odors.

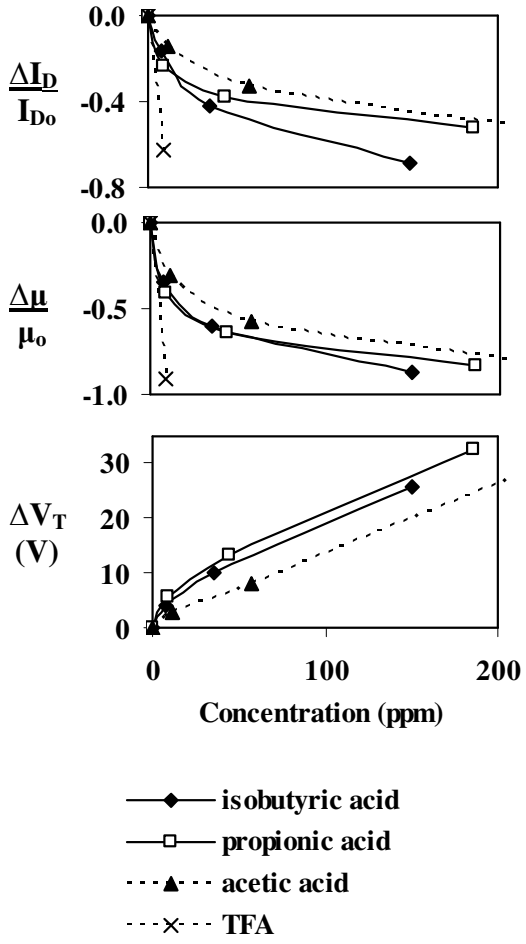

Figure 6.5: Sensor response calibration curves.
The multiparameter response of a P3HT-benzylamine OTFT gas sensor to a range of acidic analytes is shown.

A cross section of the library of reference calibration curves taken at 40 ppm analyte concentration is shown in Figure 6.6. The functionalized polythiophenes showed significant sensor response differentiation from P3HT, as desired for electronic nose application. P3HT-aniline exhibited the most similar responses to P3HT. This could be due to a weakening of the functionality of the aniline group due to its π-conjugation with the backbone thiophene system.

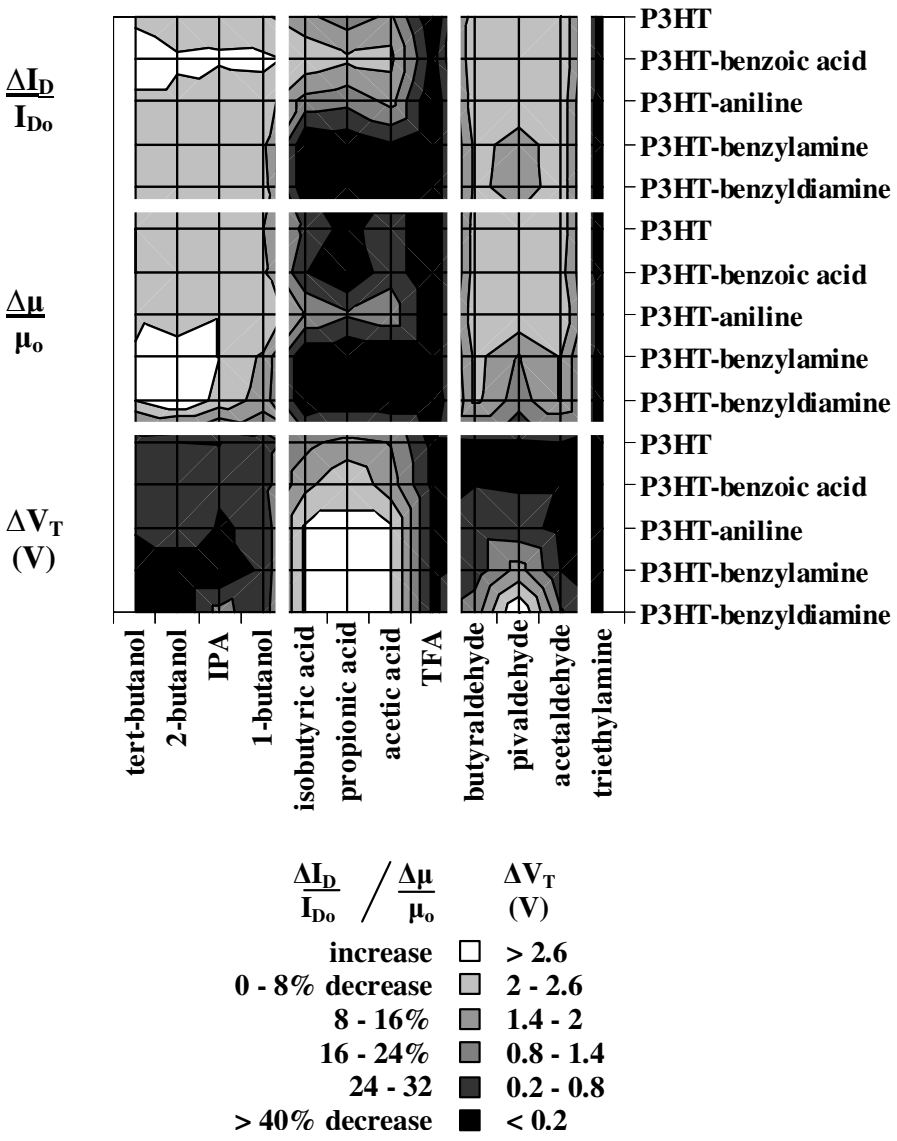

Figure 6.6: Total sensor array response to a variety of chemicals.
Baseline operation is established for operation in ambient conditions, and sensor response is measured after a 2 minute exposure to 40 ppm of each analyte.

P3HT-benzylamine responded significantly more strongly than P3HT to all analytes tested, and P3HT-benzyldiamine responded similarly but even more strongly than P3HT-benzylamine, as expected due to its higher concentration of functional groups. P3HT-benzylamine and -benzyldiamine showed particularly strong responses to carboxylic acids, a

result that is predicted by to the basicity of the amine functional group. The sensor responses of P3HT-benzoic acid were milder than that of the -amine materials, but were also the least correlated to the responses of the other materials. This is particularly true for alcohol analytes, in which the acid and bases exhibited nearly opposite responses (Figure 6.7). While P3HT-benzoic acid responded to all alcohols with increased I_{on}, P3HT-benzylamine and P3HT-benzyldiamine both exhibited strong I_{on} decreases. Since μ_{FET} responses are qualitatively similar, the disparity is caused predominately by V_T shifts in generally opposite directions, indicating a differential change in dopant concentration, interface charge distribution, or trap distribution.

This difference in sensor responses of the functionalized P3HT materials confirms that the added functional groups do, indeed, participate in and modify the sensor response. These functional groups may modify sensor response by changing the solubility of analytes in the sensor, thus affecting the partition coefficient of the analyte-sensor system. Alternately, charge transfer or other forms of direct interaction between the functional group and the analyte are possible. It is anticipated that other functional groups, such as thiols, alkyl halides, or phosphates may also elicit distinct sensor-analyte interactions. In designing new materials, it is interesting to note that the effects on sensor response of the functional groups studied here were all fairly consistent with predictions that would be made based on the electronegativity and concentration of the functional group. The well-known chemistries of most fundamental functional groups should therefore make it possible to design a sensor array in a fairly systematic fashion.

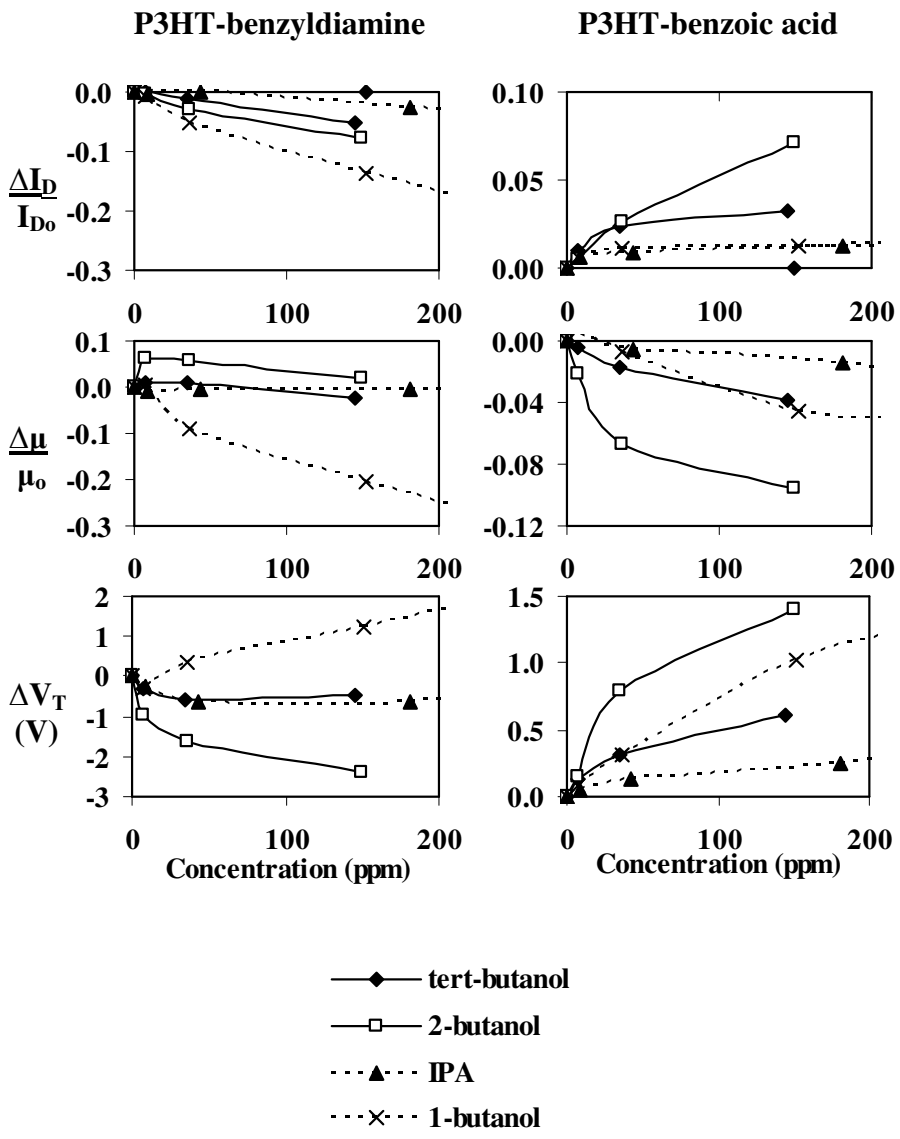

Figure 6.7: Comparison of the P3HT-benzyldiamine and P3HT-benzoic acid response to a collection of alcohols. The sensors show qualitatively opposite responses in I_{on} and V_T.

In a gas sensor array, sensor responses that are specific to a particular analyte-sensor pair are useful for enhancing the specificity and discriminatory power of the array. Our results so far seem to indicate that analyte-sensor interactions do play a role in OTFT sensing. Here, we study the extent of analyte-sensor response specificity using the methods outlined by Bissell *et*

al [97]. The gas phase concentration required to produce a 2.5% drop in I_D (C_g) was plotted against the saturated vapor pressure of the analyte at room temperature (SVP) in a log($1/C_g$) vs. log (1/SVP) plot, revealing a linear relationship for the response of P3HT-benzylamine and P3HT-benzyldiamine to a series of alcohols and carboxylic acids with varying steric hindrance (Figure 6.8a). The linear relationship between log(1/SVP) and log ($1/C_g$) here indicates that the sensor response is not sensitive to differences in molecular size, shape, or functionality in these cases, and that the dominant cause of differential sensor responses to the various analytes is differential diffusion of the analyte into the sensing material.

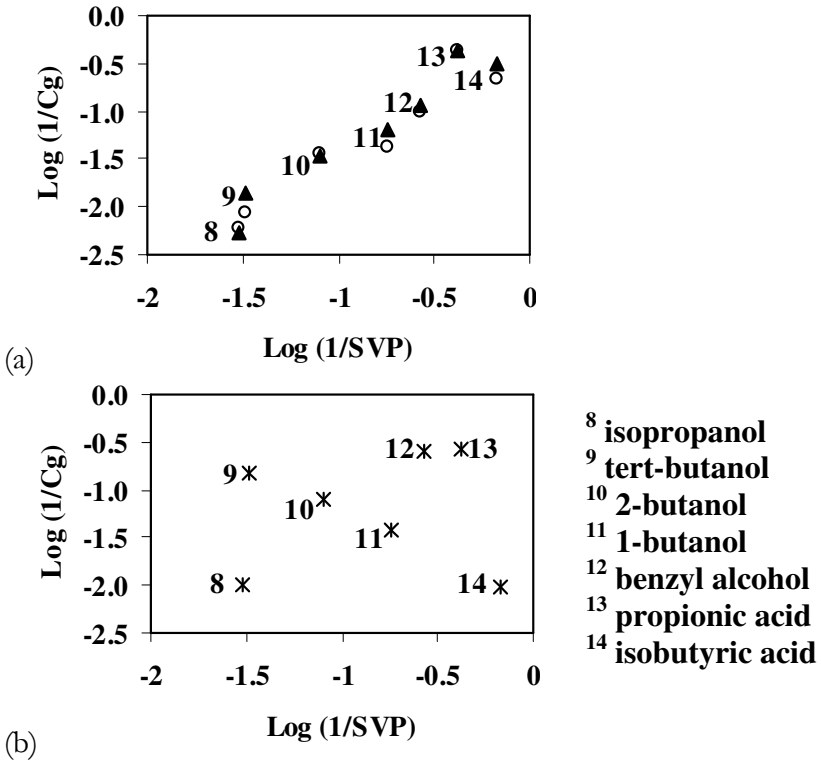

Figure 6.8: Specific and non-specific partitioning of alcohols and carboxylic acids into functionalized P3HT.
The sensor response at the $\Delta I_D/I_{Do}$=2.5% level is used. (a) Response of P3HT-benzylamine (○) and P3HT-benzyldiamine (▲) to a range of alcohols and carboxylic acids with varying steric hindrance also appears to be diffusion-controlled. (b) On the other hand, P3HT-benzoic acid (*) appears to have a non-volatility driven sensor response to the same set of alcohols and carboxylic acids.

The sensor response of P3HT-benzoic acid (Figure 6.8b), however, was clearly not driven by analyte volatility. This is consistent with the fact that the P3HT-benzoic acid sensor response was very different from the other polythiophene-based sensors, especially for alcohol analytes. P3HT-benzoic acid is the only material to show an increase rather than decrease in I_{on} when exposed to alcohol. The lack of correlation between SVP and C_g and the increase in I_{on} in response to alcohols both indicate that the sensor response is not driven by mechanical effects such as swelling. This result is particularly interesting, because it confirms that adding functionalized end groups with end-group-to-monomer ratios as low as 1:20 can both quantitatively and qualitatively change the sensor response of polythiophene OTFT gas sensors.

6.5 Conclusion

An array of soluble, semiconducting, functionalized polythiophene materials were generated by the incorporation of functionalized end-capping groups. When used as the active layer in OTFT gas sensors, these materials exhibited differential sensor responses which allow discrimination between a range of analytes including alcohols, carboxylic acids, aldehydes, and amines. Differentiation in the sensor response followed patterns consistent with the chemical nature of the functional group, meaning that the sensing behavior of other differently functionalized polythiophenes may be predicted to some extent. The solubility of the poly-alkyl-thiophene starting materials was retained during the functionalization process, making these sensor materials potentially compatible with print-based fabrication processes. Chapter 7 explores the exploitation of this property, using the functionalized polythiophene sensor materials presented in this chapter to make integrated sensor arrays with fabrication techniques compatible with low-cost manufacturing.

6.6 References

[93] K.J. Albert, N.S. Lewis, C.L. Schauer, G.A. Sotzing, S.E. Stitzel, T.P. Vaid, and D.R. Walt, "Cross-Reactive Chemical Sensor Arrays," Chem. Rev., 100, 2595, 2000.

[94] S.J. Higgins, F. Mouffouk, S.J. Brown, N. Sedghi, B. Eccleston, and S. Reeman, "Functionalized regioregular polyalkylthiophene for biosensing Applications," Organic Thin-Film Electronics, edited by A.C. Arias, N. Tessler, L. Burgi, and J.A. Emerson (Mater. Res. Soc. Symp. Proc. 871E, Warrendale, PA), I1.3, 2005.

[95] J. Liu, R.D. McCullough, "End Group Modification of Regioregular Polythiophene through Postpolymerization Functionalization," Macromolecules, 35, 9882, 2002.

[96] J. Liu, T. Tanaka, K. Sivula, A.P. Alivisatos, and J.M.J. Fréchet, "Employing End-Functional Polythiophene To Control the Morphology of Nanocrystal-Polymer Composites in Hybrid Solar Cells," J. Am. Chem. Soc., 126, 6550, 2004.

[97] R.A. Bissell, K. C. Persaud and P. Travers, "The influence of non-specific molecular partitioning of analytes on the electrical responses of conducting organic polymer gas sensors," Phys. Chem. Chem. Phys., 4, 3482, 2002.

Chapter 7: LOW-COST INTEGRATION

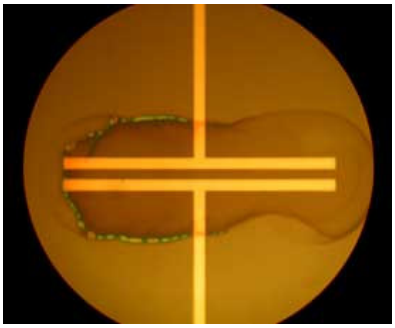

Figure 7.1: OTFT gas sensor with ink-jet printed active layer.

A major reason for the high cost of electronic noses is the difficulty of integrating multiple sensors and their signal processing support circuitry onto a single substrate. In traditional electronics, putting many different materials onto the same substrate is expensive because yield decreases quickly with the number of different materials integrated into a fabrication process, and traditional fabrication techniques require extensive subtractive processing. Many electronic nose systems forgo integration altogether and simply wire together separate sensing elements. Furthermore, signal processing in modern electronic noses is often done on a computer microprocessor, and is not integrated into the sensing systems.

The motivation behind the development of solution-processable sensor "inks" in Chapter 6 was to enable the use of low-cost fabrication methods such as printing for the construction of OTFT gas sensors. Using an inkjet printer loaded with cartridges of different sensor inks, integrating multiple sensor materials onto the same substrate could be as simple as printing a multi-colored cheese wrapper. These inks could be printed directly onto silicon chips containing circuitry for signal processing, or for an all-printed solution, they could be paired with OTFT-based circuitry.

In this chapter, techniques that have been developed for the integration of sensor arrays are reviewed. Then, an overview is given of concepts relevant to printed electronics, including ink development, printing techniques, and roll-to-roll fabrication. Finally, the construction of an integrated sensor array on a silicon substrate using the materials developed in Chapter 6 is presented. Simple circuitry for proving signal processing using integrated circuit components connected on a prototyping breadboard is also demonstrated. The next step, incorporation of OTFT-driven signal processing, will be discussed in Chapter 8.

7.1 Previous work on integrated sensor arrays

The drive to lower the cost of sensor arrays began as soon as the technology first appeared. Because silicon-based circuitry is the most widely available and well-developed electronics solution, a majority of this work focused on ways of integrating sensor components into existing silicon microfabrication processes. Compatibility with CMOS processes and process simplicity are the two main factors that would help to lower cost. In addition, solution processing of other sensors based on other classes of materials such as conducting polymers or composite materials such as carbon black mixtures have been pursued.

7.1.1 Microfabricated metal oxide sensors

Most reports of integrated gas sensor arrays are based on the integration of inorganic metal oxide sensors into traditional microfabrication process flows. This would lower costs by allowing sensors to be easily integrated with silicon processing circuitry. The primary challenges were to satisfy the need for high temperature operation of metal oxide sensors and to provide material differentiation on a single substrate. Typically, high temperatures are provided by resistive heating elements. To achieve high enough temperatures at reasonable

power dissipation, these heater are placed together with the sensing metal oxide thin-films on suspended thin silicon nitride membranes, which reduces the volume of material to be heated and thus increases the heating efficiency of the resistor [98][99]. More recently, the use of surface micro-machined micro-hotplates has been proposed in which the silicon nitride membranes are replaced with a more sophisticated suspended hotplate structure [100]. Sensors constructed on suspended silicon bridges have also been demonstrated [101].

A variety of strategies have been demonstrated for achieving sensor diversity in integrated metal oxide sensor arrays. Gardner *et al* drop-casted suspensions of differently doped tin oxide onto an integrate chip which was then annealed at 600ºC to form polycrystalline films [98]. The solution-based deposition used here is interesting for low-cost manufacturing, though the high temperature anneal required afterwards is not compatible with low-cost substrates. Around the same time, Nayak *et al* [102] used sputtered tin oxide sensors with successive layers of photoresist masking to create four differently doped sensors on a single substrate. These sensors were shown to be able to distinguish between various alcohols and alcoholic beverages [103]. Moon *et al* [101] also used photolithography and masking layers to pattern adjacent areas of copper oxide- and platinum-doped tin oxide films. While effective, this fabrication method requires multiple masking layers and numerous processing steps, and is thus time-consuming and expensive.

Carné *et al* fabricated an array of three tin oxide gas sensors, each paired with an independently controlled heater. By heating the films to different temperatures, differential sensor responses were obtained [99]. However, responses were still highly correlated due to the use of the same sensing material for all sensors. Ehrmann *et al* demonstrated a simplified method of generating sensor arrays through the used of continuous gradients. Differentiation was introduced by

operating the sensors with an applied temperature gradient, or by coating the sensors with a layer of silicon dioxide with a graded thickness. Tin oxide and tungsten oxide sensor arrays were demonstrated, and shown capable of differentiating between normal human breath and bad breath. The simplicity of this approach offers the potential of lowered fabrication costs, but again, the use of a single material limits the range of sensor diversity achievable through the gradient technique.

Another variable that can be modified is the grain size of a thin film sensor material. Taurino *et al* [104] demonstrated that a supersonic cluster beam of titanium could be used to deposit titania films with controlled nanocrystalline grain size. Varied grain size resulted in correspondingly varied sensitivity and selectivity. The resulting sensors were used to successfully distinguish between methanol, propanol, and ethanol. Differential sensitivity can also be achieved with the same materials by taking advantage of different transduction mechanisms. Hagleitne *et al* [105] fabricated an integrated sensor chip which monitored three separate transduction mechanisms in metal oxide films. A micromachined resonating cantilever provided information about the mass of sorbed analytes, a thermoelectric calorimeter monitored the heat of absorption, and a capacitive responded to changes in the volume and dielectric properties of the sensing layer with sorbed analytes. The most impressive aspect of this demonstration was its integration with on-chip signal conditioning and analog/digital conversion. The use of three separate transduction mechanisms did, indeed provide orthogonal sensor information, and significantly enhanced the amount of information obtainable from a single material. However, the integration of multiple materials is still difficult, and the range of the array is thus still limited.

7.1.2 Conductive polymers

Conducting polymer arrays for gas sensing with multiple sensing materials integrated on a single substrate were demonstrated in the early 1990's. In 1994, Hatfield *et al* fabricated a sensor array with ten different conducting polymers deposited on a ceramic substrate and integrated with a custom designed application specific integrated circuit (ASIC) for signal processing. To construct the sensor array, gold electrodes were patterned on the ceramic substrates using photolithography, and a seed layer of polypyrrole was deposited and patterned, also using photolithography. Then, the array was attached to a customized ASIC, which controlled the sequential, localized electrodeposition of the various conducting polymers. The ASIC also controlled operation of the array during measurement. Localized electrodeposition has been widely used for the fabrication of conducting polymer arrays, and is cheaper than sequentially sputtering and removing multiple inorganic materials for metal oxide sensors. However, the sequential process of electrodepositing different polymers is time-consuming and the sensitivity of the process to deposition conditions makes batch processing difficult. Recently, an alternate technique was demonstrated in which localized electropolymerization of conducting polymers was achieved by applying a bias between electrodes in a monomer vapor [107]. This method has the advantage of self-alignment, since the polymers only deposit between the electrodes, and are automatically aligned to them. The vapor-based deposition is also compatible with other microelectronics techniques.

The use of conducting polymers as gates for otherwise traditionally fabricated silicon devices is another effort to integrate the sensitivity of conducting polymers into stream-lined CMOS technology. Polk *et al* demonstrated the integration of CMOS-based sensors and signal processing units in 1999 [108]. To maintain wafer-level processing for the structures, they

suggested the fabrication of all gates out of the same conducting polymer, polyaniline, and the employment of post-processing modifications to adjust sensitivity. Options for such modifications include electrochemical anion exchange, soaking in dopant solutions, or exposure to radiation such as ultraviolet light [109].

7.1.3 Carbon black arrays

While conducting polymers have the potential to be soluble, the majority of conducting polymers used for sensing today are not soluble. Polymer composites, however, are a related class of sensing materials that are typically solution processed. This class of materials refers to mixtures of a conductive filler, either carbon black or polypyrrole, and a non conductive, but chemically sensitive polymer.

Polypyrrole composites are fabricated by chemically polymerizing pyrrole in solution in the presence of the insulating polymer. The resulting solution is then dip cast or spin-cast to form thin films [110]. Carbon black composites are constructed by suspending conductive carbon black powder in a solvent containing the insulating polymer. The ratio of conductive to insulating material is chosen to be near the percolation threshold, that is, the minimum amount of conductive material is used such that conduction through the film by percolation of charge along networks of connected conductive material clusters is still possible [111].

While both polypyrrole and carbon black composites are solution-processed, there have been no reports of using inkjet printing to deposit these materials. Rather, they are either spun-cast, dip cast, or drop cast [113]-[115]. Drop casting using syringes has been used to demonstrate arrays of carbon black sensors integrated onto a single chip. To achieve better sensor uniformity and smaller dimensions using drop casting, Zee *et al* used a substrate with isolated

wells micromachined between electrodes. Sensor materials were deposited by filling each well with a different carbon black polymer composite and allowing it to dry. The wells improved control over film positioning and thickness [116]-[118].

7.2 Printed electronics

Roll-to-roll manufacturing based on print-based patterning of electronically active inks offers the tantalizing prospect of ultra-low-cost electronics. While it is unlikely that any technology will ever compete with silicon-based electronics at a cost-per-transistor level, printed electronics remains a potentially disruptive technology in the area of large-area, flexible electronics with low performance requirements. Engineers and business analysts alike agree that printed electronics are nearing its last stages of development before commercialization. Technologies nearing production include printed displays, memories, batteries, OTFTs, and photovoltaics [119]. Among the earliest products to go to market are all-printed displays, including printed OTFT backplanes, to be introduced by Plastic Logic in the first half of 2006 [120].

Due to the unique demands of printed electronics, throughput for printing of electronics still lags far behind that of printed graphic arts. For example, Plastic Logic's initial prototype manufacturing line, including inkjet printing and laser patterning, is not roll-to-roll, and will only support a throughput of 100 35cmX35cm substrates per week [120]. So far, the fastest demonstrated process, unveiled in late 2005 by the Institute for Print and Media Technology at Chemnitz University in Germany, can produce all-printed OTFT-based ring oscillators at the rate of at 0.8 m/s [121]. This relatively high throughput is obtained at the price of

performance, however. The mass-printed circuits have a structural resolution of 100 μm, which limits the speed of these ring oscillators to 1 Hz.

Though progress in this field has been promising, significant infrastructure, materials, and technological developments are necessary before ultra-low cost printed electronics becomes a reality. In this section, candidate printing technologies are compared, and the issues associated with electronic ink development are reviewed.

7.2.1 Printing techniques

Technologies being evaluated for printed electronics include contact techniques such as flexography, gravure printing, and screen printing as well as digital printing techniques such as thermal and inkjet printing. Each technique is associated with unique ink specifications, set-up and equipment costs, pattern fidelity, resolution, field size, overlay accuracy, throughput, and patterning flexibility.

Flexography is a low-cost technique currently used for printing everything from grocery bags to cardboard boxes, frozen food packages, and business envelopes. Raised images of the desired patterns are created on a flexible plate, which is then attached to a rotating cylinder. During printing, the patterned plate is simultaneously rolled against another cylinder which transfers a uniform layer of ink to the raised surfaces and a substrate upon which the pattern is printed. Flexographic plates are robust and relatively inexpensive to make, easy to operate, relatively tolerant of substrate roughness, and can print substrates at rates of up to 1500 feet per minute. One major advantage of flexography for printed electronics is the ability to control film thickness of the printed ink, allowing uniform coverage of large areas. However, pattern fidelity suffers from distortion of the flexible plate during printing, and a resolution of 76 μm

is the best that has been demonstrated. Thus, this technique would be best suited for the high-speed printing of large features with loose dimensional requirements [122].

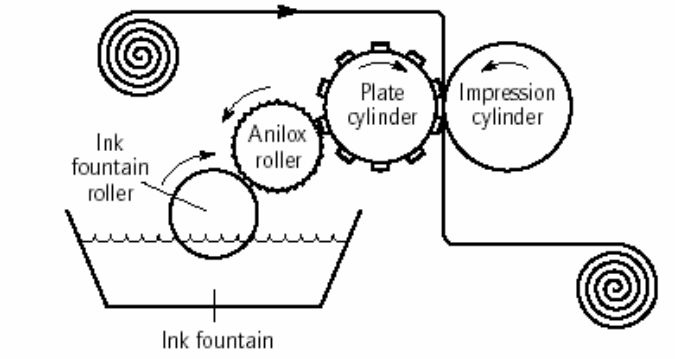

Figure 7.2: Schematic flexography printing process.
(Courtesy: Pira)

Unlike flexography, patterns in gravure printing are engraved to form a recessed blueprint on a metal cylinder. During the printing process, the surface of the roll is covered with ink, which is then scraped off of the non-recessed portions of the surface with a doctor blade. The remaining ink is then transferred to a substrate as the cylinder is rolled across the substrate. Gravure printing provides high print quality, good pattern fidelity, long cylinder lifetime, and line resolution down to 15 μm. It can provide a maximum throughput of around 300 fpm, and at slower speeds, can achieve a registration tolerance of up to 50μm. However, it has a low tolerance for substrate roughness, and can suffer both from unpainted spots where the ink fails to transfer and misplaced spots of ink in areas where the doctor blade fails to completely remove the ink. Because of its resolution, registration, and throughput, gravure is one of the most likely candidates for large area printed electronics [122].

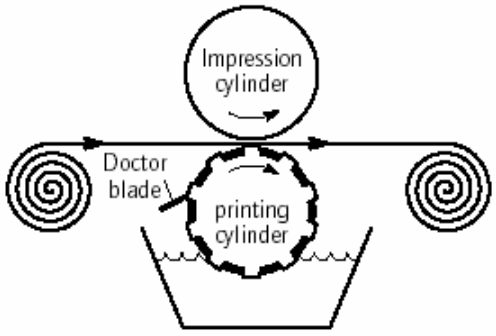

Figure 7.3: Schematic gravure printing process.
(Courtesy: Pira)

Screen printing involves dragging a layer of ink across the surface of a screen which is in contact with the substrate. A pattern of holes in the screen allows ink to be selectively transferred to the substrate only in localized areas. This technique is already widely used in the microelectronics industry for the manufacture of printed wiring boards. Its main advantage is flexibility. Screen printing is efficiently employed used both for small scale and large scale operations, is compatible with a wide range of inks and substrates, and can print layers with thickness ranging from less than one micron to hundreds of microns.

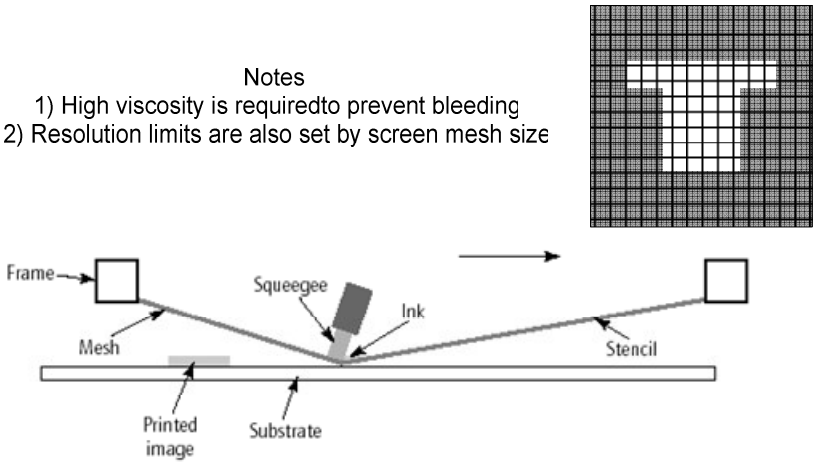

Figure 7.4: Schematic screen printing process.
(Courtesy: Pira)

Compared to the printing methods already discussed, digital printing with techniques such as thermal or inkjet printing is a relatively modern technology. Patterning is achieved directly from a computer image, and does not require a physical mask or pattern, providing flexibility, fast prototyping, a small overhead per run, and quick turnaround. In thermal printing, dye is selectively transferred from a carrier film to the substrate through localized heating and sublimation. While a few electronic materials such as pentacene are amenable to such a sublimation process, most are not. Therefore, inkjet printing is considered to have a greater potential for use with electronics.

In inkjet printing, droplets of ink are physically propelled towards a substrate, and patterning is achieved by adjusting the relative positions of the print head and substrate between each drop deposition. Ink droplets can be supplied in three ways. In continuous inkjet printing, a stream of droplets is passed through a set of electrodes, which selectively deflect single droplets towards the substrate when needed. This method typically has poor drop placement accuracy, and is used in low-cost applications. Alternately, ink can be fed into piezo-electric crystal or bubble jet print heads, which offer the ability to generate droplets on demand. The application of a voltage to the piezo-electric print head initiates a pressure wave which forcefully expels a controlled amount of ink. In bubble jet printing, a similar forceful expulsion of droplets is powered by the thermal expansion of a gas bubble created by the local boiling of the ink using a high speed, localized heater.

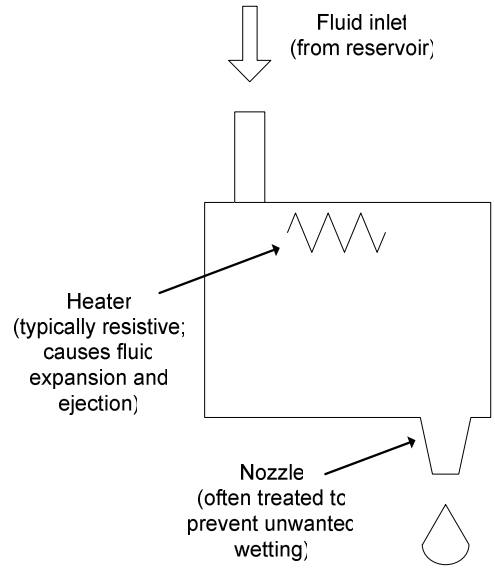

Figure 7.5: Schematic bubble inkjet printing system.
(Courtesy: Pira)

So far, most demonstrations of printed OTFTs have been based on piezo-electric inkjet printing. Because of the serial nature of inkjet printing, throughput is lower than in roll-based techniques such as gravure. Also, the digital nature of the patterning makes inkjet less adept at forming uniform, smooth films over large areas. On the other hand, drop size, drop placement accuracy and alignment to other features can be continually monitored and adjusted during printing, and the resolution and registration of inkjet printing has the potential to exceed other printing techniques. Moreover, the use of multiple print heads allows simultaneous printing of different inks, which makes inkjet printing ideal for the deposition of small quantities of many different materials next to each other, as is required for gas sensor arrays [123]. A final advantage of ink-jet printing is that it requires lower viscosity inks than most other printing methods, allowing the elimination of binders or other additives which are typically used to thicken inks. This allows the printing of higher purity films.

7.2.2 Electronic inks

One of the most critical steps in setting up a printing process is ink design. Printing method, substrate, and desired characteristics of the final film all place constraints on the ink properties. The printability of an ink is largely determined by its rheology and surface energy. In addition, the final characteristics of the dried film are affected by the drying speed and adhesion/cohesion interactions.

The rheology of an ink refers to how "thick" or "thin" it is, that is, how it deforms and flows under varying conditions of applied force, temperature, and shear. For pattern transfer techniques such as flexography or gravure, the ink must be thick enough to remain on the cylinder even when held sideways or upside down. For inkjet, on the other hand, the ink should be thin enough to flow easily through the print head and tubing leading up to the print head.

Surface energy is one factor which determines whether the ink will tend to bead up or spread out on a given surface. Other factors include the surface energy of the substrate and the interfacial tension between the ink and the substrate. Thus, the desired surface energy of an ink depends on the properties of the surfaces it will come in contact with, including plates or cylinders for pattern transfer, print heads, and substrates. For this reason, it will often be necessary to customize inks to specific processes, especially when printing on different substrates or layering materials over one another. The final ink-substrate surface interactions affect the thickness of the printed films, pattern fidelity, and minimum achievable resolution.

In flexography and gravure, inks are typically based on water, organic solvents, or UV curable polymers, and a viscosity of 0.05 to 0.5 Pa-s is required. Inks must be designed to adhere

preferentially to the substrate over the patterned cylinder. High viscosity inks provide better pattern fidelity, especially for gravure, while low viscosity inks spread across the substrate more readily, providing a smoother, more uniform film over large areas. Screen printing is compatible with a much wider range of ink viscosities [122]. Ideally, an ink should have a high viscosity at rest and a low viscosity during sheer. In inkjet printing, drop expulsion depends on a complex set of interactions between the ink and the print head, and compatibility between the two materials is especially important. The two must often be mutually engineered for compatibility with each other. When ink properties are constrained by the electronic material to be printed, engineering must focus on using coatings to modify surface properties of the cylinder or print head [123].

7.3 Droplet-on-demand integrated sensor array

For the sensor material evaluation described in Chapters 5 and 6, sensors were fabricated using spin-coated active layers. While spin-coating is a useful tool for testing new materials due to its simplicity, it is not a suitable technique for fabrication of integrated sensor chip arrays, in which multiple sensing materials on a single substrate are required. In this situation, inkjet printing is an ideal approach.

The solubility of the functionalized polythiophenes developed in Chapter 6 makes them compatible with inkjet printing, but the development of solutions suitable for printing requires further engineering of ink characteristics. While printing of polythiophenes has been demonstrated by other groups [120],[124]-[126], the development of inks is highly specific to the inkjet heads and substrates used, and it is thus non-trivial to reproduce such results (see Section 7.2.2). Thus, for this work, high precision droplet-on-demand using micropipettes

mounted on micromanipulators was used to simulate inkjet printing. P3HT, P3HT-benzoic acid, and P3HT-benzylamine inks were prepared by dissolution into anisole at concentrations of 4mg/mL, with mild heating used to promote solvation. Solutions were filtered, and then deposited onto adjacent prepatterned gold electrodes on prepared substrate-gated, bottom-contact silicon substrates. While inkjetted films with thicknesses comparable to spun-cast films have been demonstrated using smaller droplet volumes and more dilute inks, the films generated using this droplet-on-demand technique resulted in films that were approximately ten times thicker than the spun-cast films.

Material deposition was performed in nitrogen, and after deposition of all three materials, the integrated chips were annealed in nitrogen at 120ºC for 20 minutes. The chips were stored in nitrogen for up to two weeks, and removed to air at least an hour before testing.

The integrated OTFT sensor chips were tested for sensitivity to a range of volatile organic compounds, including tert-butanol, hexanol, isobutyric acid, acetic acid, and hexylamine. Sensing tests were performed at room temperature in an isolated chamber with controlled gas flow (Figure 5.3), probed remotely with an HP 4145 parameter analyzer with a 3% duty cycle to avoid bias stress. I_{on}, μ_{FET}, and V_T were monitored in real-time. A fan within the chamber ensured swift distribution of gas analytes, and purging was performed using compressed air, which provided consistent ambient humidity.

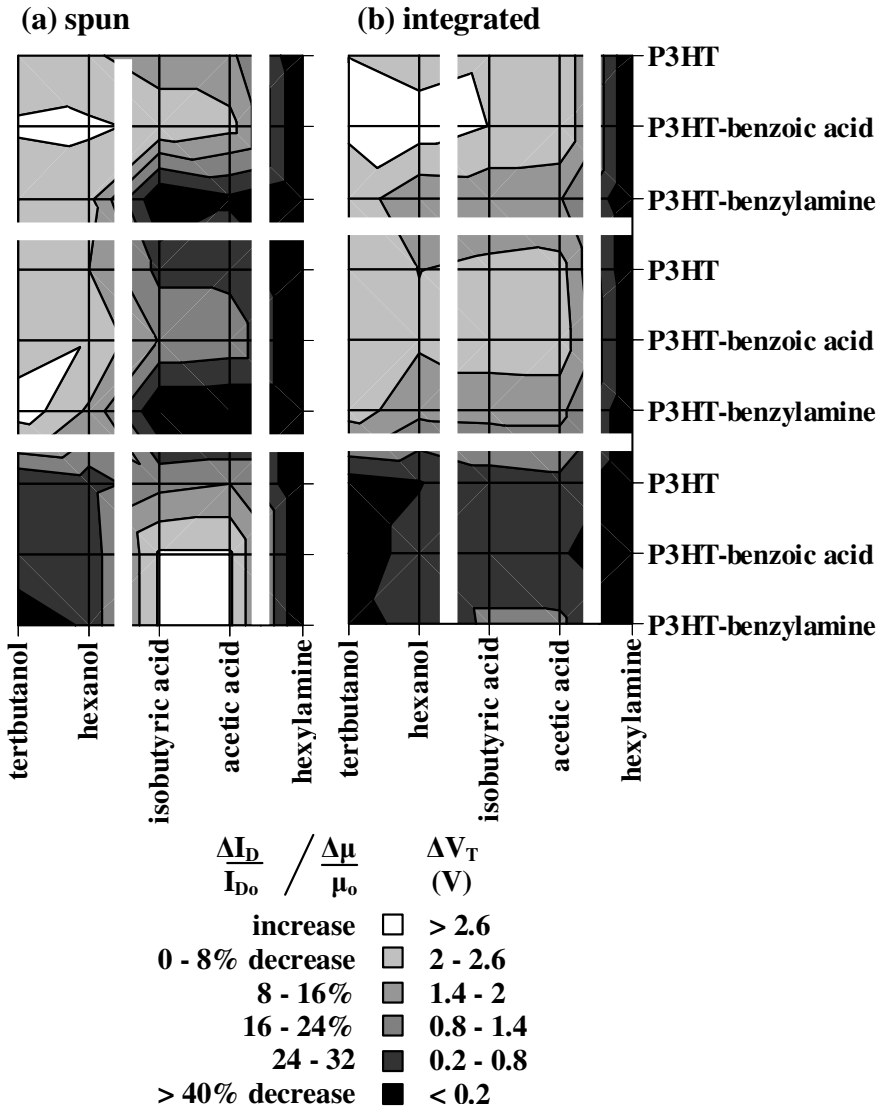

Figure 7.6: Comparison of integrated (drop-cast) and spun-cast gas sensor array.
Total array response of (a) a non-integrated, spin-coated array and (b) a droplet-on-demand, integrated array. The active layer of the drop-cast devices are approximately 10x thicker, resulting in a similar, but muted sensor response.

The integrated OTFT gas sensors suffered from degraded uniformity and yield, but operated properly, exhibiting sensor responses to a range of volatile organic compounds. Differential responses to the various odors were observed, with trends similar to that exhibited in the

spun-cast devices (Figure 7.6). As in the spun-cast sensors, integrated P3HT-benzylamine and P3HT-benzoic acid sensors had opposite I_{on} responses to the alcohols, and P3HT-benzylamine generally exhibited the strongest sensor responses, especially to the acids.

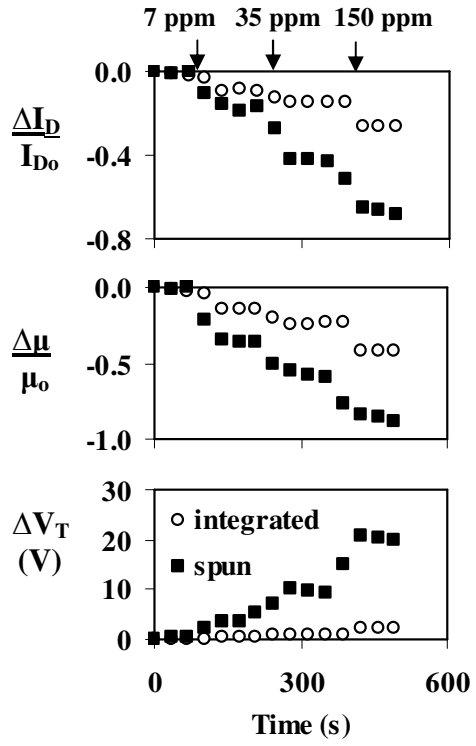

Figure 7.7: Comparison of integrated (drop-cast) and spun-cast P3HT-benzylamine OTFT gas sensors.
The time response of the sensors to increasing concentrations of isobutyric acid is shown.

While qualitatively similar, the integrated sensors exhibited quantitatively milder responses. This is not unexpected, due to their thicker active layers. Because TFT behavior is dominated by material near the dielectric interface, it is strongly influenced by active material thickness, and V_T response should be especially dampened in the thicker drop cast devices. An example of the muted sensor response, with a particularly muted V_T response, is shown in Figure 7.7. Due to active layer thickness nonuniformities in the integrated sensors quantitative chip to

chip variations in sensor response was significantly enhanced compared to spun-cast devices. Consequently, for a reliable sensor system, thickness control in the printing process will be critical.

Nevertheless, the integrated sensors still exhibited good sensitivity, with P3HT-benzylamine demonstrating a discernible sensor response to as little as 7 ppm of isobutyric acid. All sensors showed very strong responses to hexylamine, immediately becoming non-conductive with exposeure to 10 ppm of the analyte.

7.4 CMOS signal processing for sensor array

The OTFT gas sensor fabrication process is compatible with postprocessing over microfabricated CMOS chips. Three additional microfabricated layers would be required after completion of the CMOS back-end of line: a metal layer for the OTFT gate electrodes, a dielectric, and an additional metal layer for the OTFT source and drain electrodes. In addition, contact vias would be required through the dielectric and between the CMOS and OTFT layers. All of these can be low-temperature processing steps. The metal layer could be evaporated aluminum patterned with a wet etch. The dielectric can be silicon dioxide or silicon nitride deposited with plasma enhanced chemical vapor deposition, with vias patterned with wet or dry etching. Finally, the source and drain electrodes could be evaporated gold patterned patterned with lift-off. The highest temperature the substrate would be exposed to in these steps would be during the deposition of the dielectric, which can be done at under 200ºC, and is well under the thermal budget of any CMOS process. Alternately, an organic dielectric, spun on at room temperature and annealed at under 200ºC could be used.

After this processing, the source and drain electrodes would be on top, resulting in a structure that would appear very similar from the top as the silicon substrates used in this work. The final step would be to inkjet the sensing material between the patterned electrodes. Most likely, the area requirement of the chip would be dominated by the area occupied by the inkjetted drops, and the precision with which they can be placed with respect to one another, especially if many different sensing materials are used. Thus, for minimizing cost, it would be critical to achieve small droplet sizes and good alignment with the inkjet printing process.

Depending on the size of the array and the complexity of the targeted sensing tasks, the complexity of the signal processing circuitry can span a large range. The circuitry should handle analog amplification of the sensor response into a voltage signal, analog to digital conversion, digital processing of the data, as well as output to a display.

The circuitry diagramed in Figure 7.8 was used to demonstrate a simple sensing application. Three OTFT gas sensors and three matching OTFT reference devices were used to differentiate between ethanol and acetic acid, which are two of the most relevant volatile organic compounds associated with wine aging. The system could distinguish between mixture of the two analytes as well.

The sensing materials used for this demonstration were P3HT-benzoic acid, P3HT-benzylamine, and M2. M2 is an air stable modification of P3HT provided by Merck Chemical, Ltd., and provides sensor responses similar to those of P3HT (see Sections 4.2 and 4.3). For this sensing task, the opposite I_{on} responses of P3HT-benzoic acid and P3HT-benzylamine to ethanol was exploited, as well as the strong response of P3HT-benzylamine to acetic acid.

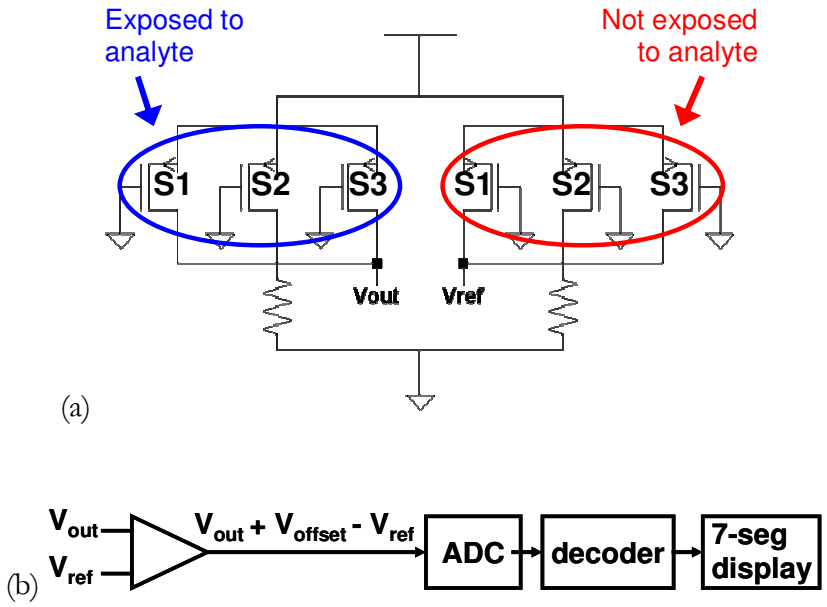

Figure 7.8: Simple example of signal processing circuitry for an OTFT gas sensor array.

Due to the simplicity of the sensing task, a single linear combination of the sensor response (Equation 7.1) was used as the sensing signal.

$$V_{out} = R * (2*I_{on,P3HT\text{-}benzoic\ acid} + I_{on,P3HT\text{-}benzylamine} + I_{on,M2}) \qquad \text{Equation 7.1}$$

For a more complex task, principle component analysis could be used to find one or more of the most relevant linear combinations of sensor responses to use (see Section 2.5.2). The circuitry in Figure 7.8a provides the amplified signal V_{out} and a matching reference signal V_{ref} from a set of reference OTFT sensors which are not exposed to the analyte, but used to cancel out the affects of bias stress during operation. The two resistors Figure 7.8a were adjusted to compensate for any initial mismatch between V_{out} and V_{ref}. V_{ouf} and V_{ref} were then fed into a series of integrated circuit components (Figure 7.8b) for further amplification and conversion to a digital signal. The output signal was read with a simple 7-segment display.

7.5 Conclusion

The integration of multiple OTFT sensor devices onto a single sensor chip was demonstrated. The integrated sensor chip exhibited a sensor response to a range of organic vapors at concentrations of below 10 ppm, and provided the differential signals necessary for electronic nose operation. The integrated OTFT sensors were fabricated on a silicon substrate, and feasibility of incorporating CMOS processing circuitry into this silicon substrate was explored.

7.6 References

[98] J. W. Gardner, A. Pike, N. F. De Rooij, M. Koudelka-Hep, P. A. Clerc, A. Hierlemann and W. Göpel, "Integrated array sensor for detecting organic solvents," Sensors and Actuators B, 26-27, 135, 1995.

[99] C. Cané, I. Gràcia, A. Götz, L. Fonseca, E. Lora-Tamayo, M. C. Horrillo, I. Sayago, J. I. Robla, J. Rodrigo and J. Gutiérrez, "Detection of gases with arrays of micromachined tin oxide gas sensors," Sensors and Actuators B, 65, 244, 2000.

[100] P.C.H. Chan, G. Yan, L. Sheng, R.K. Sharma, Z. Tang, J.K.O. Sin, I.-M. Hsing, Y. Wang "An integrated gas sensor technology using surface micro-machining," Sensors and Actuators B, 82 277, 2002.

[101] B.-U. Moon, J.-M. Lee, C.-H. Shim, M.-B. Lee, J.-H. Lee, D.-D. Lee, J.-H. Lee, "Silicon bridge type micro-gas sensor array," Sensors and Actuators B 108, 271, 2005.

[102] M.S. Nayak, R. Dwivedi and S.K. Srivastava, "Integrated sensor array for detection of alcohols and alcoholic beverages." Journal of Institution of Engineers (India)—ET, 75, 94, 1995.

[103] R. R. Das, K. K. Shukla, R. Dwivedi and A. R. Srivastava, "Discrimination of individual gas/odor using responses of integrated thick film tin oxide sensor array and fuzzy-neuro concept," Microelectronics Journal, 30, 793, 1999.

[104] A.M. Taurino, S. Capone, P. Siciliano, T. Toccoli, A. Boschetti, L. Guerini, S. Iannotta, "Nanostructured TiO2 thin films prepared by supersonic beams and their application in a sensor array for the discrimination of VOC," Sensors and Actuators B, 92, 292, 2003.

[105] C. Hagleitner, A. Hierlemann, D. Lange, A. Kummer, N. Kerness, O. Brand, and H. Baltes, "Smart single-chip gas sensor microsystem," Nature, 414, 293, 2001.

[106] J.V. Hatfield, P. Neaves, P.J. Hicks, K. Persaud, and P. Travers, "Towards an integrated electronic nose using conducting polymer sensors," Sensors and Actuators B, 18-19, 221, 1994.

[107] M. Su, L. Fu, N. Wu, M. Aslam, and V.P. Dravid, "Individually addressed large-scale patterning of conducting polymers by localized electric fields," Appl Phy. Lett, 84, 828, 2004.

[108] B. Polk, J.A. Smith, S.P. DeWeerth, Z. Zhou, J. Janata, and K. Domansky, "Design of solid state array for simultaneous potentiometric and impedance sensing in gas phase," Electroanalysis, 11, 707, 1999.

[109] B.J. Polk and J. Janata, "ChemFET Arrays for Chemical Sensing Microsystems" IEEE Sensors Conference, Orlando, Florida, 5.13, 2002.

[110] K.J. Albert, N.S. Lewis, C.L. Schauer, G.A. Sotzing, S.E. Stitzel, T.P. Vaid, and D.R. Walt, "Cross-Reactive Chemical Sensor Arrays," Chem. Rev., 100, 2595, 2000.

[111] E.J. Severin, Array-based vapor sensing using conductive carbon black-polymer composite thin film detectors, dissertation submitted to California Institute of Technology, 1999.

[112] Y.S. Kim, "Microheater-integrated single gas sensor array chip fabricated on flexible polyimide substrate," Sensors and Actuators B, 114, 410, 2006

[113] B.C. Sisk and N.S. Lewis, "Comparison of analytical methods and calibration methods for correction of detector response drift in arrays of carbon black-polymer composite vapor detectors," Sensors and Actuators B: Chemical, 104, 249, 2005
[114] T. Gao, E.S. Tillman, and N.S. Lewis, "Detection and Classification of Volatile Organic Amines and Carboxylic Acids Using Arrays of Carbon Black-Dendrimer Composite Vapor Detectors," Chem. Mater., 17, 2904, 2005
[115] B. Matthews, J. Li, S. Sunshine, L. Lerner, and J.W. Judy, "Effects of Electrode Configuration on Polymer Carbon-Black Composite Chemical Vapor Sensor Performance", IEEE Sensors Journal, 2, 160, 2002
[116] F. Zee, J.W. Judy, "Micromachined polymer-based chemical gas sensor array," Sensors and Actuators B: Chemical, 72, 120, 2001.
[117] F. Zee and J.W. Judy, "Micromachined MEMS Chemical Gas Sensor using a Polymer-Based Array", International Solid-State Sensor and Actuator Conference Digest of Technical Papers (Transducers '99), 680, 1999.
[118] F. Zee and J.W. Judy, "Miniaturization of A Carbon Black/Polymer Array Electronic Nose," 6th International Symposium - Olfaction and Electronic Nose, Tübingen, Germany September 20-22, 1999.
[119] Printed Electronics Europe, Cambridge, Cambs, United Kingdom, April 2006
[120] C.J. Curling, "14" Prototype line for manufacturing flexible active matrix displays," USDC Flexible Displays & Microelectronics, Phoenix Arizona, Feb 2006.
[121] Plastics Electronics trade fair, Frankfurt, Germany, October 2005.
[122] D.R. Gamota, P. Brazis, K. Kalyanasundaram, and J. Zhang (Ed.), Printed organic and molecular electronics, Kluwer Academic Publishers: New York, NY, 2004.
[123] L. T. Creagh and M. McDonald, "Design and performance of inkjet print heads for non-graphic-arts applications," MRS Bulletin, 807, November 2003.
[124] H. Sirringhaus, T. Kawase, R. H. Friend, T. Shimoda, M. Inbasekaran, W. Wu, E. P. Woo, "High-resolution inkjet printing of all-polymer transistor circuits," Science, 290, 2123, 2000.
[125] C. Arias, S. E. Ready, R. Lujan, W. S. Wong, K. E. Paul, A. Salleo, M. L. Chabinyc, R. Apte, Robert A. Street, Y. Wu, P. Liu, and B. Ong, "All jet-printed polymer thin-film transistor active-matrix backplanes," Appl. Phys. Lett., 85, 3304, 2004.
[126] W. Clemens, W. Fix, J. Ficker, A. Knobloch, and A. Ullmann, "From polymer transistors toward printed electronics," J. Mater. Res., 19, 1963, 2004.

Chapter 8: OTFT MODELING & CIRCUIT SIMULATION

AS the field of organic electronics continues to make steady strides towards commercialization, development of accurate OTFT device models for circuit simulations is becoming more important. While the technology is not yet ready to handle the requirements of electronic noses, circuit simulations are useful for gaining insight into what performance factors are still lacking, and how technology development efforts should be best focused. In this chapter, different models for charge transport in organics are reviewed, and a compact SPICE model for printed OTFTs is presented. The model is implemented in Verilog and based on experimental data measured from printed pentacene OTFTs fabricated on plastic [127].

8.1 Charge transport models

A good transport model is essential not only for the development of accurate analytical models, but also so that material and device structures can be intelligently engineered, and so that stability and degradation issues can be addressed more effectively. However, after a decade of animated debate, perhaps the only definite conclusion that may be drawn is that no single charge transport model can successfully explain the widely varying—and often contradictory—observations that have been made by different groups over the years.

In one notable case, pentacene OTFTs reported on by the same group fabricated under nominally identical conditions exhibited wildly different transport behaviors, ranging from thermally activated to temperature-independent charge transport [128]. Though such variation is rarely reported in literature, it is probably not uncommon in the laboratory. In light of the strong effect of processing conditions on device performance in organic electronics, which has

been frequently cited [129]-[132], the ability to choose the most applicable model given a specific experimental system is particularly important. This requires a good understanding of the various charge transport mechanisms that have been proposed.

As discussed in Section 3.3.2, the current-voltage characteristics of OTFTs are not well-described by the square-law behavior exhibited in many other field effect transistors. Rather, this traditional analysis must be modified to account for features such as gate-bias-dependent mobility, thermally activated transport, and gradual turn-on characteristics.

8.1.1 Gate-bias dependent mobility

Field effect mobility (μ_{FET}) in OTFTs was defined and described in Section 3.3.3. It has been universally observed that μ_{FET} in OTFTs changes with gate-bias, typically exhibiting a gate-activated behavior in which it increases with increasing (negative) bias. A number of explanations have been offered to explain this effect. An early explanation invoked the Poole-Frenkel mechanism, which states that high applied field lowers Coulombic potential barriers between localized states, increasing the tunneling rate between those sites. For cases in which significant conduction is assumed to occur through the tunneling of trapped charges between localized states, the mobility at high fields is expected to depend exponentially on applied field according to Equation 8.1.

$$\mu \propto e^{\frac{\sqrt{E}}{kT/q}}$$

Equation 8.1

μ = charge carrier mobility
E = applied electric field
k = Boltzmann constant
T = temperature
q = elementary charge

Dimitrakopoulos *et al* discounted the Poole-Frenkel theory by separating the effect of charge carrier concentration (N) and electric field (E), and showing that calculated mobility increases with increasing gate bias due to increased N, rather than increased E [134]. This dependence of mobility on charge density is also predicted by numerical simulations assuming a Gaussian density-of-states function (see Section 8.1.7) [133].

In an effect also related to charge density, the trapping models predict a gate-bias dependent mobility due to the gate-bias induced filling of traps. Variable range hopping (VRH) [135] and multiple trap and release (MTR) [136][137] charge transport models both predict a power-law relationship (Equation 8.2).

$$\mu_{FET} = K\,(-V_{GS} + V_T)^{\alpha} \qquad \text{Equation 8.2}$$

K, α = constants

In this equation, α is expected to fall between 0 and 1. Equation 8.2 has been successfully fit to a range of experimental OTFT data [138]. In VRH, the increase of gate bias results in the filling of deeper traps, activating more shallow, higher energy traps from which hopping can more easily occur. For MTR, on the other hand, a constant free carrier mobility μ_o is assumed, with a gate bias dependence resulting from the fact that the experimentally extracted μ_{FET} is an average of the mobility of trapped and free carriers. As traps are filled, the number of trapped carriers decrease, resulting in an increase in the average, extracted mobility.

In contrast, the grain boundary trapping (GBT) model predicts an exponential increase of mobility with gate bias due to the screening of grain boundary barriers by charges in the accumulated channel (Equation 8.3) [139].

$$\mu_{FET} = \mu_o e^{s/V_{GS}}$$ Equation 8.3

s = constant

This model has also been used to successfully fit experimental pentacene OTFT I-V curves [140]. In practice, however extracted μ_{FET}'s rarely show a purely power law or exponential dependence on V_G, so it is difficult to distinguish between the various models purely based on how μ_{FET} changes with V_G, especially over a limited range of V_G.

8.1.2 Temperature-dependent mobility

Though operation of OTFTs at very high or low temperatures is not interesting for most practical applications due to degraded lifetime and reliability, variable temperature measurements are a powerful tool for discerning transport mechanisms. Generally, mobility is expected to decrease with increasing temperature in band-like transport due to phonon scattering, and increase with increasing temperature in hopping-based mechanisms, where thermal activation is essential for the transport of carriers in localized states. Reports of temperature-independent transport probably indicate either that temperature effects are relatively weak, or that a combination of localized and delocalized (band) transport is taking place.

Experimentally, all possible behaviors have been observed by different groups; μ_{FET} in OTFTs has been separately reported to increase, decrease, and stay constant. Mobilities measured with subpicosecond transient photoconductivity on single crystals of pentacene indicate that band-

like transport does occur at time scales shorter than the carrier trapping time constants [141], while in most thin films, μ_{FET} shows strong thermal activation [128].

Another mechanism for low-mobility transport in materials such as organic semiconductors which exhibit polaron behavior is the Holstein small polaron model. This model predicts competing temperature effects, with hopping-type behavior at higher temperatures and coherent band-like behavior at lower temperatures, as well as anisotropic conduction in single crystals [142]. However, the small polaron model also predicts a drain-bias dependent mobility [143], which is not generally observed in OTFTs. Nevertheless, the model has found some experimental support in rubrene single crystal field effect transistors [144], and oligothiophene OTFTs [143][145].

The most commonly observed temperature behavior, an Arrhenius-like dependence of the form given in Equation 8.4, is predicted by any model involving thermally activated hops, including VRH [135], MTR [137], and GBT [139].

$$\mu = \mu_o e^{-\frac{E_a}{kT/q}} \qquad \text{Equation 8.4}$$

μ_o = intrinsic mobility
E_a = activation energy

In VRH and MTR, larger activation energy E_A indicates a wider, deeper trap distribution [130], and E_A decreases with increasing gate bias. As the Fermi level moves closer to the valence band, deep traps become filled, and the remaining shallower traps are more easily thermally activated. Reports of relatively temperature independent behavior could be explained by a shallow, narrow trap distribution above the valence band. In GBT, E_A corresponds to the barrier height at grain boundaries, with a larger trap distribution causing a larger barrier height.

Saleo *et al* report that both VRH and MTR models provide a good fit for a fairly extensive set of experimental polythiophene OTFT data, noting that the two models are indistinguishable within the temperature range accessible for organic materials. They reject the VRH in favor of the MTR model solely on the basis of a more physical interpretation of the final fitted parameter values [135].

8.1.3 Grain boundary trapping model

In the grain boundary trapping model, outlined by Levinson *et al* for inorganic thin films [149], polycrystalline material can be described as crystalline material punctuated by localized trap densities. Filling of these traps results in the formation of an energy barrier which impedes the flow of mobile carriers. As described above, GBT predicts both gate-bias and temperature-dependent charge transport. In addition, it predicts a strong dependence on doping concentration. The model assumes grain boundaries of zero thickness, so the effective width of the energy barrier is determined by the width of the depletion region it creates. The more heavily doped the crystalline region, the thinner the energy barriers, and the higher the effective charge mobility. This increase of effective mobility with increased doping has, in fact, been reported in polythiophenes, polythienylene vinylenes [150], and pentacene [151], but the relationship is difficult to rigorously verify experimentally because organic materials are rarely intentionally doped. Rather, dopants are usually unintentional impurities such as oxygen which have absorbed into the film in unregulated amounts. In addition, attempts to verify this relationship are confusticated by the fact that increased dopant concentration should also cause an increased mobile charge density, which is predicted to increase mobility in all of the other models as well. GBT does predict that dopant induced charge will boost mobility much more strongly than gate-bias induced charge [151]. To test this prediction, two otherwise

identical devices are required, one with high dopant density and measured at low gate bias, and the other with low dopant density but measured at a gate bias high enough to induce the same amount of mobile charges as were present in the first device. Unfortunately, accurate estimates of charge induced by either dopant density or gate bias are generally unavailable, and this sort of experiment would be difficult to set up.

Another possibility for distinguishing GBT from other mechanisms is to look for an increasing variation of measured μ_{FET} in OTFTs as channel length is scaled down to the same length scale as the grain boundaries themselves. The observation of band like transport in a thin film device built on a single grain would be strong evidence that traps are, indeed, localized to grain boundaries. In fact, devices have been fabricated on single grains [152], but no drastic improvement was observed by elimination of grain boundaries in the OTFT channel. However, this is not conclusive evidence against GBT since it has been shown that the grain structure in the first layer of an organic semiconductor, where most charge transport occurs, is not necessarily the same as the grain structure in the rest of the thin film.

8.1.4 Multiple Trap and Release

The grain boundary model assumes that the ratio of mobile charges to trapped charges is small, and free carriers are assumed to remain freely mobile in extended band-like states. If, however, the number of traps is large compared to the induced mobile charge (if significant trap states are present in the crystalline grain as well, for example, or if the grain size becomes very small and the grain boundary area large), then it becomes likely that all free carriers will be trapped. MTR and VRH (Section 8.1.5) are models based on variations of this assumption that all mobile carriers will be trapped. In MTR, most carriers are trapped in shallow states from

which they can eventually escape with the help of thermal energy. Thus, carriers tend to be repeatedly trapped and released; charge transport occurs predominantly through the movement of charges while they are in the extended band-like states, and tunneling or hopping of localized charges is ignored.

In its basic form, the MTR model predicts that μ_{FET} will be related to its intrinsic mobility by the ratio of extended states to trap states and the rate of thermally-activated release from trapped states (Equation 8.5) [142][154].

$$\mu_{FET} = \mu_o \alpha e^{-\frac{E_t}{kT}} \qquad \text{Equation 8.5}$$

μ_o=intrinsic charge mobility
α = ratio of extended states to trap states
E_a = activation energy of trap states

More complicated models have been developed involving differently shaped band tails [135], different analytical approaches to calculating physical parameters [137], and even energy-dependent mobility in the band tail [155]. Not surprisingly, the most important physical parameter in this model is the width and shape of the band tail. A steeper band tail allows the accumulation of more mobile charges with less gate bias, and is thus important in determining subthreshold slope characteristics of an OTFT. Though its validity is now in question, this was a popular model for amorphous silicon TFTs, and is perhaps the most cited transport model for "high performance" OTFTs.

8.1.5 Variable Range Hopping

Variable range hopping is also based on an exponential band tail, but assumes a wider, deeper distribution of traps than MTR, so that trapped charges are confined to localized states and

transport occurs predominately through tunneling or hopping from state to state. Also, materials that exhibit MTR at higher temperatures may convert to a VRH-like mechanism when carriers no longer have the energy to escape from traps into extended band-like states.

This model may be most appropriate for materials such as amorphous polymer thin films, where charges are assumed to be delocalized along portions of the polymer backbone, but laterally confined to the polymer chain. In VRH, the statistical probability of charge transfer between localized states, either through tunneling or hopping, is combined with an assumed random spatial distribution of states and analyzed using percolation theory to produce a complicated expression for mobility which includes both a gate-bias and temperature dependence [156]. Within experimentally accessible temperature ranges, however, the gate-bias and temperature dependency of μ_{FET} in VRH reduce to the same form as those of MTR, and the two cannot be readily distinguished.

For the development of an accurate analytical OTFT model, then, distinguishing between MTR and VRH is not important, since they predict the same functional relationships within all relevant operating conditions. Physically, though, the parameters extracted for one of the models may make more sense. As disorder is increased in the same material, for example, parameters related to disorder, such as band tail width, should change, while parameters related to intrinsic material properties, such as intrinsic mobility, should remain constant. Unfortunately, the VHR fitting parameters are more difficult to interpret physically than the MTR parameters.

MTR predicts thin film mobilities closer to the intrinsic mobility of a material, while VRH predicts much lower mobilities. Though the intrinsic mobilities of organic semiconductors is

not known, they are often assumed to be between 1 and 10 cm^2/V-s. Thus, materials with mobilities below ~0.01 cm^2/V-s can be fairly safely assumed to fall under VRH, since an MTR analysis would likely predict intrinsic mobilities well outside of this 1 to 10 cm^2/V-s range.

8.1.6 Polycrystalline polymer model

In recent years, the performance of polymer OTFTs has improved dramatically, and room temperature mobilities as high as 0.1 cm^2/V-s have been reported. Though VRH seems to be the most appropriate model for amorphous polymer organic thin films, these high mobilities hint that a new model is needed. Street *et al* [155] argues that high-performance thin films should, indeed, be analyzed as polycrystalline systems, with band-like transport coupled with localized tail states as described in the MTR model. By treating polymer thin films as interwoven regions of crystalline and amorphous materials, he proposes a density of states (DOS) distribution in which the amorphous regions, due to their shorter conjugation lengths, have a larger band gap than the crystalline regions. These disordered regions also have long, wide band tails, but, because of the valence band offset from the larger band gap, the effective trapping tail seen by mobile carriers is shallower, resulting in a boosted μ_{FET}. In addition, Street *et al* observes that transport along some grain boundaries should be easier than others, due to a better alignment of ordered regions or overlap of polymer chains. As a result, charge transport may further accelerated due to percolation of carriers through favorable paths.

8.1.7 Gaussian Density of States

The band structure of organic crystals results from the superposition of the HOMO and LUMO levels of many individual organic molecules. This is analogous to the splitting of atomic energy levels in inorganic molecules to form energy bands in inorganic crystals.

However, organic molecules are not as regularly spaced as inorganic atoms in a crystal because of the relative weakness of the van der Waals forces that hold them together. In addition, the specific HOMO and LUMO configuration of each organic molecule depends on many factors, including conjugation length, orientation, and surrounding conditions.

Perhaps the greatest unknown in trying to model charge transport in an organic material is the shape of the density-of-states function (DOS). How narrow are the bands? How steep are the band edges, and how long are the tail states? Is the distribution Gaussian or exponential? Are there trap states within the band? Which aspects of the DOS corresponding to material properties that can be controlled? The ability to experimentally extract the shape of a material's DOS distribution and correlate it with the both fabrication processes that caused it and the transport behavior that it results in would solve most of the remaining mysteries concerning charge transport in organic materials.

Unfortunately, DOS is rather difficult to deduce experimentally. Methods available for such attempts often produce data that are difficult interpret, and separate data sets are usually difficult to reconcile. Typically, states are filled with carriers either thermally, electrically, or optically, and then current levels or other indicators are monitored while the trapped carriers are released in a controlled manner. Alternatively, the Fermi level is ramped up slowly, and the filling up of traps is monitored.

A recent extraction of the DOS in single-crystalline pentacene [158] revealed an extended band tail resembling those typically observed in amorphous inorganic solids. This DOS distribution was inferred from a combination of several optical and electrical techniques, and though the various data sets did not completely reconcile, they did show an encouraging level of

qualitative agreement. Interestingly, the energy of the singlet exciton peak seems to correspond to the energy level of hydrogen- or oxygen-induced defects in pentacene predicted through first-principles calculations [159].

For the purposes of numerical device simulation, researchers have found it fruitful to simply use a Gaussian-shaped DOS at the band edge. This assumption, though questionable in polycrystalline material where complete randomness does not apply, is convenient mathematically. Importantly, it allows the development of numerical models which, though perhaps not entirely accurate, can lend powerful insight into the basic effects of disorder on charge transport.

Researchers at Technion [133][157] have derived a number of interesting charge transport dependencies based solely on varying the width of the Gaussian DOS as a disorder parameter. Most importantly, the spread in density of states results in a shifting of the charge density centroid so that it is almost always adjacent to the band edge. Disordered materials such as organic semiconductors must therefore be considered degenerate in all practical cases, and Boltzmann statistics cannot be applied. Roichman *et al* [157] also found that many of the effects of a Gaussian DOS can be summarized as a modification to the Einstein relation between diffusion coefficient and mobility:

$$\frac{D}{\mu} = n\frac{kT}{q}$$

Equation 8.5

D = diffusion coefficient
μ = charge mobility
n = proportionality constant
k = Boltzmann constant
T = temperature
q = elementary charage

Other results include a charge-density-dependent mobility and reduced subthreshold slope. Roichman *et al* also show that, by tweaking characteristic parameters, a Gaussian DOS can mimic the behavior of an exponential DOS within all reasonable ranges of operation. Conclusions drawn from Gaussian DOS calculations are therefore probably applicable, with some modification, to other DOS distributions as well.

8.1.8 Transport model summary

The field of organic electronics has matured to the point where OTFTs with reproducible—and even predictable—I-V curves can be reliably designed and manufactured. However, subtleties of the charge transport in organic thin films remains unknown. In many experimental situations, multiple transport models can be fit reasonably well to the same data. However, a few general conclusions may be drawn from the past decade of debate on these issues. The multiple trap and release mechanism, in which a mobility edge separates mobile carriers from local carriers, is the likely the most relevant model currently available for "high" mobility materials around with μ_{FET}'s of ~0.1 to 1 $cm^2/V\text{-}s$. For lower mobility materials, variable range hopping may be more appropriate. In polycrystalline polymer materials with high mobilities, transport may be accelerated by factors highlighted in the polycrystalline polymer model. Finally, the qualitative effects of introducing more disorder, calculated using the Gaussian DOS, model is probably relevant to most organic systems.

8.2 Compact DC model for OTFTs

The OTFTs used for model extraction were fabricated and measured by Steven Molesa [127], and were chosen because they possessed the characteristics necessary for low-cost OTFT logic applications: an individually addressable gate, low-cost plastic substrate, and an almost entirely

solution-based fabrication process. The first step in device fabrication involved spinning a layer of polyvinylphenol onto the plastic substrate to create a smooth surface. Then, gold gate electrodes were evaporated onto the plastic through a shadow mask. This was the only fabrication step that was not based on solution processing. The gate electrodes could have been printed as well, but the printing technology available to the researcher could not achieve the small line widths (<20μm) and film smoothness required for good device operation. Thus, the evaporated gold lines were used to simulate the lines that could be printed using state-of-the-art inkjet printers currently being developed for printed electronics.

On top of the gold electrodes, a thin layer of cross-linked polyvinylphenol was spun on and annealed to provide the gate dielectric. Then, gold source and drain electrodes were inkjet printed on either side of the gold electrodes. Finally a soluble pentacene precursor was printed between each pair of contact electrodes, and then converted to pentacene through a nitrogen anneal. The resulting devices had extracted μ_{FET}s of ~0.05 cm^2/v-s. Output and transfer characteristics are shown in Figure 8.1-Figure 8.3 for a device with a channel width of 59 μm, a channel length of 26 μm, and a dielectric thickness of 38 nm.

As discussed previously, square-law models do not describe OTFT behavior well. Figure 8.1 illustrates the poor fitting obtained by using a pure square law model (Equation 3.2) to fit the printed OTFT. This is the model from which reported μ_{FET} and V_T values are typically extracted; thus, the result in Figure 8.1 is a good one to keep in mind when considering such extracted values, both in this work and other reports.

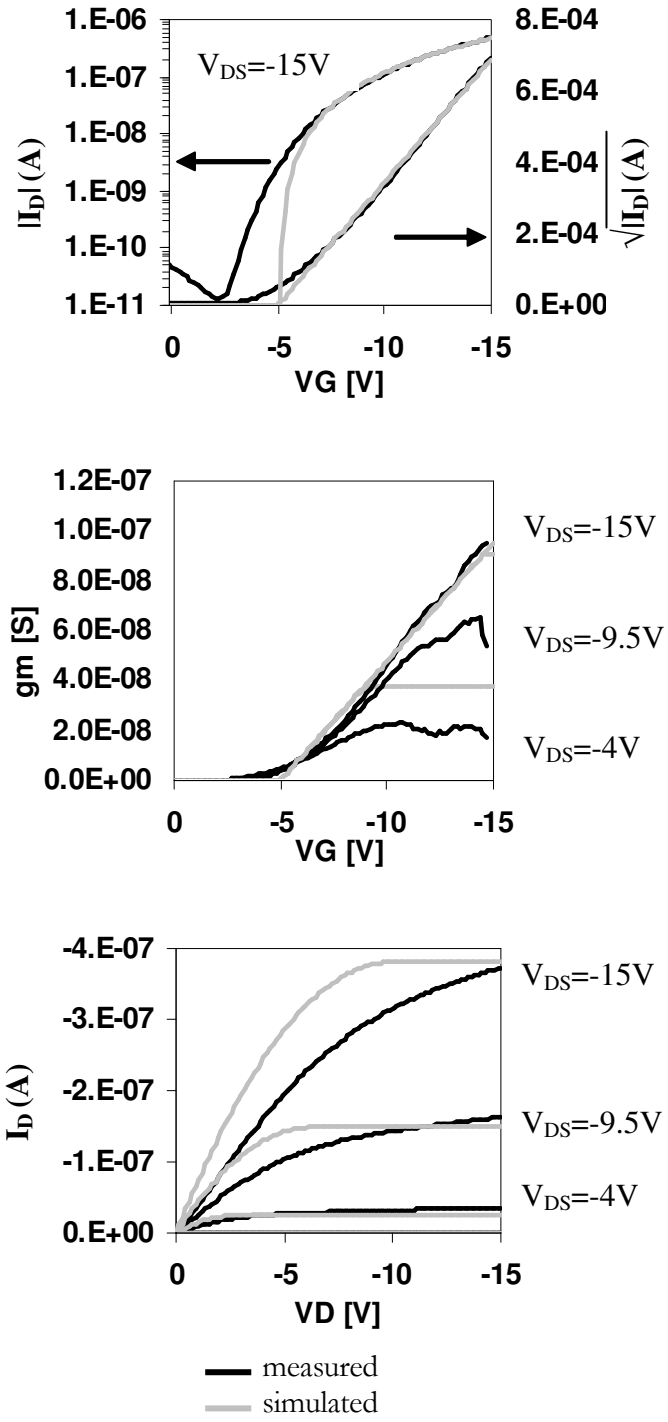

Figure 8.1: OTFT transfer and output characteristics fitted using square-law equations.

Modifying the compact model to include a power-law gate-bias dependent mobility according to Equation 8.2 results in a better fit of the transfer characteristics (Figure 8.2). Note that the subthreshold region is fairly well modeled by the gate bias dependent mobility alone, without requiring any separate model for the subthreshold region. In the compact model, the current is simply set to zero when the device is below threshold, and the exponential character of the subthreshold region comes entirely from square-law equations modified by gate-bias activated mobility.

In silicon CMOS, subthreshold current is modeled to be an exponential function of V_{GS} due to the exponential build up of inversion charge as V_{GS} moves the Fermi level closer to the band edge when the channel is first forming. In contrast, the high trap densities in organic materials pins the Fermi level, and the accumulation of charge in the channel is due to V_{GS}-induced filling of traps. Thus, it is not surprising that a gate-bias activated mobility describes the turn-on characteristics of OTFTs well.

Another distinguishing characteristic of OTFTs is the drain-dependent nature of the subthreshold region. Transfer characteristics of an OTFT are routinely observed to be shifted by applied drain bias, even in long-channel devices. In silicon devices, current in the subthreshold region is considered to be due to diffusion rather than drift. As a result, subthreshold behavior should not depend strongly on V_{DS}. In modern devices, this is not the case, since drain-induced barrier lowering (DIBL) can actually modify the effective threshold voltage, and thus shift subthreshold behavior. However, DIBL is a short channel effect in silicon devices, that is, it is only observed when devices were scaled down to submicron channel lengths. Thus, DIBL is not a good explanation of the drain-dependent nature of the

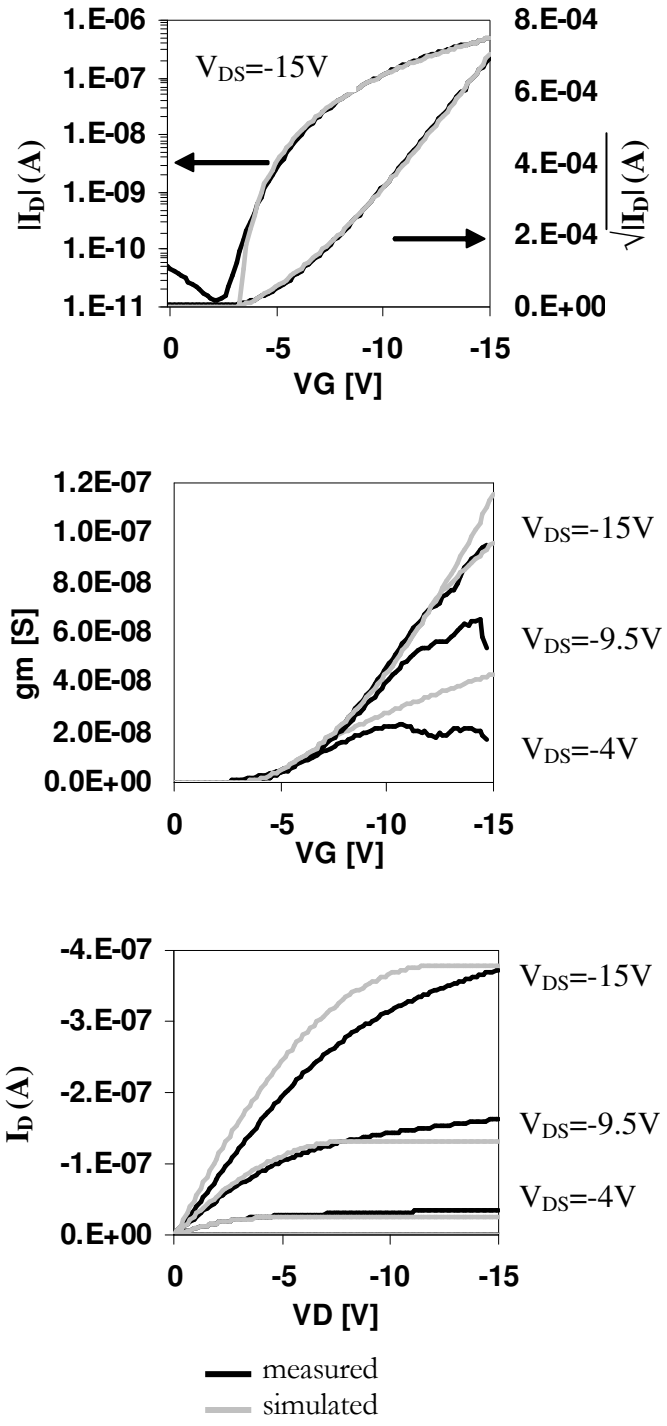

Figure 8.2: OTFT transfer and output characteristics fitted using V_{GS}-dependent μ_{FET}.

subthreshold region observed in long-channel OTFTs. However, if the subthreshold current is considered to be due to the drift of carriers with a gate-activated mobility, then a V_{DS} dependence is expected.

Contact issues are an important factor in OTFT performance. Perfect alignment between the source and drain work function and the organic semiconductor band edge is nearly impossible, since choosing a different metal is currently pretty much the only way of adjusting source/drain work function. Thus, a contact barrier is expected. Moreover, increased disorder at the metal/semiconductor interface is nearly always observed, especially in bottom contact structures where the semiconductor is deposited on top of the contacts. The difference in surface characteristics of the contact metal and the dielectric film results in a non-uniform surface for organic semiconductor film growth and/or re-organization after deposition. Borders between different surface characteristics, which correspond to the contact regions of the OTFT, are thus areas of enhanced disorder.

Contact resistance and contact barriers have a strong affect on the shape of the output characteristics, and on the behavior of the device in linear operation. Thus, while the simulated transfer characteristics in Figure 8.2 show good matching with the experimental data, the output characteristics do not. Incorporation of contact resistance into the compact model results in a much improved fit of both the output characteristics and the g_m curves for linear region operation (Figure 8.3).

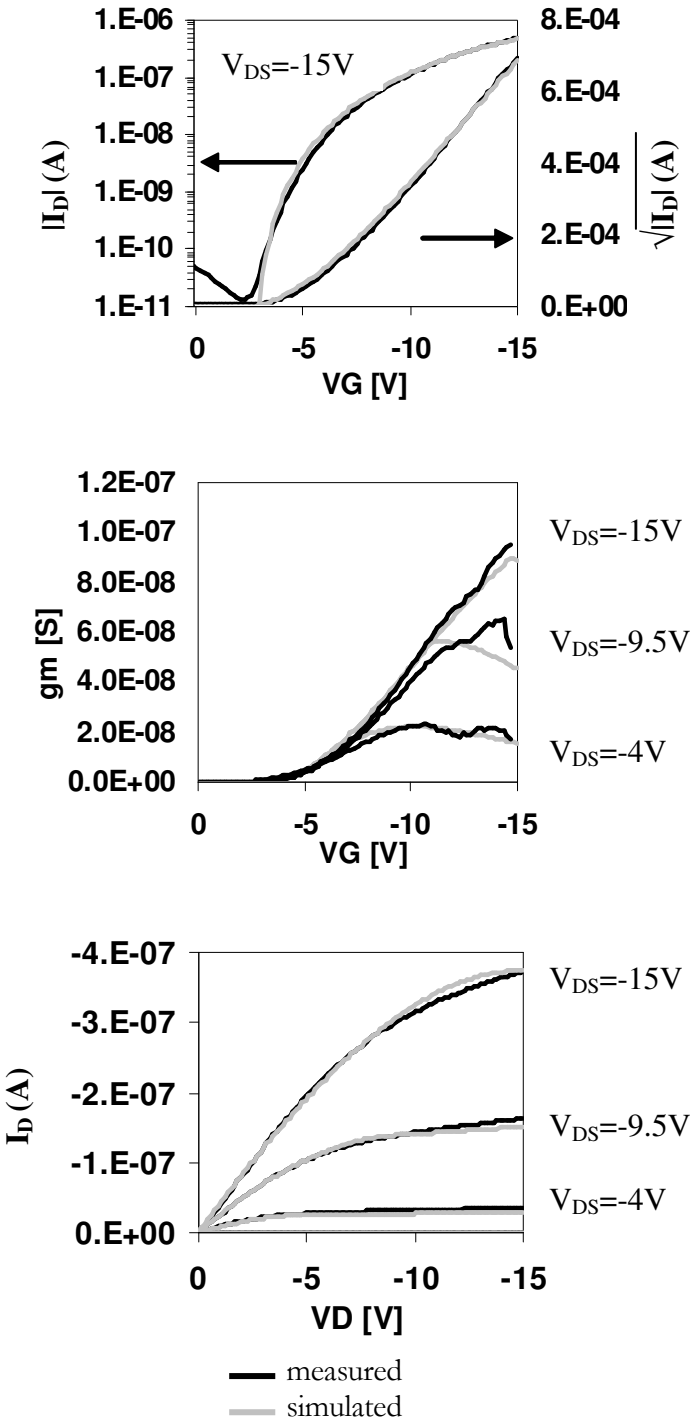

Figure 8.3: OTFT transfer and output characteristics fitted using V_{GS}-dependent μ_{FET} and series resistance.

8.3 Analog/Digital conversion using OTFT logic

A compact SPICE model based on the model illustrated in Figure 8.3, incorporating both V_{GS} dependent mobility and series resistance, was implemented using Verilоga. Using this model, several simple circuits were simulated. Figure 8.4 diagrams a circuit for providing signal amplification and analog to digital conversion of a sensor signal. The sensor signal is modeled as a differential change in current between an exposed OTFT gas sensor and a matching reference OTFT which is not exposed to the analyte. This differential change in current is converted to a differential voltage using a Wheatstone Bridge, and then fed into a three-bit flash analog to digital converter (ADC). In this structure, a ladder of resistors is used to provide a sequence of reference voltages, with each reference voltage associated with a digital output. Reference voltages larger than the voltage signal will trigger a high output level, and reference voltages smaller than the voltage signal will trigger a low output level. To allow detection of both positive and negative changes in I_{on} in the sensor OTFT, one end of the

.

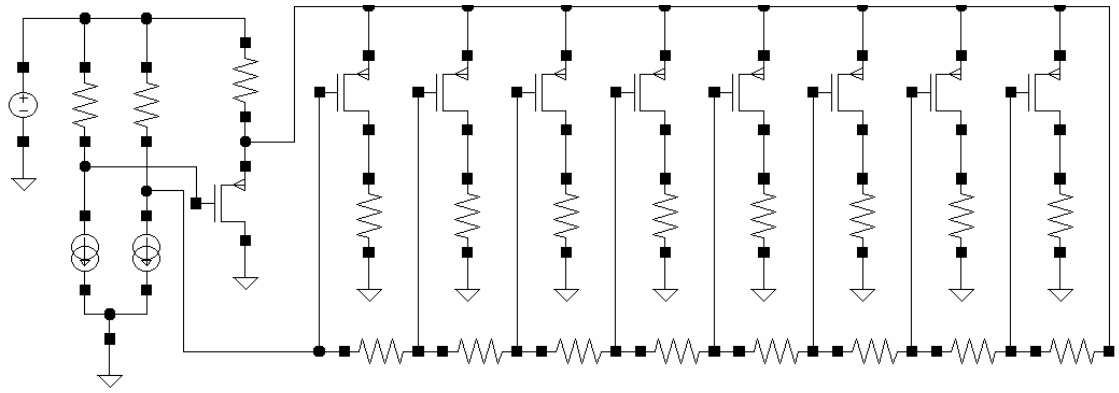

Figure 8.4: OTFT circuit to provide amplification and analog/digital conversion of sensor signal.
A Wheatstone Bridge amplified the sensor signal, one end of the differential signal is level shifted, and the resulting potential is fed into a flash ADC.

differential signal from the Wheatstone Bridge is level-shifted before feeding the signal into the flash ADC.

The transfer curve of the eight digital outputs as the sensor signal (I_{in}) is swept in relation to the reference signal (I_{ref}) is shown in Figure 8.5. The outputs flip from low to high sequentially as I_{in}-I_{ref} is varied from -200nA to 200nA, providing an eight-level, or three-bit resolution. Higher resolution can be achieved by simply increasing the length of the resistor chain in the flash ADC. However, the maximum useful resolution in an actual circuit will be limited by noise and variability in the device parameters. V_T control is particularly poor in OTFTs, since there exists no good knob for tuning V_T in organic semiconductors. Also, V_T is very sensitive to trap distributions, which can be quite variable due to the random nature of film formation from solution. To test sensitivity to V_T variability, the circuit in Figure 8.4 was simulated for V_T's ranging from -0.75V to -1.25V (the original simulation assumed a V_T of -1V). The arrows in Figure 8.5 show the variation of the transfer curves of the 1st, 2nd, 3rd, 5th, and 8th output of the flash ADC. The first output is shifted only by ΔV_T, which would limit the resolution of the ADC to the variation in V_T. However, the shift in output characteristics becomes more severe as the reference voltage level it corresponds to grows. The final output shifts by $\Delta V_T*(V_{in,max}/V_{T,\ nominal})$, where $V_{in,\ max}$ is the maximum value of V_{out}-V_{ref} that can be detected by the flash ADC. The error in the last bit is large enough to overlap both the 6th and 7th bit. Thus, even with a V_T control of +/- 0.25V, which is already probably better than what can be currently achieved in OTFT fabrication processes, adequate ADC resolution cannot be provided.

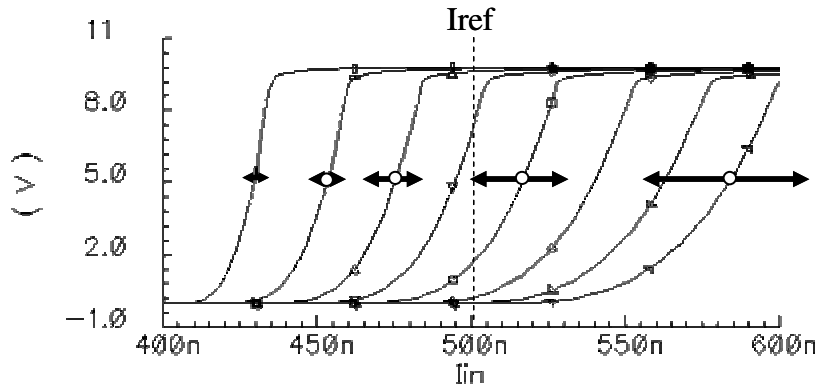

Figure 8.5: Outputs of flash ADC diagrammed in Figure 8.4. The arrows indicated the extent to which the indicated output transfer characteristic shifts as V_T is varied by +/- 0.25V.

An alternate ADC design in which resolution may be less sensitive to variability in device parameters is a pipeline ADC, illustrated in Figure 8.6. In this circuit, resolution is limited by the accuracy of the 2x gain stages. Given an amplifier with high gain and good control over resistor ratios, feedback can be used to provide accurate 2x gain stages which are relatively insensitive to variations in device parameters such as transconductance, output resistance, and V_T. Thus, this is a very attractive design for OTFT-based ADCs.

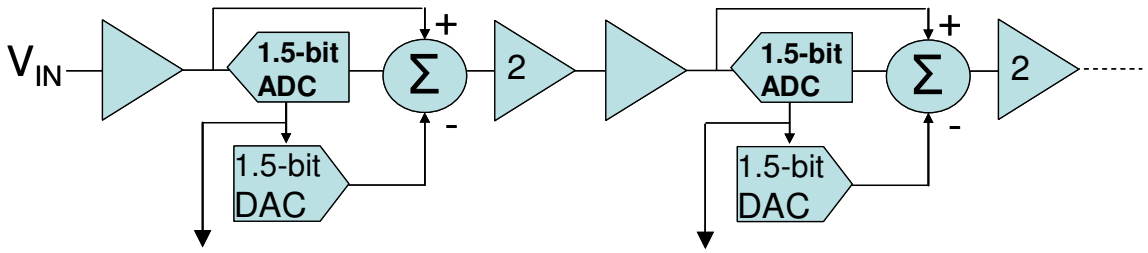

Figure 8.6: Block diagram of a pipeline ADC.

Relatively high-precision, high-resistance printed resistors can be made using resistive inks such as carbon black. The other required element is high gain amplifiers. Unfortunately, the OTFTs used for this simulation tend to have low transconductance (g_m) and low small-signal output impedances (R_{out}) compared to the large-signal channel resistance, two characteristics that make it difficult to provide high gain. The highest g_m*R_{out} observed in the printed pentacene OTFTs used for the SPICE model extraction was ~30. The average value was closer to 10. This is not quite enough to provide variability-insensitive feedback gain stages.

The effect of variations in μ and V_T on several basic gain stages, including an inverter, a feedback amplifer, and a differential amplifier are shown in Figure 8.7-Figure 8.9. None of them show good immunity to variability in V_T or μ, and so the greater complexity of implementing a pipeline ADC instead of a flash ADC is not justified with the currently available OTFT technology.

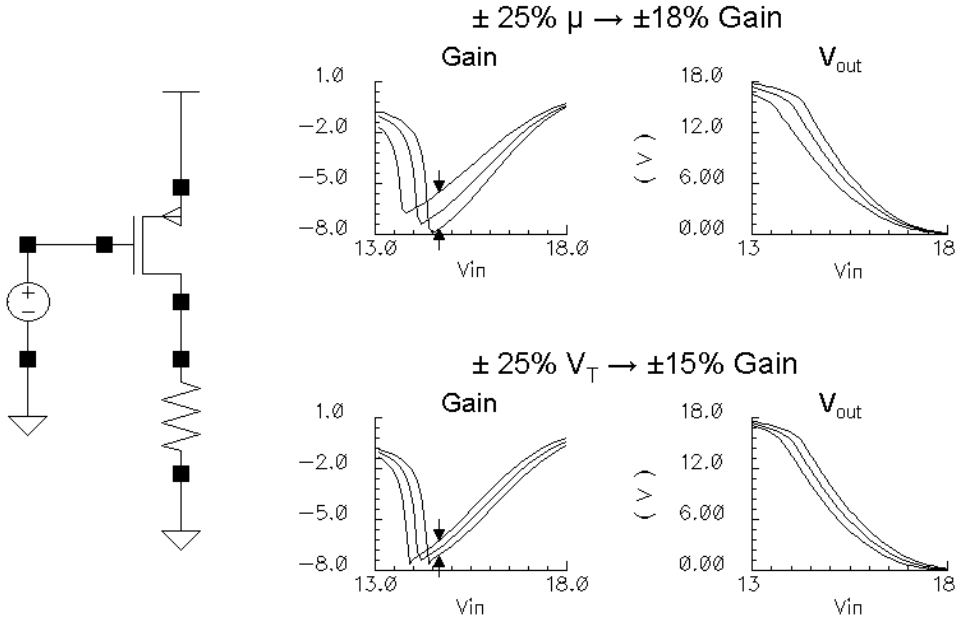

Figure 8.7: Effect of g_m and V_T variability on the gain and transfer characteristics of an inverter.

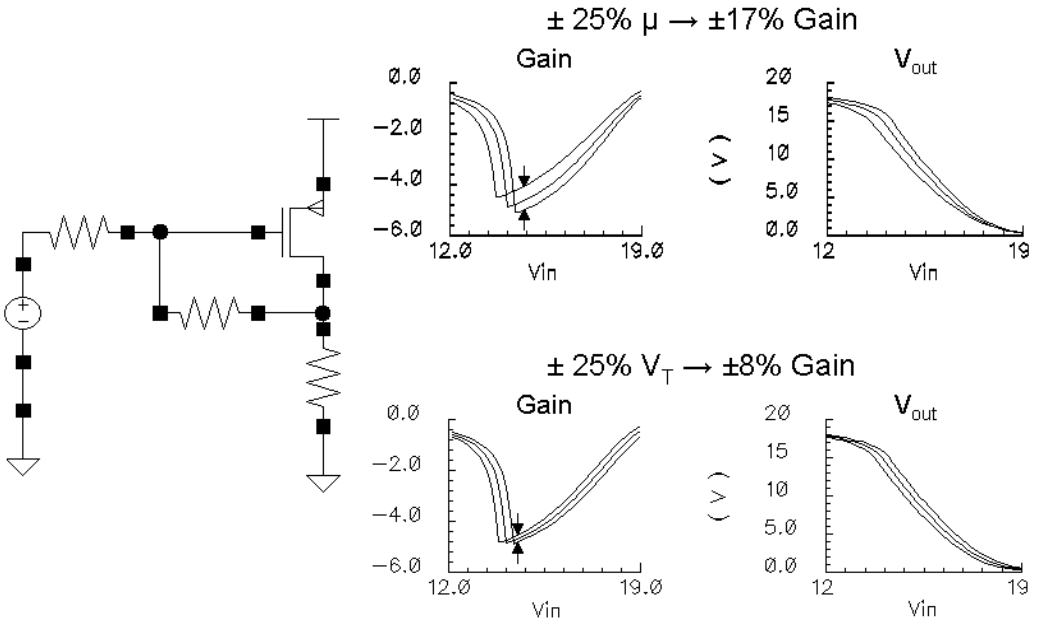

Figure 8.8: Effect of g_m and V_T variability on the gain and transfer characteristics of a feedback amplifier.

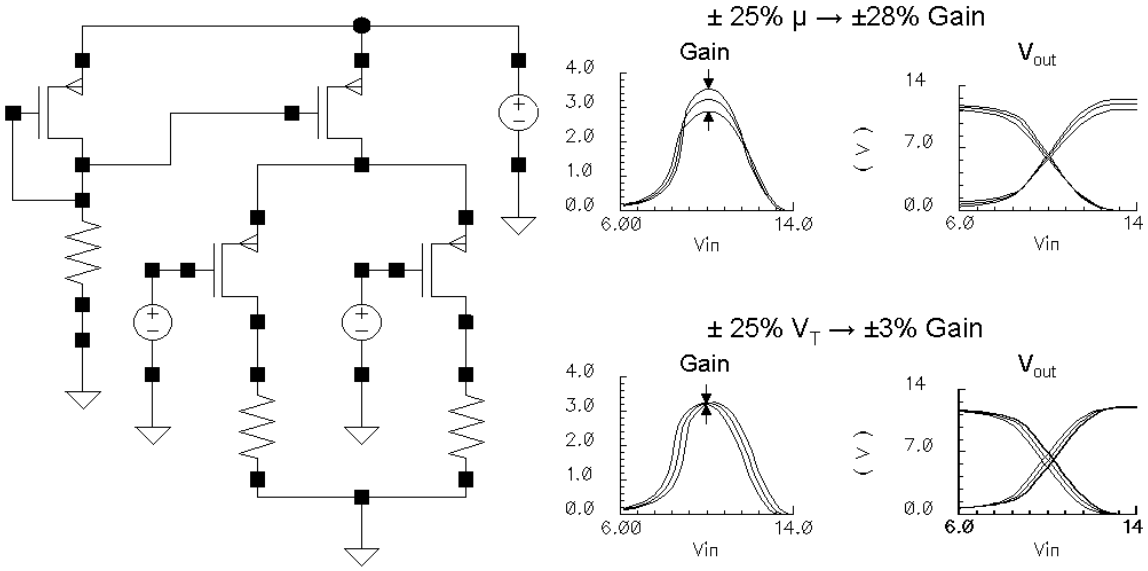

Figure 8.9: Effect of g_m and V_T variability on the gain and transfer characteristics of a differential amplifier

8.4 Conclusion

A compact model for OTFTs was developed based on a power law dependence of charge mobility on gate bias, which is predicted by both the variable range hopping and multiple trap and release charge transport models. An OTFT device with a structure compatible with low-cost printed circuits was used to extract modeling parameters. Using the developed SPICE model, the design of an ADC using current printed OTFT technology was explored. It was shown that the variability in V_T and other OTFT device characteristics will be a major challenge in the use of OTFTs to provide signal processing circuitry such as ADCs for electronic nose sensors.

8.5 References

[127] S.E. Molesa, A. de la Fuente Vornbrock, P.C. Chang, V. Subramanian, "Low-Voltage Inkjetted Organic Transistors for Printed RFID and Display Applications," Int. Electron Devices Meeting, Sec. 5.4, 2005.

[128] S. F. Nelson, Y.-Y. Lin, D. J. Gundlach, and T. N. Jackson, "Temperature-independent transport in high-mobility pentacene transistors," Appl. Phys. Lett., vol. 72, pp. 1854-1856, April 1998.

[129] O. Marinov, M. J. Deen, J. Yu, G. Vamvounis, S. Holdcroft, and W. Woods, "Variable current transport in polymer thin films transistors," J. Vac. Sci. Technol. A, vol. 22, pp. 755-759, June 2004.

[130] D. Knipp, R. A. Street, and A. R. Völkel, "Morphology and electronic transport of polycrystalline pentacene thin-film transistors," Appl. Phys. Lett., vol. 82, pp. 3907-3909, June 2003.

[131] D. J. Gundlach, Y. Y. Lin, T. N. Jackson, S. F. Nelson, and D. G. Schlom, "Pentacene Organic Thin-Film Transistors—Molecular Ordering and Mobility, IEEE Elec. Dev. Lett., vol. 18, pp. 87-89, March 1997

[132] R. Schroeder, L. A. Majewski, and M. Grell, "A study of the threshold voltage in pentacene organic field-effect transistors," Appl. Phys. Lett., vol. 83, pp. 3201-3202, Oct. 2003.

[133] Y. Roichman, Y. Preezant, and N. Tessler, "Analysis and modeling of organic devices," Phys. Stat. Sol., vol. 201, pp. 1246-1262, May 2004.

[134] C. D. Dimitrakopoulos, S. Purushothaman, J. Kymissis, A. Callegari, J. M. Shaw, "Low-Voltage Organic Transistors on Plastic Comprising High Dielectric Constant Gate Insulators," Science, vol. 283, pp. 822-

[135] A. Salleo, T.W. Chen, and A. R. Völkel, "Intrinsic hole mobility and trapping in a regioregular poly(thiophene)," Phys. Rev. B, vol. 70, 115311, Sep. 2004.

[136] G. Horowitz, M.E. Hajlaoui, "Grain size dependent mobility in polycrystalline organic field effect transistors," Synth. Met., vol. 122, pp. 185-189, 2001.

[137] M. Shur and M. Hack, "Physics of amorphous silicon based alloy field-effect transistors," J. Appl. Phys., vol. 55, pp. 3831-3842, May 1984.

[138] P. V. Necliudov, M. S. Shur, D. J. Gundlach and T. N. Jackson, "Modeling of organic thin film transistors of different designs," J. Appl. Phys., vol. 88, pp. 6594-6597, Dec 2000.

[139] R. A. Street, D. Knipp, and A. R. Vökel, "Hole transport in polycrystalline pentacene transistors," Appl. Phys. Lett., vol 80, pp. 1658-1660, March 2002.
[140] A. Bolognesi, M. Berliocchi, M. Manenti, A. Di Carlo, P. Lugli, D. Lmimouni, and C. Dufour, "Effects of grain boundaries, field-dependent mobility, and interface trap states on the electrical characteristics of pentacene TFT," IEEE Trans. Elec. Devices, vol 51, pp. 1997-2003, Dec. 2004.
[141] O. Ostroverkhova, D. G. Cooke, S. Shcherbyna, R. F. Egerton, and F. A. Hegmann, "Bandlike transport in pentacene and functionalized pentacene thin films revealed by subpicosecond transient photoconductivity measurements," Phys. Rev. B, vol. 71, 035204, Jan. 2005.
[142] G Horowitz, "Organic Field-Effect Transistors," Adv. Mater., vol. 10, pp. 365-377, 1998.
[143] K. Waragai, H. Akimichi, S. Hotta, and H. Kano, "Charge Transport in thin films of semiconducting oligothiophenes," Phys. Rev. B, vol. 52, pp. 1786-1792, July 1995.
[144] V. Podzorov, E. Menard, A. Borissov, V. Kiryukhin, J. A. Rogers, and M. E. Gershenson, "Intrinsic Charge Transport on the Surface of Organic Semiconductors," Phys Rev.Lett., vol. 93, 086602, Aug 2004.
[145] L. Torsi, A. Dodabalapur, L.J. Rothberg, A.W.P. Fung and H.E. Katz, "Intrinsic Transport Properties and Performance Limits of Organic Field-Effect Transistors," Science, vol. 272, pp. 1462-1464, June 1996
[146] Y-Y. Lin; D.I. Gundlach S. F. Nelson, and T. N. Jackson, "Pentacene-based organic thin-film transistor," IEEE Trans. on Elec. Dev. vol 44, pp. 1325 – 1331, Aug. 1997.
[147] T. Lindner, G. Paasch, and S. Scheinert, "Influence of distributed trap states on the characteristics of top and bottom contact organic field-effect transistors," J. Mater. Res., vol.19, pp. 2014-2027. July 2004.
[148] A. R. Völkel, R. A. Street, and D. Knipp, "Carrier transport and density of state distributions in pentacene transistors," Phys. Rev. B, vol. 66, 195336, Nov. 2002.
[149] J. Levinson, F.R. Shepherd, P. J. Scanlon, W. D. Westwood, G. Este, and M. Rider, "Conductivity behavior in polycrystalline semiconductor thin film transistors," J. Appl. Phys., vol. 53, pp. 1193-1202, August 1981.
[150] E. J. Meijer, C. Detcheverry, P. J. Baesjou, E. van Veenendaal, D. M. de Leeuw, and T. M. Klapwijk, "Dopant density determination in disordered organic field-effect transistors," J. Appl. Phys., vol. 93, pp. 4831-4835, April 2003.
[151] S. Verlaak, V. Arkhipov, and P. Heremans, "Modeling of transport in polycrystalline organic semiconductor films," Appl. Phys. Lett., vol 82, pp. 745-747, Feb 2003.
[152] T. Minari, T. Nemoto, and S. Isoda, "Fabrication and characterization of single-grain organic field-effect transistor of pentacene," J. Appl. Phys., vol 96, pp. 769-772, July 2004
[153] P.G. Le Comber and W. E. Spear, "Electronic transport in amorphous silicon films," Phys. Rev. Lett., vol. 25, pp. 509-511, Aug 1970.
[154] G. Horowitz, R. Hajlaoui, and P. Delannoy, "Temperature dependence of the field-effect mobility of Sexithiophene. Determination of the Density of Traps," J. Phys. III France, vol. 5 pp. 355-371, April 1995
[155] R.A. Street, J. E. Northrup, and A. Salleo, "Transport in polycrystalline polymer thin-film transistors," Phys. Rev. B, vol. 71, 165202, April 2005.
[156] M. C. J. M. Vissenberg, M. Matters, "Theory of the field-effect mobility in amorphous organic transistors," Phys. Rev. B, vol 57, 12964-12967, May 1998.
[157] Y. Roichman and N. Tessler, "Generalized Einstein relation for disordered semiconductors—implications for device performance," Appl. Phys. Lett., vol. 80, pp. 1948-1950, March 2002.
[158] D.V. Lang,1, X. Chi, T. Siegrist, A.M. Sergent, and A. P. Ramirez, "Amorphouslike Density of Gap States in Single-Crystal Pentacene," Phys. Rev. Lett., vol 93, 086802, August 2004.
[159] J. E. Northrup and M. L. Chabinyc, "Gap states in organic semiconductors: hydrogen- and oxygen-induced states in pentacene," Phys. Rev. B, vol. 68, 041202, 2003.

Chapter 9: **FUTURE WORK**

The demonstration of the gas sensing properties of printable organic semiconductors and the ability to modify this sensitivity through synthetic chemistry represent important initial steps towards the development of a printed gas sensor array. However, much work remains before a full-fledged low-cost electronic nose system can be realized.

First, the stability issues described in Chapter 4 must be addressed through materials engineering and signal processing. While repeatable and reversible sensor responses were demonstrated in this work, they were observed in gas sensors operated in an enclosed chamber under consistent ambient conditions. The exposure of gas sensors to varying temperature, humidity, and lighting conditions will heighten the challenge of maintaining and properly interpreting sensor responses. All organic semiconductor gas sensors investigated in this work exhibited especially strong sensor responses to humidity changes, and humidity was maintained at a constant level for all experiments due to its interfering effect on other sensor responses. In some applications, such as spoilage detection for refrigerated milk or sealed pharmaceutical packages, the requirement of a constant humidity level may be acceptable. However, there are many applications in which variable humidity must be dealt with. While a properly engineered sensor array may provide enough information to decouple the effect of humidity from the other sensor responses, a disproportionately strong response to water vapor will make this task difficult. It is likely that innovations in material engineering will be required in order to reduce the sensor response to water vapor relative to other odors of interest.

Another major task that remains is the engineering of the sensor inks for printability. While the solubility of the sensor materials demonstrated in Chapter 7 makes them compatible with inkjet printing, they have only been tested with a limited range of solvents and deposition conditions. The development of a printable ink involves an extensive search for proper solvents, solute concentrations, and printing conditions, all of which depend as much on the print head and substrate used as on the material to be printed.

Also, the library of printable inks developed in this work will need to be greatly expanded. The end-cap functionalization described in Chapter 6 is a viable synthetic route for the generation of such a library, but significant effort will still be required to synthesize and characterize these additional sensing materials. The careful selection of functional groups to provide maximum orthogonality of response will be vital to the eventual sensitivity and selectivity of the electronic nose system.

Finally, to complete the electronic nose system, supporting circuitry must be provided for the gas sensor array. For each new sensor array, a unique response library will need to be collected for odors of interest, and data processing techniques will need to be implemented to match observed response patterns to known odors. To handle a large number of sensing elements and complex odors, the required data processing will be orders of magnitude more complex than that of the circuits described in Section 7.4. At the same time, for low-cost applications, software running on a generic microprocessor is not an option, and a stand-alone system will be necessary. As a first step, a silicon-based application-specific integrated circuit fabricated in the traditional method would suffice. This solution could be coupled with an off-the-shelf power source and display to provide an electronic nose system with lowered costs due solely to

the advantage of printing the gas sensing elements. Later, with advancements in both OTFT and other printed technologies, an ultra-low-cost, all-printed solution may be possible.

The core motivating idea in this work is that a printed gas sensor array could enable the drastic lowering of the cost of electronic noses. OTFT gas sensing elements were chosen as a model system because there are currently extensive research efforts worldwide to print and optimize the printing of OTFTs. However, OTFTs are not the only gas sensor technology amenable to printing, and the printing of other sensing structures such as conducting polymer or polymer composite chemoresistors should certainly be considered as well.

In conclusion, OTFT gas sensors have been shown to be a promising solution for printed gas sensor arrays. OTFTs made with solution-processed polythiophene sensing material exhibit a response to a wide range of vapors, and functionalization of the polythiophene can modify this sensor response in a predictable fashion. These results encourage the pursuit of low-cost electronic noses based on printed OTFT gas sensor arrays.